Convective heat transfer in coarse-grained porous media

A numerical investigation of natural and mixed convection

Chakkingal, M.

DOI
10.4233/uuid:a5428de8-dc6b-4a45-b0de-d4ac1ad54697

Publication date
2020

Document Version
Final published version

Citation (APA)
Chakkingal, M. (2020). *Convective heat transfer in coarse-grained porous media: A numerical investigation of natural and mixed convection.* [Dissertation (TU Delft), Delft University of Technology]. https://doi.org/10.4233/uuid:a5428de8-dc6b-4a45-b0de-d4ac1ad54697

Important note
To cite this publication, please use the final published version (if applicable).
Please check the document version above.

CONVECTIVE HEAT TRANSFER IN COARSE-GRAINED POROUS MEDIA

A NUMERICAL INVESTIGATION OF NATURAL AND MIXED CONVECTION

CONVECTIVE HEAT TRANSFER IN COARSE-GRAINED POROUS MEDIA

A NUMERICAL INVESTIGATION OF NATURAL AND MIXED CONVECTION

Dissertation

for the purpose of obtaining the degree of doctor
at the Delft University of Technology,
by the authority of the Rector Magnificus prof. dr. ir. T.H.J.J. van der Hagen,
chair of the Board of Doctorates,
to be defended publicly on 14 September 2020 at 10.00 hrs

by

Manu CHAKKINGAL

Master of Technology in Engineering Mechanics, Indian Institute of Technology, Delhi
born in Kerala, India.

This dissertation has been approved by the promotors.

promotor: Prof. dr. ir. C. R. Kleijn
promotor: Prof. dr. S. Kenjereš, Dipl-Ing.

Composition of the doctoral committee:

Rector Magnificus,	chairperson
Prof. dr. ir. C. R. Kleijn,	Delft University of Technology, promoter
Prof. dr. S. Kenjereš, Dipl-Ing,	Delft University of Technology, promoter
Independent members:	
Prof. J. Padding,	Delft University of Technology
Prof. dr. ir. J.R. van Ommen,	Delft University of Technology
Prof. dr. ir. T.H. van der Meer,	University of Twente
Prof. dr. ir. D.M.J. Smeulders,	Eindhoven University of Technology
Ir. D. van der Plas,	TATA Steel, The Netherlands

This research was carried out under project number S41.5.14526a in the framework of the Partnership Program of the Materials innovation institute M2i (www.m2i.nl) and the Technology Foundation TTW (www.stw.nl), which is part of the Netherlands Organization for Scientific Research (www.nwo.nl). This work is also partly funded by TATA Steel in Europe.

Keywords: Natural convection, mixed convection, packed bed, simulations

Printed by: Ridderprint

Front & Back: Temperature distribution in a lid-driven cavity under mixed convection.

ISBN 978-94-6416-089-5

An electronic version of this dissertation is available at
`http://repository.tudelft.nl/`.

uddhared ātmanātmānaṁ nātmānam avasādayet
ātmaiva hyātmano bandhur ātmaiva ripur ātmanaḥ

Use the power of your mind, to grow
and not to degrade yourself,
for the mind can be your friend and also the enemy.

Bhagavad Gita: Chapter 6, Verse 5

CONTENTS

SUMMARY

Heat transfer by the motion of fluids, referred to as convective heat transfer, is ubiquitous. Convective heat transfer in enclosures packed with solid obstacles, is of great importance in various engineering and real-life applications, such as in blast furnaces, refrigeration devices, distribution transformers, nuclear waste disposal, energy storage, etc. Both natural convection, where the heat transfer occurs due to the flow induced by density differences, and mixed convection, where the combined influence of natural convection and forced convection is of importance, play an important role in these applications.

The particular application that motivated our research is molten iron production in the hearth of a blast furnace. Here we deal with natural convection due to thermal gradients between the hot molten metal and the cooled walls, whereas the tapping of molten metal from the blast furnace adds the influence of forced convection. The large, unburnt coke particles in the hearth create a coarse-grained porous packing. This plays an important role in the convection within the furnace and thus the power required to cool it. In the blast furnace, and all the other applications mentioned above, the flow and thermal length scales can be comparable to those of the pore-spaces of the porous media. Therefore, there is a strong interaction between pore geometry and the flow, and hence the geometrical effects of the porous media cannot be neglected. The thermal conductivity of the porous media can also influence the heat transfer and the temperature distribution in the cavity.

Indeed, some experimental studies reported in literature hint at a strong influence of the pore-spacing and thermal properties of porous media on the heat transfer. However, the existing numerical modelling techniques are not able to capture these effects. To better understand the heat transfer mechanism in such coarse-grained porous media and to improve the existing models, it is important to understand the local pore-scale flow and temperature distribution, and the resulting global heat transfer.

In this work, we carry out pore-structure resolved numerical simulations in a simplified geometry- a cubical enclosure filled with spherical beads. We investigate the role of the strength and direction of the forced and natural convective flow, and the role of the local wall temperature distribution in the heat transfer mechanism. We compare our pore-structure resolved simulation results with the results obtained with the representative volume averaging approach of modelling porous media. This helps us to better understand how the local pore-structure, the thermal properties of the spherical bead packing, the direction and strength of the forced convective flow, etc. influence the heat transfer mechanism.

Our results are validated against experiments conducted in a parallel Ph.D. study by Dr. Iman Ataei Dadavi. We thus provide an experimentally validated numerical model to solve heat transfer in porous-media to our industrial partner, TATA steel. With our work,

we aim at improving the understanding of the various factors influencing heat transfer in the hearth of the blast furnace.

SAMENVATTING

Warmteoverdracht door stromende vloeistoffen, convectieve warmteoverdracht genoemd, is alomtegenwoordig. Convectieve warmteoverdracht in behuizingen waarin zich obstakels bevinden is van groot belang in verschillende toepassingen, zoals in (hoog)ovens, koelapparatuur en koelhuizen, transformatoren, opslagplaatsen voor kernafval, energieopslag, enz. Zowel natuurlijke convectie, waar de warmteoverdracht plaatsvindt door de stroming veroorzaakt door dichtheidsverschillen, en gemengde convectie, waarbij de gecombineerde invloed van natuurlijke convectie en geforceerde convectie van belang is, speelt bij deze toepassingen een belangrijke rol.

De specifieke toepassing die ons onderzoek heeft gemotiveerd, is de productie van gesmolten ijzer in de haard van een hoogoven. Hier hebben we te maken met natuurlijke convectie door thermische gradiënten tussen het hete gesmolten metaal en de gekoelde wanden van de hoogoven, terwijl het tappen van gesmolten metaal uit de hoogoven leidt tot additionele geforceerde convectie. De grote, onverbrande cokesdeeltjes in de haard creëren een grofkorrelige poreuze stapeling. Dit beïnvloedt de convectie binnen de oven en dus het vermogen dat nodig is om deze te koelen.

In de hoogoven en alle andere hierboven genoemde toepassingen kunnen de afmetingen van stromingspatronen en thermische structuren van dezelfde orde grootte zijn als de afmetingen van de holten tussen de vaste objecten. Daarom is er een sterke interactie tussen de geometrie van deze holten en de stroming en kunnen de geometrische effecten van de grofkorrelige poreuze stapeling niet worden verwaarloosd. De thermische eigenschappen van de vaste objecten kunnen bovendien ook de warmteoverdracht en de temperatuurverdeling in de holten en in de gehele behuizing beïnvloeden.

Experimentele studies in de literatuur duiden inderdaad op een sterke invloed van de geometrie van de holten en van de thermische eigenschappen van de vaste objecten op de lokale en globale warmteoverdracht. Bestaande numerieke modelleringstechnieken, zoals die bijvoorbeeld worden gebruikt om processen in hoogovens te simuleren en optimaliseren en waarin de geometrische en thermische eigenschappen van de vaste objecten worden uitgemiddeld over de ruimte, zijn echter niet in staat deze lokale effecten correct mee te nemen. Om het mechanisme van warmteoverdracht in dergelijke grofkorrelige stapelingen beter te begrijpen en om de bestaande modellen te verbeteren, is het belangrijk om de lokale stromings- en temperatuurverdeling op holteschaal te begrijpen, alsmede hun invloed op de grootschalige warmteoverdracht.

In dit werk bestuderen we, met behulp van numerieke simulaties, de stroming en warmteoverdracht in de kanalen van een vereenvoudigde geometrie, namelijk een kubusvormige omhulling gevuld met verschillend gestapelde bollen. We onderzoeken de invloed van de grootte en richting van de geforceerde en natuurlijke convectiestroming op de lokale wandtemperatuurverdeling en op het grootschalige warmteoverdrachtsmechanisme. We vergelijken onze simulatieresultaten, waarin de stapeling in detail is gesimuleerd, met simulatieresultaten die zijnverkregen met veelgebruikte grofschalige

simulatietechnieken waarin de invloed van de vaste objecten wordt gemiddeld over de ruimte. Dit helpt ons om beter te begrijpen hoe de lokale kanaalstructuur, de thermische eigenschappen het vaste materiaal, de richting en sterkte van de gedwongen convectiestroom, etc. het warmteoverdrachtsmechanisme beïnvloeden.

Onze resultaten zijn gevalideerd aan de hand van experimenten die zijn uitgevoerd in een parallelle promotiestudie door Dr. Iman Ataei Dadavi. Zo heeft onze studie geleid tot een experimenteel gevalideerd numeriek simulatiemodel, waarmee onder andere onze inustrieële partner Tata-steel de stroming en warmteoverdracht in de haard van hoogovens kan modelleren en optimaliseren met het oog op bijvoorbeeld staalkwaliteit en energiezuinigheid.

1

INTRODUCTION

1.1. APPLICATION BACKGROUND

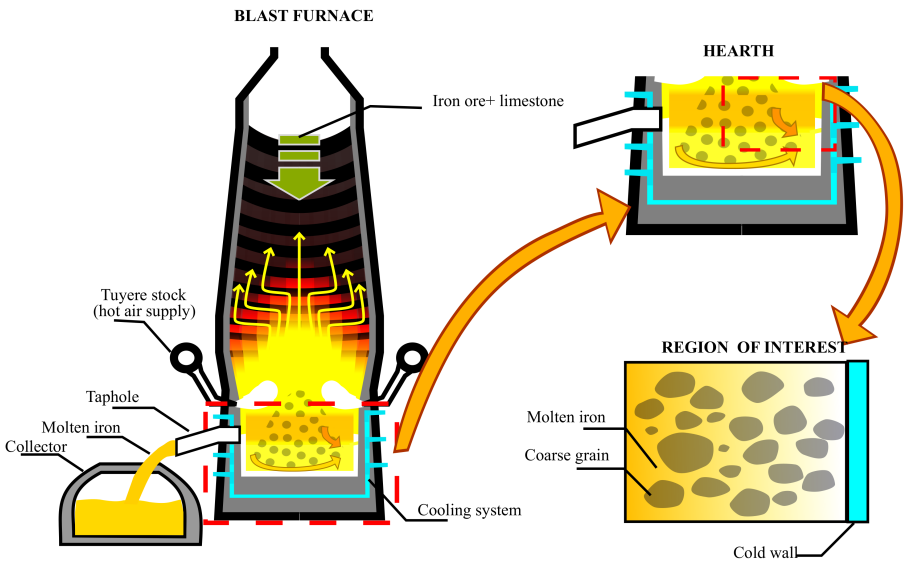

Figure 1.1: Schematic representation of a blast furnace. The image is an adapted version available in [1]. The hearth of the blast furnace is simplified as a side-heated side-cooled cavity filled with porous media.

The blast furnace, used for smelting to produce industrial metals, converts iron ore into hot liquid metal. The liquid metal is collected at the bottom of the furnace, in the so-called hearth, and tapped off. The hearth is made of refractory materials and is cooled from its sides. The hearth (5-7 m in height [2]) is filled with a coarse-grained (typical

diameter 10-40mm) porous carbon structure through which the hot metal (at a temperature $\approx 1500^{\circ}C$) flows from the top (Fig.1.1).
The cooling of the hearth walls with water at room temperature results in a natural convective flow of the molten metal. The tapping off process results in a forced convective flow inside the hearth ($\mathbf{u} \approx 2-8 m/s$ [3]). The combined effects of natural convection and forced convection in molten metal (Rayleigh number $\approx 10^{11}$, Richardson number ≈ 1), which is a low Prandtl number fluid ($\approx 0.1-0.3$), results in flow asymmetries and a complex temperature distribution at the walls. Regions with high local temperature, termed as hot-spots, are observed at the walls, leading to the reduction in the lifetime of the hearth and negative impact on productivity. The flow being opaque and at high temperatures, it is difficult to carry out experimental studies. Thus, computational fluid flow modeling is the only available tool to study and optimize this liquid metal flow.

To understand the heat transfer mechanism in such a complex domain, it is important to understand the natural convective and mixed convective flow in simplified fluid and porous-media filled-cavities. In this chapter, we first discuss natural convective and mixed convective flow in fluid-only cavities to explain the influence of fluid properties, enclosure characteristics and wall temperatures on the local and global flow and heat transfer. Later in this chapter, we discuss the influence of porous media in systems with the natural convective and mixed convective flow.

1.2. NATURAL CONVECTION IN FLUID-ONLY CAVITIES

Natural convection is observed in fluids when a driving force for the flow is generated by gravity and the density variation due to a temperature/concentration gradient. Convective thermal turbulence is observed in earth's mantle [4, 5], the atmospheric boundary layer [6] and ocean circulation [7]. Natural convective flows also play an important role in various engineering and industrial applications like electronic cooling [8, 9], passive safety of nuclear reactors [10], ventilation of rooms [11], thermal energy storage [12], etc. These convective currents are characterized by local ascending and descending vertical movements of the fluid.

The fluid motion in a thermally-driven flow with relatively small temperature differences can be described by the incompressible Navier-Stokes equations with the Boussinesq assumption to account for buoyancy effects [13].

$$\nabla \cdot \mathbf{u} = 0 \tag{1.1}$$

$$\frac{\partial \mathbf{u}}{\partial t} + \mathbf{u} \cdot \nabla \mathbf{u} = -\frac{1}{\rho} \nabla p + \nu \nabla^2 \mathbf{u} + \mathbf{g} \beta (T - T_{ref}) \tag{1.2}$$

$$\frac{\partial T}{\partial t} + \mathbf{u} \cdot \nabla T = \alpha \nabla^2 T \tag{1.3}$$

where $\mathbf{u}$, p, $\mathbf{g}$, T, T_{ref}, β, α are the velocity, pressure, acceleration due to gravity, temperature, reference temperature, volume expansion coefficient and thermal diffusivity, respectively.

When non-dimensionalized, the convective heat transfer can be characterized by three control parameters, namely the Rayleigh number (Ra), Prandtl number (Pr) and

aspect ratios (Γ), and by two response parameters- Reynolds number (Re) and Nusselt number (Nu).

Studies on natural convection for enclosures of different types like cubical, cylindrical etc. are widely reported in literature. Among them, the influence of the control parameters on the response is extensively reported for the most famous classical problems on natural convection, *viz.*

- Rayleigh–Bénard convection (RBC), driven by a vertical temperature gradient. It is extensively studied with cubical and cylindrical enclosures.
- Natural convection in differentially heated cavities characterized by a horizontal temperature gradient. It is studied mostly with cubical enclosures.

Thus, in our current study, we use cubical enclosures with horizontal and vertical temperature gradient. The major findings in the above classical problems can be classified into:

1. *Influence of Ra and Pr on Nu* [14–25]
   The non-dimensional heat transfer, Nu increases with the increase in Ra and is strongly dependent on Pr for low-Pr fluids, but becomes weakly dependent on Pr, at $Pr > 1$. In a bottom-heated top-cooled cavity, the global heat transfer approaches $Nu \sim Ra^{1/2}$ at very high Ra and small to moderate Pr. In a side-heated cavity, $Nu \sim Ra^{1/4}$ for laminar flows and is close to $Nu \sim Ra^{1/3}$ for turbulent flows. Calculation of Nu for the most downstream part alone in turbulent side-heated cavities shows that it follows the classical $Ra^{1/3}$ scaling for turbulent flows.

2. *Effect of aspect ratio and boundary conditions on local and global heat transfer* [23, 26–29]

   In bottom-heated top-cooled rectangular cavities filled with fluids of $Pr \geq 0.5$, for a fixed Ra, the global heat transfer increases with an increase in width to height ratio and is observed to attain a maximum. With further increase in the ratio the heat transfer decreases. With the increase in Pr, maximum heat transfer enhancement is observed in cavities with a smaller width to height ratio. While in bottom-heated top-cooled cylindrical cavities, at low Ra, the heat transfer initially decreases with diameter to height ratio, reaches a minimum and then increases. With further increase in the aspect ratio, the heat transfer becomes independent of it. With the increase in Ra, the aspect ratio does not influence the heat transfer. However, in side-heated side-cooled cavities no strong influence of aspect ratio on heat transfer is observed.

3. *Boundary layer characteristics* [24, 25, 30, 31]
   The global scaling of the thickness of thermal and viscous boundary layers follows a power law *w.r.t* Ra, both in cavities with a vertical and horizontal temperature gradient. The multiplication pre-factor and the power are found to be sensitive to Pr, the aspect ratio and the orientation of the cavity. At high Ra, intermittent and complex large scale turbulent flows result in strong spatial inhomogeneities of the thermal and viscous boundary layers in bottom-heated top-cooled cavities.

While in side-heated cavities, the boundary layers remain laminar up to regions (upstream part) where gravity waves start to disrupt the boundary layer, ejecting eddies from the boundary layer to the core. With the increase in Ra, the point where this transition occurs moves upstream of the boundary layers.

4. *Large scale flow structure* [29, 32–40]
   The large scale circulation in bottom-heated cavities is strongly influenced by the aspect ratio and Pr. This in-turn affects the global heat transfer. For low Pr fluids, the modification in LSC with change in inclination of the cavity, results in heat transfer enhancement when compared to RB convection. An increase in the number of vertical (LSC) roles increases the heat-carrying capacity of the fluid, in laminar and weakly turbulent flows. However at really high Ra, the Nu seems to be less sensitive to changes in LSC. In side-heated cavities, large-scale spiral structures are observed in turbulent thermal convective flows, which lead to the reduction in enstrophy production thus preserving its topology.

5. *Thermal plumes* [41–46]
   In cavities with a vertical temperature gradient, thermal plumes initiate the large-scale motions at high Ra. The mean wind is thus due to the organization of thermal plumes to a large scale circulation. The eruption of thermal plumes is enhanced in cavities with rough surfaces, which in-turn enhances the total heat transfer. The interaction of the LSC with the rough surface results in this behaviour.

From the above discussion, we can see that the geometrical features, the thermal properties of the fluid and the temperature boundary conditions result in different flow behaviours and thus different local/global heat transfer. Flow features like the thickness of thermal boundary layers and thermal plumes play an important role in heat transfer in cavities filled with coarse-grained porous media (discussed later in Section 1.5), where the length scales of the pore-structure are comparable to the flow and thermal scales.

1.3. MIXED CONVECTION IN FLUID-ONLY CAVITIES

Mixed convection flow is observed in many natural situations and engineering applications like dynamics of a lake, crystal growth, thermal hydraulics of nuclear reactors, etc. It is a flow and heat transfer mechanism in which flow velocities due to forced convection and natural convection of comparable magnitude occur. When non-dimensionalized, the convective heat transfer can be characterized by four control parameters, Rayleigh number (Ra), Prandtl number (Pr), Reynolds number (Re) and geometrical aspect ratio (Γ). The ratio between natural and forced convection is quantified by the Richardson number Ri, defined as $Ra/(Pr \times Re^2)$. Mixed convection is observed when $Ri = O(1)$. A value of $Ri \gg 1$ indicates natural convection dominated flow, while a smaller value $Ri \ll 1$ indicates forced convection dominated flow.

Similar to the studies on natural convection, the studies on mixed convective flow and heat transfer in fluid-only cavities investigate the influence of Prandtl number [47–49], large scale flows [49–52], oscillations and turbulent fluctuations [50, 53–55], flow transitions [48, 56, 57], etc. Also, studies on the influence of the relative strength of the

natural convection and forced convection [53, 58–63] are reported in the literature. However, unlike in the cavities with natural convection alone, the studies on the control parameters and the responses are not that extensive for mixed convection.

The heat transfer is observed to strongly depend on Pr, while the flow pattern is only influenced by Pr at high Ri. Cavities with vertical temperature gradient show a great sensitivity as analysed using proper orthogonal decomposition. When $Ri >> 1$, most of the energy is carried by the first mode. A decrease of the energy of the first mode and an increase in the number of energy carrying modes is observed with the onset of a buoyancy-induced secondary flow when $Ri = O(1)$.

In cavities with a horizontal temperature gradient, researchers have also investigated the influence of the relative direction of forced flow *w.r.t* natural convection, mostly by studying mixed convection in cavities with moving walls and temperature differences [64–67]. In assisting mixed convection, in which buoyancy and shear forces assist each other, the flow follows the direction of moving walls. The heat transfer increases with the decrease in Ri and approaches the heat transfer by forced convection alone, at very low Ri.

However, in the case of opposing mixed convection in which the buoyancy and shear forces oppose each other, a shear cell is formed adjacent to the moving boundary, while a buoyancy cell fills the rest of the cavity. The size of the cell depends on Ri. With the increase in the opposing nature of the shear force, the heat transfer rate decreases until a minimum is reached at $Ri = 1$. Further increase in the shear force results in the increase of heat transfer rate due to the formation of a shear dominant regime. For $Ri << 1$, the heat transfer is independent of the direction of the movement of the walls when they move in the opposite direction (forced convection dominant), while For $Ri >> 1$, the heat transfer is fully governed by natural convection.

Thus from above, we could infer that the flow and thermal features are strongly influenced by the strength of forcing, the thermal properties of the fluid, geometric features and on the relative direction of the forced and natural convection.

1.4. FLOW THROUGH POROUS MEDIA

Before we discuss convection in porous media, it is important to understand the concept of Darcy's law [68] which relates the superficial flow velocity ($\mathbf{u_d} = \phi\mathbf{u}$) in porous media to the pressure gradient.

$$\nabla P = -\frac{\mu}{K}\mathbf{u_d} \tag{1.4}$$

where $\phi = 1 - \dfrac{\text{Volume of solid media}}{\text{Total volume of the cavity}}$, P, μ, K, $\mathbf{u}$, $\mathbf{u_d}$ are the porosity, pressure, dynamic viscosity, permeability, average fluid velocity and superficial flow velocity, respectively. However, this linear relation is only valid at low Reynolds numbers, based on pore-scale length and superficial velocity. An increase in $\mathbf{u_d}$ increases the form drag due to the solid obstacles, resulting in the breakdown of the linearity. A modified form of Darcy's equation, the Forchheimer's equation [69],

$$\nabla P = -\frac{\mu}{K}\mathbf{u_d} - C_F K^{-0.5}\rho_f |\mathbf{u_d}|\mathbf{u_d} \tag{1.5}$$

where C_F and ρ_f are form-drag constant and density of the fluid, was developed to account for this effect. The effect of an increase in form drag is modelled with the second term on the right-hand side of the equation. Darcy's equation was also modified into the so-called Brinkman equation [70] to account for the viscous resistance by adding a term proportional to the Laplacian of the average flow velocity [71]. However, these relations do not reduce to the fluid-only Navier-Stokes equations when $\phi = 1$. A generalized form of the flow and heat transfer equations in porous media satisfying the above, was reported in [72, 73].

In this approach, the continuum equations are averaged over a representative elementary volume (REV) occupied by both solid and fluid phases.

$$\nabla \cdot \mathbf{u} = 0 \tag{1.6}$$

$$\frac{\partial \mathbf{u}}{\partial t} + \mathbf{u}\cdot\nabla\mathbf{u} = -\frac{1}{\rho_f}\nabla p + \nu\nabla^2\mathbf{u} + \mathbf{g}\beta(T_p - T_{ref}) + \frac{1}{\rho_f}\mathbf{S} \tag{1.7}$$

$$(\rho c_p)_{eff}\frac{\partial T}{\partial t} + (\rho c_p)_f \phi\mathbf{u}\cdot\nabla\mathbf{T} = (\rho c_p)_f \alpha_{eff}\nabla^2 T \tag{1.8}$$

where,

- $(\rho c_p)_{eff} = \phi(\rho c_p)_f + (1-\phi)(\rho c_p)_s$, with f referring to the fluid and s referring to the solid. ρ is the density andc_p is the specific heat capacity of the fluid and the solid.
- $\alpha_{eff} = \dfrac{\lambda_{eff}}{(\rho C_p)_{eff}}$ with an effective thermal conductivity, $\lambda_{eff} = \phi\lambda_f + (1-\phi)\lambda_s$.

The source term, **S** in Eq.(1.7) is implemented as:

$$\mathbf{S} = -\frac{\mu}{C_0}\phi\mathbf{u} - C_1\frac{1}{2}\rho_f\phi\mathbf{u}\,|\,\phi\mathbf{u}\,| \tag{1.9}$$

For a packed bed cavity, C_0 and C_1 may be calculated using Ergun's equation as:

$$C_0 = \frac{d^2}{150}\frac{\phi^3}{(1-\phi)^2} \tag{1.10}$$

$$C_1 = \frac{3.5}{d}\frac{1-\phi}{\phi^3} \tag{1.11}$$

where d and ϕ are the diameter of the spherical beads and local porosity, respectively.

1.5. NATURAL AND MIXED CONVECTION IN POROUS MEDIA

Natural convective heat transfer in porous media has been extensively studied owing to its occurrence in various industrial and technological applications like greenhouses [74], energy storage [75], solid waste treatment [76], etc. Heat transfer in porous media gets more complex due to the influence of size [77–81], shape [79, 81–83] and thermal properties [78, 79, 81, 84–86] of the porous media. As in fluid-only natural convection, the global heat transfer is observed to follow a power-law correlation with Ra when Ra and Nu are calculated using effective properties of the medium, when convection is not dominant. When the convection is dominant, the heat transfer follows a power-law correlation with both Nu and Ra calculated using fluid properties.

The global heat transfer is observed to be strongly dependent on the morphology of the porous medium. Thus the heat transfer obtained using numerical simulations with the REV approach [79, 85, 87–90] with uniform porosity, deviate from that obtained with experiments. Similar to the studies on natural convection in porous media filled cavities, numerical studies on mixed convective heat transfer in porous media are also based on Darcy/Darcy-Forchheimer [91–93] and REV approach [94–100] assuming a uniform porosity. Thus the flow and thermal features observed closely resemble that in fluid-only mixed convective flows. Mixed convective heat transfer has also been experimentally investigated [101–104]. Experimental results on heat transfer are reported to deviate from simulations applying the Darcy model. Even at $Ri > 10$, the influence of mixed convection is observed in the flow through the porous media. In cavities with a horizontal temperature gradient, studies on the influence of assisting and opposing forced convective contribution of varying strength (different Ri) are also reported in the literature [103–107]. Similar to that reported in fluid-only cavities the heat transfer increases with Ra and Re in assisting mixed convection, whereas for the opposing mixed convection it decreases with Re and reaches a minimum and then again starts to increase. It is also observed that the pore-scale velocity [104] is dependent on the pore-density and has important effects on the buoyancy induced secondary flows.

1.6. RESEARCH OBJECTIVE

From the above studies on natural and mixed convective flow and heat transfer in porous media filled enclosures it was found that the intrinsic geometric features of the porous medium can lead to unreliable results with REV approach, when the pore-scale is comparable to flow and thermal length scales. The interaction between the porous media and the flow and thermal structures is expected to be different in cavities with a vertical and horizontal temperature gradient, due to the difference in the flow features, *viz.*

- formation of thermal plumes in enclosures with vertical temperature gradient,
- formation of thermal boundary layers at the vertical walls in enclosures with horizontal temperature gradient.

The interaction between the porous media and thermal boundary flow structures is also expected to vary significantly in mixed convective flows with assisting and opposing forced convective contributions. These interactions can influence the local flow and temperature distribution close to walls, for instance, of the blast furnace hearth and play a significant role in the formation of hot-spots at the walls. An understanding of the above is only possible by analyzing the flow and thermal features at the scale of the pore-spaces in the porous media. To provide an insight into this, we carry out pore-structure resolved numerical simulations of bottom-heated top-cooled natural convection, side-heated side-cooled natural convection and lid-driven assisting/opposing mixed convection with horizontal temperature gradient. We carry out our numerical simulations in a simplified geometry *viz.* a cubical cavity filled with spherical beads arranged in a structured packing and we address:

1. **What is the influence of coarse-grained porous media on local and global heat transfer in a natural convective flow environment?**
   An understanding of the regions with high local heat transfer can help us in identifying the hot-spots in the hearth of the furnace. To address this issue the local flow and temperature distribution in cavities

   - fully and partially filled with spherical beads
   - with different location of spherical beads *w.r.t* the isothermal walls
   - filled with spherical beads of different thermal properties *w.r.t* the working fluid

   are investigated at different Rayleigh numbers. In side-heated side-cooled cavities, we study the influence of local wall temperature distribution *w.r.t* the location of the spherical beads on the local and global heat transfer. The simulations are also compared with fluid-only simulations and porous media simulations.

2. **What is the influence of coarse-grained porous media on local and global heat transfer in a mixed convective flow environment?**
   In side-heated side-cooled cavities filled with spherical beads, we investigate the influence of assisting and opposing forced convection of different strengths on the local flow and temperature distribution. We also investigate the interaction of the

thermal boundary layers with the spherical beads and compare it with REV simulations to better understand local and global heat transfer in a mixed convective flow environment.

We validate our results by comparing them with experiments conducted by another Ph.D. student in the group, Iman Ataei Dadavi [108–110]. Thus, we provide an experimentally validated numerical model to our industrial partner, TATA steel. Our work will help them to improve the understanding of the various factors influencing the heat transfer in the hearth of the blast furnace. Based on our preliminary investigation, we also suggest further numerical and experimental studies with double-scalar convection to identify the locations with serious dissolution of the carbon lining in the hearth of a blast furnace, to better understand the hot-spot formations in the hearth.

1.7. OUTLINE

We numerically investigate the flow and heat transfer due to natural convection and mixed convection in cubical enclosures fully (partially) filled with coarse-grained porous media. The study on natural convective heat transfer is carried out with two arrangements, bottom heated and side heated arrangements. To analyze mixed convective heat transfer we consider a side-heated cavity with moving walls. The numerical schemes, the solvers and the geometries considered are described in each chapter.

The chapters in this thesis are self-contained and have been published in /submitted to scientific journals. In Chapter 2 and 3 we study bottom-heated top-cooled arrangements with uniform wall temperature. In Chapter 2 we discuss heat transfer in a bottom-heated cavity filled with adiabatic beads, with different heights and locations of the packing. We compare the pore-scale flow and thermal features with the REV approach based results. In Chapter 3 we extend our investigation to the influence of thermal properties of the porous media on the heat transfer. As in most real-life scenarios the temperatures are non-uniform, in Chapter 4 we study a side-heated cavity both with uniform- and non-uniform wall temperatures. We compare the flow behaviour and the associated heat transfer to that in a fluid-only cavity to explain the role of pore-space on the heat transfer mechanism. The heat transfer in a porous-media filled side-heated cavity is further analysed with the combined effect of natural and forced convection in Chapter 5. Here we discuss the influence of the strength and direction of the mixed convective flow on the heat transfer, local flow and temperature distribution in porous media-filled cavities. In Chapter 6 we summarize our findings and discuss the possible application of our findings in research at R&D TATA steel, IJmuiden and provide an outlook to future research possibilities in this field.

REFERENCES

[1] W. Commons, *File:blast furnaces temperatures.svg — wikimedia commons, the free media repository,* https://commons.wikimedia.org/w/index.php?title=File:Blast_furnaces_temperatures.svg&oldid=218478723 (2016).

[2] A. Babich and D. Senk, *Recent developments in blast furnace iron-making technology,* in *Iron Ore* (Elsevier, 2015) pp. 505–547.

[3] L. Nelson and R. Hundermark, *The tap-hole - key to furnace performance,* Journal of the Southern African Institute of Mining and Metallurgy **116** (2016), 10.17159/2411-9717/2016/v116n5a12.

[4] W. J. Morgan, *Convection plumes in the lower mantle,* Nature **230**, 42 (1971).

[5] D. P. Mckenzie, J. M. Roberts, and N. O. Weiss, *Convection in the earth's mantle: towards a numerical simulation,* Journal of Fluid Mechanics **62**, 465 (1974).

[6] D. L. Hartmann, L. A. Moy, and Q. Fu, *Tropical convection and the energy balance at the top of the atmosphere,* Journal of Climate **14**, 4495 (2001).

[7] J. Marshall and F. Schott, *Open-ocean convection: Observations, theory, and models,* Reviews of Geophysics **37**, 1 (1999).

[8] A. Bar-Cohen and W. M. Rohsenow, *Thermally optimum spacing of vertical, natural convection cooled, parallel plates,* Journal of Heat Transfer **106**, 116 (1984).

[9] S. Banerjee, A. Mukhopadhyay, S. Sen, and R. Ganguly, *Natural convection in a bi-heater configuration of passive electronic cooling,* International Journal of Thermal Sciences **47**, 1516 (2008).

[10] E. Krepper, E.-F. Hicken, and H. Jaegers, *Investigation of natural convection in large pools,* International Journal of Heat and Fluid Flow **23**, 359 (2002).

[11] H. Awbi and A. Hatton, *Natural convection from heated room surfaces,* Energy and Buildings **30**, 233 (1999).

[12] H. Liu and H. B. Awbi, *Performance of phase change material boards under natural convection,* Building and Environment **44**, 1788 (2009).

[13] D. J. Tritton, *Physics of Fluid Dynamics*, 1^{st} ed. (Oxford University Press, New York, 1977) pp. 180–220.

[14] T. Versteegh and F. Nieuwstadt, *A direct numerical simulation of natural convection between two infinite vertical differentially heated walls scaling laws and wall functions,* International Journal of Heat and Mass Transfer **42**, 3673 (1999).

[15] J. L. Lage and A. Bejan, *The Ra-Pr domain of laminar natural convection in an enclosure heated from the side,* Numerical Heat Transfer, Part A: Applications **19**, 21 (1991).

[16] S. Grossmann and D. Lohse, *Scaling in thermal convection: a unifying theory,* Journal of Fluid Mechanics **407**, 27 (2000).

[17] S. Grossmann and D. Lohse, *Fluctuations in turbulent Rayleigh–Bénard convection: The role of plumes,* Physics of Fluids **16**, 4462 (2004).

[18] D. Lohse and F. Toschi, *Ultimate state of thermal convection,* Physical Review Letters **90**, 034502 (2003).

[19] E. Siggia, *High Rayleigh number convection,* Annual Review of Fluid Mechanics **26**, 137 (1994).

[20] C. Sun, L.-Y. Ren, H. Song, and K.-Q. Xia, *Heat transport by turbulent Rayleigh–Bénard convection in 1 m diameter cylindrical cells of widely varying aspect ratio,* Journal of Fluid Mechanics **542**, 165 (2005).

[21] C. Sun, H. D. Xi, and K. Q. Xia, *Azimuthal symmetry, flow dynamics, and heat transport in turbulent thermal convection in a cylinder with an aspect ratio of 0.5,* Physical Review Letters (2005), 10.1103/PhysRevLett.95.074502.

[22] C. Sun, K. Q. Xia, and P. Tong, *Three-dimensional flow structures and dynamics of turbulent thermal convection in a cylindrical cell,* Physical Review E - Statistical, Nonlinear, and Soft Matter Physics (2005), 10.1103/PhysRevE.72.026302.

[23] K. L. Chong, S. Wagner, M. Kaczorowski, O. Shishkina, and K.-Q. Xia, *Effect of Prandtl number on heat transport enhancement in Rayleigh-Bénard convection under geometrical confinement,* Physical Review Fluids **3** (2018), 10.1103/physrevfluids.3.013501.

[24] F. Trias, A. Gorobets, M. Soria, and A. Oliva, *Direct numerical simulation of a differentially heated cavity of aspect ratio 4 with Rayleigh numbers up to* 10^{11}*–part II: Heat transfer and flow dynamics,* International Journal of Heat and Mass Transfer **53**, 674 (2010).

[25] C. S. Ng, A. Ooi, D. Lohse, and D. Chung, *Vertical natural convection: application of the unifying theory of thermal convection,* Journal of Fluid Mechanics **764**, 349 (2015).

[26] S. S. Hsieh and C. Y. Wang, *Experimental study of three-dimensional natural convection in enclosures with different working fluids,* International Journal of Heat and Mass Transfer **37**, 2687 (1994).

[27] R. A. W. M. Henkes and P. Le Quéré, *Three-dimensional transition of natural-convection flows,* Journal of Fluid Mechanics **319**, 281 (1996).

[28] R. Verzicco and R. Camussi, *Numerical experiments on strongly turbulent thermal convection in a slender cylindrical cell,* Journal of Fluid Mechanics **477** (2003), 10.1017/S0022112002003063.

[29] J. Bailon-Cuba, M. S. Emran, and J. Schumacher, *Aspect ratio dependence of heat transfer and large-scale flow in turbulent convection,* Journal of Fluid Mechanics **655**, 152 (2010).

[30] F. Trias, A. Gorobets, M. Soria, and A. Oliva, *Direct numerical simulation of a differentially heated cavity of aspect ratio 4 with Rayleigh numbers up to* 10^{11}*–part I: Numerical methods and time-averaged flow,* International Journal of Heat and Mass Transfer **53**, 665 (2010).

[31] J. D. Scheel and J. Schumacher, *Local boundary layer scales in turbulent Rayleigh–Bénard convection,* Journal of Fluid Mechanics , 344 (2014), arXiv:1409.3385 .

[32] G. Ahlers, E. Brown, and A. Nikolaenko, *The search for slow transients, and the effect of imperfect vertical alignment, in turbulent Rayleigh–Bénard convection,* Journal of Fluid Mechanics **557**, 347 (2006).

[33] G. Ahlers and X. Xu, *Prandtl-number dependence of heat transport in turbulent Rayleigh-B'enard convection,* Phys. Rev. Lett. **86**, 3320 (2001).

[34] T. Rayleigh, J. J. Niemela, and K. R. Sreenivasan, *Turbulent convection at high Rayleigh numbers and aspect ratio 4,* Journal of Fluid Mechanics **557**, 411 (2006).

[35] H.-D. Xi, Q. Zhou, and K.-Q. Xia, *Azimuthal motion of the mean wind in turbulent thermal convection,* Phys. Rev. E **73**, 056312 (2006).

[36] S. Xin and P. L. Quéré, *An extended chebyshev pseudo-spectral benchmark for the 8:1 differentially heated cavity,* International Journal for Numerical Methods in Fluids **40**, 981 (2002).

[37] M. Wang, S. Fu, and G. Zhang, *Large-scale spiral structures in turbulent thermal convection between two vertical plates,* Physical Review E - Statistical, Nonlinear, and Soft Matter Physics **66**, 1 (2002).

[38] Q. Zhou, C. Sun, and K.-Q. Xia, *Morphological evolution of thermal plumes in turbulent Rayleigh-Bénard convection.* Physical Review Letters **98**, 074501 (2007).

[39] L. Zwirner and O. Shishkina, *Confined inclined thermal convection in low-prandtl-number fluids,* Journal of Fluid Mechanics **850**, 984 (2018).

[40] S. Kenjereš, *Heat transfer enhancement induced by wall inclination in turbulent thermal convection,* Phys. Rev. E **92**, 053006 (2015).

[41] Y. Du and P. Tong, *Turbulent thermal convection in a cell with ordered rough boundaries,* Journal of Fluid Mechanics **407**, 57 (2000).

[42] O. Shishkina and C. Wagner, *Analysis of thermal dissipation rates in turbulent Rayleigh–Bénard convection,* Journal of Fluid Mechanics **546**, 51 (2005).

[43] O. Shishkina and C. Wagner, *Analysis of sheet-like thermal plumes in turbulent Rayleigh–Bénard convection,* Journal of Fluid Mechanics **599**, 383 (2008).

[44] S. Kenjereš and K. Hanjalić, *Transient analysis of Rayleigh–Bénard convection with a RANS model,* International Journal of Heat and Fluid Flow **20**, 329 (1999).

[45] S. Kenjereš and K. Hanjalić, *Numerical insight into flow structure in ultraturbulent thermal convection,* Physical Review E - Statistical, Nonlinear, and Soft Matter Physics (2002), 10.1103/PhysRevE.66.036307.

[46] S. Kenjereš and K. Hanjalić, *LES, T-RANS and hybrid simulations of thermal convection at high Ra numbers,* International Journal of Heat and Fluid Flow **27**, 800 (2006).

[47] M. K. Moallemi and K. S. Jang, *Prandtl number effects on laminar mixed convection heat transfer in a lid-driven cavity,* International Journal of Heat and Mass Transfer **35**, 1881 (1992).

[48] T. S. Cheng, *Characteristics of mixed convection heat transfer in a lid-driven square cavity with various Richardson and Prandtl numbers,* International Journal of Thermal Sciences **50**, 197 (2011).

[49] P. P. Shevkar, G. S. Gunasegarane, S. K. Mohanan, and B. A. Puthenveettil, *Effect of shear on coherent structures in turbulent convection,* Physical Review Fluids **4** (2019), 10.1103/physrevfluids.4.043502.

[50] D. Schmeling, A. Westhoff, M. Khün, J. Bosbach, and C. Wagner, *Large-scale flow structures and heat transport of turbulent forced and mixed convection in a closed rectangular cavity,* International Journal of Heat and Fluid Flow (2011), 10.1016/j.ijheatfluidflow.2011.06.006.

[51] D. Schmeling, J. Bosbach, and C. Wagner, *Oscillations of the large-scale circulation in turbulent mixed convection in a closed rectangular cavity,* Experiments in Fluids **54** (2013), 10.1007/s00348-013-1517-3.

[52] D. Schmeling, J. Bosbach, and C. Wagner, *Simultaneous measurement of temperature and velocity fields in convective air flows,* Meas. Sci. Technol. Measurement Science and Technology Meas. Sci. Technol **25**, 35302 (2014).

[53] A. Westhoff, J. Bosbach, D. Schmeling, and C. Wagner, *Experimental study of low-frequency oscillations and large-scale circulations in turbulent mixed convection,* International Journal of Heat and Fluid Flow **31**, 794 (2010).

[54] D. Schmeling, A. Westhoff, J. Bosbach, and C. Wagner, *Flow Structure Formation of Turbulent Mixed Convection in a Closed Rectangular Cavity,* Notes on Numerical Fluid Mechanics and Multidisciplinary Design (NNFM) **112**, 571 (2010).

[55] D. Schmeling, J. Bosbach, and C. Wagner, *Temperature oscillations in turbulent mixed convective air flows,* in *Turbulence and Interactions* (Springer, 2014) pp. 157–163.

[56] A. K. Prasad and J. R. Koseff, *Combined forced and natural convection heat transfer in a deep lid-driven cavity flow,* International Journal of Heat and Fluid Flow (1996), 10.1016/0142-727X(96)00054-9.

[57] N. O. Moraga and S. E. López, *Numerical simulation of Three DImensional mixed convection in an air cooled cavity,* Numerical Heat Transfer, Part A: Applications **45**, 811 (2004).

[58] S. Mergui, *Caracte´risation expe´rimentale des e´coulements d'air de convection naturelle et mixte dans une cavite´ ferme´ e, the'se de l'Universite´ de Poitiers, France (In French),* (1993).

[59] H. Van Santen, C. R. Kleijn, and H. E. A. Van Den Akker, *Mixed convection in radial flow between horizontal plates — I. Numerical simulations,* International Journal of Heat and Mass Transfer **43**, 1523 (2000).

[60] H. V. Santen, C. R. Kleijn, and H. E. V. D. Akker, *Mixed convection in radial flow between horizontal plates—II. experiments,* International Journal of Heat and Mass Transfer **43**, 1537 (2000).

[61] H. van Santen, C. R. Kleijn, and H. E. van den Akker, *On multiple stability of mixed-convection flows in a chemical vapor deposition reactor,* International Journal of Heat and Mass Transfer **44**, 659 (2001).

[62] Z. Zhang, W. Zhang, Z. J. Zhai, and Q. Y. Chen, *Evaluation of Various Turbulence Models in Predicting Airflow and Turbulence in Enclosed Environments by CFD: Part 2—Comparison with Experimental Data from Literature,* HVAC&R Research **13**, 871 (2007).

[63] R. Ezzouhri, P. Joubert, F. Penot, and S. Mergui, *Large Eddy simulation of turbulent mixed convection in a 3D ventilated cavity: Comparison with existing data,* International Journal of Thermal Sciences **48**, 2017 (2009).

[64] O. Aydm, *Aiding and opposing mechanisms of mixed convection in a shear- and buoyancy-driven cavity,* International Communications in Heat and Mass Transfer **26**, 1019 (1999).

[65] A. Raji and M. Hasnaoui, *Mixed convection heat transfer in ventilated cavities with opposing and assisting flows,* Engineering Computations , 556 (2000).

[66] S. Singh and M. A. R. Sharif, *Mixed Convective Cooling of a Rectangular Cavity With Inlet and Exit Openings on Differentially Heated Side Walls,* Numerical Heat Transfer, Part A: Applications **44**, 233 (2003).

[67] H. F. Oztop and I. Dagtekin, *Mixed convection in two-sided lid-driven differentially heated square cavity,* International Journal of Heat and Mass Transfer **47**, 1761 (2004).

[68] H. P. G. Darcy, *The public fountains of the city of Dijon. Exposure and application of principles 'a to follow and formulas à to use in questions of water distribution, etc* (1856).

[69] P. Forchheimer, *Water movement through soil: Journal of the Association of German Engineers, v. 45,* (1901).

[70] H. C.Brinkman, *On the permeability of media consisting of closely packed porous particles,* Flow, Turbulence and Combustion **1** (1949), 10.1007/bf02120318.

[71] D. A. Nield, A. Bejan, *et al.*, *Convection in porous media*, Vol. 3 (Springer, 2006).

[72] K. Vafai, *Convective flow and heat transfer in variable-porosity media,* Journal of Fluid Mechanics **147**, 233 (1984).

[73] P. Nithiarasu, K. N. Seetharamu, and T. Sundararajan, *Natural convective heat transfer in a fluid saturated variable porosity medium,* International Journal of Heat and Mass Transfer **40**, 3955 (1997).

[74] S. Reichrath and T. W. Davies, *Using CFD to model the internal climate of greenhouses: past, present and future,* Agronomie **22**, 3 (2002).

[75] H. Nazir, M. Batool, F. J. Bolivar Osorio, M. Isaza-Ruiz, X. Xu, K. Vignarooban, P. Phelan, Inamuddin, and A. M. Kannan, *Recent developments in phase change materials for energy storage applications: A review,* International Journal of Heat and Mass Transfer **129**, 491 (2019).

[76] J. Zhang, X. Kan, Y. Shen, K.-C. Loh, C.-H. Wang, Y. Dai, and Y. W. Tong, *A hybrid biological and thermal waste-to-energy system with heat energy recovery and utilization for solid organic waste treatment,* Energy **152**, 214 (2018).

[77] J. W. Elder, *Steady free convection in a porous medium heated from below,* Journal of Fluid Mechanics **27**, 29 (1967).

[78] N. Seki, S. Fukusako, and H. Inaba, *Heat transfer in a confined rectangular cavity packed with porous media,* International Journal of Heat and Mass Transfer **21**, 985 (1978).

[79] N. Kladias and V. Prasad, *Experimental verification of darcy-brinkman-forchheimer flow model for natural convection in porous media,* Journal of Thermophysics and Heat Transfer **5**, 560 (1991).

[80] H. Sakamoto and F. A. Kulacki, *Buoyancy Driven Flow in Saturated Porous Media,* Journal of Heat Transfer **129**, 727 (2007).

[81] D. J. Keene, *Thermal Convection in Porous Media at High Rayleigh Numbers,* Journal of Heat Transfer **137**, 1 (2015).

[82] A. Zenklusen, S. Kenjereš, and P. R. von Rohr, *Vortex shedding in a highly porous structure,* Chemical Engineering Science **106**, 253 (2014).

[83] S. Das, N. Deen, and J. Kuipers, *Multiscale modeling of fixed-bed reactors with porous (open-cell foam) non-spherical particles: Hydrodynamics,* Chemical Engineering Journal **334**, 741 (2018).

[84] M. S. Phanikumar and R. L. Mahajan, *Non-Darcy natural convection in high porosity metal foams,* International Journal of Heat and Mass Transfer **45**, 3781 (2002).

[85] C. Y. Zhao, T. J. Lu, and H. P. Hodson, *Natural convection in metal foams with open cells,* International Journal of Heat and Mass Transfer **48**, 2452 (2005).

[86] V. Kathare, J. H. Davidson, and F. A. Kulacki, *Natural convection in water-saturated metal foam,* International Journal of Heat and Mass Transfer **51**, 3794 (2008).

[87] N. Kladias and V. Prasad, *Natural Convection in Horizontal Porous Layers: Effects of Darcy and Prandtl Numbers,* Journal of Heat Transfer **111**, 926 (1989).

[88] G. Lauriat and V. Prasad, *Non-Darcian effects on natural convection in a vertical porous enclosure,* International Journal of Heat and Mass Transfer **32**, 2135 (1989).

[89] A. Merrikh and J. Lage, *From continuum to porous–continuum: The visual resolution impact on modeling natural convection in heterogeneous media,* in *Transport Phenomena in Porous Media III* (Elsevier, 2005) pp. 60–96.

[90] A. A. Merrikh and J. L. Lage, *Natural convection in an enclosure with disconnected and conducting solid blocks,* International Journal of Heat and Mass Transfer **48**, 1361 (2005).

[91] M. Haajizadeh and C. Tien, *Combined natural and forced convection in a horizontal porous channel,* International Journal of Heat and Mass Transfer **27**, 799 (1984).

[92] R. M. Islam and K. Nandakumar, *Mixed convection heat transfer in porous media in the non-darcy regime,* The Canadian Journal of Chemical Engineering **66**, 68 (1988).

[93] S. Mahmud and I. Pop, *Mixed convection in a square vented enclosure filled with a porous medium,* International Journal of Heat and Mass Transfer **49**, 2190 (2006).

[94] A. M. Al-Amiri, *Analysis of momentum and energy transfer in a lid-driven cavity filled with a porous medium,* International Journal of Heat and Mass Transfer **43**, 3513 (2000).

[95] K. Khanafer and K. Vafai, *Double-diffusive mixed convection in a lid-driven enclosure filled with a fluid-saturated porous medium,* Numerical Heat Transfer, Part A: Applications **42**, 465 (2002).

[96] H. F. Oztop, *Combined convection heat transfer in a porous lid-driven enclosure due to heater with finite length,* International Communications in Heat and Mass Transfer **33**, 772 (2006).

[97] E. Vishnuvardhanarao and M. K. Das, *Laminar mixed convection in a parallel two-sided lid-driven differentially heated square cavity filled with a fluid-saturated porous medium,* Numerical Heat Transfer, Part A: Applications **53**, 88 (2007).

[98] J. P. Kumar, J. C. Umavathi, I. Pop, and B. M. Biradar, *Fully developed mixed convection flow in a vertical channel containing porous and fluid layer with isothermal or isoflux boundaries,* Transport in Porous Media **80**, 117 (2009).

[99] A. Chattopadhyay, S. K. Pandit, S. S. Sarma, and I. Pop, *Mixed convection in a double lid-driven sinusoidally heated porous cavity,* International Journal of Heat and Mass Transfer **93**, 361 (2016).

[100] N. Biswas and N. K. Manna, *Enhanced convective heat transfer in lid-driven porous cavity with aspiration,* International Journal of Heat and Mass Transfer **114**, 430 (2017).

[101] M. A. Combarnous and P. Bia, *Combined Free and Forced Convection in Porous Media,* Society of Petroleum Engineers Journal **11**, 399 (1971).

[102] K. J. Renken and D. Poulikakos, *Mixed convection experiments about a horizontal isothermal surface embedded in a water-saturated packed bed of spheres,* International Journal of Heat and Mass Transfer **33**, 1370 (1990).

[103] W. L. Pu, P. Cheng, and T. S. Zhao, *Mixed-convection heat transfer in vertical packed channels,* Journal of Thermophysics and Heat Transfer **13**, 517 (1999).

[104] I. Kurtbas and N. Celik, *Experimental investigation of forced and mixed convection heat transfer in a foam-filled horizontal rectangular channel,* International Journal of Heat and Mass Transfer **52**, 1313 (2009).

[105] A. Guardo, M. Coussirat, F. Recasens, M. Larrayoz, and X. Escaler, *CFD study on particle-to-fluid heat transfer in fixed bed reactors: Convective heat transfer at low and high pressure,* Chemical Engineering Science **61**, 4341 (2006).

[106] N. Guerroudj and H. Kahalerras, *Mixed convection in a channel provided with heated porous blocks of various shapes,* Energy Conversion and Management **51**, 505 (2010).

[107] P. C. Huang and C. C. Chen, *Simulation of mixed convection in a vertical channel containing discrete porous-covering heat blocks,* International Journal of Heat and Mass Transfer **55**, 3147 (2012).

[108] I. Ataei-Dadavi, M. Chakkingal, S. Kenjereš, C. R. Kleijn, and M. J. Tummers, *Flow and heat transfer measurements in natural convection in coarse-grained porous media,* International Journal of Heat and Mass Transfer **130**, 575 (2019).

[109] I. Ataei-Dadavi, N. Rounaghi, M. Chakkingal, S. Kenjereš, C. R. Kleijn, and M. J. Tummers, *An experimental study of flow and heat transfer in a differentially side heated cavity filled with coarse porous media,* International Journal of Heat and Mass Transfer **143**, 118591 (2019).

[110] I. Ataei-Dadavi, M. Chakkingal, S. Kenjeres, C. R. Kleijn, and M. J. Tummers, *Experiments on mixed convection in a vented differentially side-heated cavity filled with a coarse porous medium,* International Journal of Heat and Mass Transfer **149**, 119238 (2020).

2

EFFECT OF PACKING HEIGHT AND LOCATION OF POROUS MEDIA ON HEAT TRANSFER IN A CUBICAL CAVITY: ARE EXTENDED DARCY SIMULATIONS SUFFICIENT?

We numerically investigate natural convection in a bottom-heated top-cooled cavity, fully and partially filled with adiabatic spheres (with diameter-to-cavity-size ratio $d/L = 0.2$) arranged in a Simple Cubic Packing (SCP) configuration. We study the influence of packing height and location of porous media. We carry out the simulations using water as the working fluid with Prandtl number, $Pr = 5.4$ at Rayleigh number $Ra = 1.16 \times 10^5$, 1.16×10^6 and 2.31×10^7. The applicability and suitability of Darcy-Forchheimer assumption to predict the global heat transfer is analysed by comparing it with the pore-structure resolved simulations. We found that the heat transfer in pore-structure resolved simulations is comparable to that in fluid-only cavities at high Rayleigh numbers, irrespective of the number of layers of packing and its location. Discrepancies in heat transfer between the Darcy-Forchheimer and the fully resolved simulations are observed when the porous medium is close to the isothermal wall and at high Ra, while it vanishes when the porous medium is away from the isothermal bottom wall [1].

[1] This Chapter is published in IJHFF with DOI: https://doi.org/10.1016/j.ijheatfluidflow.2020.108617

NOMENCLATURE

Greek Symbols

α Thermal diffusivity,$(\lambda/\rho c_p)$, m^2/s

β Thermal expansion coefficient, K^{-1}

λ Thermal conductivity, W/m.K

λ_{eff} Effective thermal conductivity, W/m.K

ν Kinematic viscosity of fluid, m^2/s

ϕ Porosity

ρ Density, kg/m^3

Other symbols and Abbreviations

$\mathbf{u}^*$ non-dimensional pore-scale velocity, $\dfrac{\mathbf{u}}{U_0}$

$\mathbf{u}$ Pore-scale velocity, m/s

δ_{th} Thermal boundary layer thickness,$\dfrac{L}{2Nu}$, m

$\mathbf{g}$ accel. due to gravity (acts along Z axis), m/s^2

θ Non-dimensional temperature, $\dfrac{T-T_c}{T_h-T_c}$

θ_m Time- and plane- averaged temperature

c_p Specific heat capacity, J/kg.K

d Diameter of sphere, m

d_p Diameter of pore-space, m

Da Darcy number, K/L^2

K Permeability

L Height of cavity, m

Nu Nusselt number based on fluid properties

p Pressure, N/m^2

Pr Prandtl Number

Ra Rayleigh Number based on fluid properties, $\dfrac{g\beta_f \Delta T L^3}{\nu\alpha}$

T Temperature, K

T_{ref} Reference temperature, $\dfrac{T_h+T_c}{2}$, K

V_T^{porous} Total volume of porous layer, m^3

V_T^{spheres} Volume occupied by spheres, m^3

t_0 characteristic time scale, $\frac{L}{U_0}$, s

U_0 characteristic velocity scale, $\frac{Ra^{3/7}\alpha}{L}$, m/s

X, Y, Z represents the rectangular coordinate system

D-F Darcy-Forchheimer simulation with continuum approach

P-R Pore-structure Resolved simulation

Subscripts

eff Effective

f Fluid

s Solid

2.1. INTRODUCTION

Natural convective heat transfer in porous media packed cavities is of great importance in various engineering and real-life applications. It is an important mechanism in refrigeration devices [1, 2], distribution transformers [3], nuclear waste disposal [4], air dehumidifiers [5], catalytic reactors [6, 7], blast furnace [8] etc. It can also be of crucial importance in heat exchangers [9, 10] under safety mode operation, when the forced flow is blocked. In most of the applications mentioned above the domain may be partially filled [11] with materials and the relative position of these materials may vary (like food kept at the bottom or top of a refrigerator), which demands an in-depth understanding of the heat transfer mechanism in a partially filled porous media and its relative position.

Several experimental and numerical studies on natural convection in porous media are available in literature [12]. Most of the studies are on the influence of Rayleigh number [13], Prandtl number [14, 15], conductivity [16, 17] and size of porous media [18–20]. Studies also report that the heat transfer in fully packed porous media filled cavities asymptotically approach the heat transfer in a fluid-only cavity at high Rayleigh numbers [19, 21]. All these studies concentrate on the effect of the above mentioned parameters on fully packed cavities. However, the studies on the effect of location of the porous medium and its height are limited. Studies on partially filled porous media made of metal foam report a positive influence of porous media on heat transfer enhancement [22]. The enhancement reported is mostly due to the increased conductivity of the medium. Experimental studies also report a non-monotonic change in heat transfer with packing height [23, 24]. Visualization from the top of the cavity hints at the channeling effect to be the reason for the non-monotonic heat transfer variation.

A variety of different cases and conditions were tested using Darcy assumption and other more refined Darcy models [12], with most of them being 2D simulations. Semi-analytical solution for 2-dimensional [25, 26] and 3-dimensional [27] porous media are available for conditions at which Darcy assumption is valid. 3-dimensional numerical simulation of layered porous structure with Darcy assumption [28] discusses the influence of the thermal properties of the layer in heat transfer. However, at comparatively higher flow velocities, this linear relation is valid only at lower Reynolds number [12]. Extensive studies on porous-continuum representative volume (REV) based approach [20, 29] valid at higher flow velocities, with Darcy [30, 31] and Darcy-Forchheimer [32] terms included are reported in literature. Heat transfer in partially filled cavities, obtained using REV approach with Darcy and extended Darcy assumptions show good agreement with experiments at low Ra [33, 34]. The simulations, however, deviate up to 15% from the experimental heat transfer measurements, when the Ra and Da are high, and also with the change in the location and height of the packing [35].

From our literature review, we find that the literature on the effect of pore-scale phenomena on heat transfer is mostly limited to fully packed cavities [36, 37] and almost no literature is available on the effect of location and height of packing [2]. From our previous numerical [37–39] and experimental [17, 21, 40] studies on fully-packed porous media, we find a strong influence of pore-scale features on global and local heat transfer. Consequently, detailed pore-structure resolved simulations can give us a better understanding of the effect of height and location of the packing on heat transfer as well as the reason for deviation of REV approach based simulations from experiments. In our

present work, we carry out 3D numerical simulations resolving the pore-structure and compare them to the Darcy-Forchheimer (D-F) simulations. We investigate the validity and applicability of the D-F assumption in partially filled cavities of different packing heights and locations, by comparing it with the pore-structure resolved simulations. We aim at providing an insight into the influence of local flow and thermal structures on the heat transfer in these cavities and explain the discrepancy in heat transfer between the pore-structure resolved and D-F simulations.

2.2. MATHEMATICAL FORMULATIONS AND NUMERICAL METHODS

2.2.1. GEOMETRY AND BOUNDARY CONDITIONS

We study natural convection in a cubical $L \times L \times L$ cavity filled with adiabatic spheres of diameter, $d = 0.2L$ at $Ra = 1.16 \times 10^5, 1.16 \times 10^6$ and 2.3×10^7. We use water ($Pr = 5.4$) as the working fluid. The gravity, **g** acts along the negative Z-axis of the Cartesian coordinate system. From our previous experimental study on natural convection in fully-packed cavity [21], we find that spherical beads of the dimensions mentioned above result in its influence on heat transfer at low Ra, while the effect reduces with an increase in Ra. The bottom and top walls of the cubical cavity are maintained at uniform temperatures T_h and T_c ($T_h > T_c$) respectively. All the other vertical walls are adiabatic. Effects of packing height and packing location are investigated carrying out fully resolved numerical simulations and comparing with Darcy-Forchheimer simulations.

- **Packing height:** The domain is stacked with different number of horizontal layers (Fig.2.1 and Table 2.1) of sphere-packing from the bottom wall to the top, arranged in a Simple Cubic Packing (SCP) fashion
- **Packing location:** The domain is stacked with single layer (and 2 layers) of spheres at different positions with respect to the bottom wall (Table 2.1) in an SCP fashion

No-slip boundary condition is applied at all the walls for both fully resolved and D-F simulations, and also at the spherical surfaces in the fully resolved packed bed simulations. We ensure that $\beta \Delta T << 1$ in all our simulations such that the Boussinesq approximation [41] is valid.

2.2.2. GOVERNING EQUATIONS AND NUMERICAL METHOD

The governing equations used for the simulations are split into two:

- Fully resolved simulations of fluid-only (Rayleigh-Bénard convection) and packed bed cavities using open-source finite volume CFD solver Foam Extend 4.0 [42]
- Darcy-Forchheimer (D-F) simulations using commercial software, ANSYS Fluent (v17.2)

For the fully resolved simulations using the Boussinesq approximation, we numerically solve the transient Navier-Stokes and thermal energy transport equations for Newtonian fluids:

Table 2.1: Packing name referred in the current work and the corresponding packing scheme.

Packing name	Packing Scheme	Packing name	Packing Scheme
1 Layer		5 Layer	
2 Layer		1L Middle	
3 Layer		1L Quarter	
4 Layer		2L Quarter	

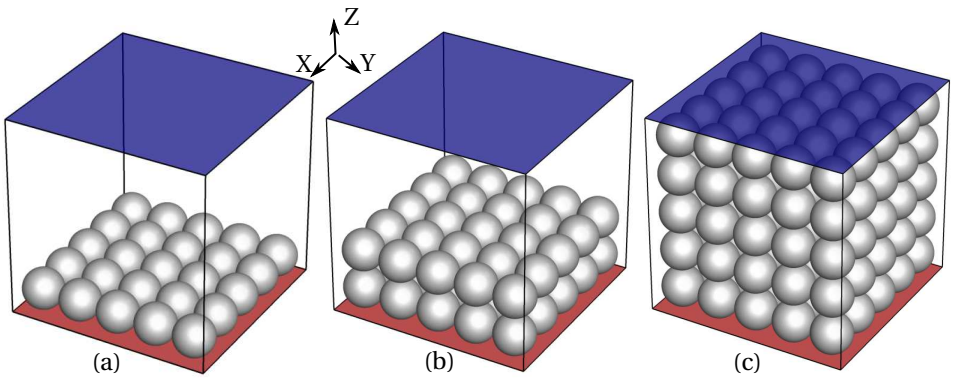

Figure 2.1: Geometrical representation of fluid-filled cubical cavity heated from the bottom (red) and cooled from the top (blue) packed with (a) 1 layer (b) 2 layers (c) 5 layers of adiabatic spherical beads.

$$\nabla \cdot \mathbf{u} = 0 \tag{2.1}$$

$$\frac{\partial \mathbf{u}}{\partial t} + \mathbf{u} \cdot \nabla \mathbf{u} = -\frac{1}{\rho}\nabla p + \nu \nabla^2 \mathbf{u} + \mathbf{g}\beta(T - T_{ref}) \tag{2.2}$$

$$\frac{\partial T}{\partial t} + \mathbf{u} \cdot \nabla T = \alpha \nabla^2 T \tag{2.3}$$

To perform fully resolved numerical simulations in our complex geometry, we use Foam Extend 4.0 (a fork of OpenFOAM). We use unstructured polyhedral grids [43, 44] to carry out numerical simulations for the packed bed cavities and structured grids for the reference (fluid only) Rayleigh-Bénard convection simulations. The above set of equations, Eq.(2.1)-(2.3) are discretized and fully resolved numerical simulations are carried

out using the standard solver **buoyantBoussinesqPisoFoam**. The solver is validated by comparing the heat transfer obtained at different Ra in fluid-only cavities to that reported in the literature [21, 45, 46]. A detailed solver validation is also reported in [47]. The heat transfer in cavity fully-filled with adiabatic spherical beads (discussed later) at the highest Ra reported, is compared to that obtained with glass beads, experimentally [21]. At $Ra = 2.31 \times 10^7$, for a cavity fully-filled with adiabatic spherical beads we obtain a Nusselt number, $Nu = 18.2$. From experiments it is observed that, at the same Ra, in a cavity filled with glass beads of the same size and packing [21] we obtain a Nusselt number $Nu = 17.9$ (interpolated from data). The heat transfer obtained numerically with adiabatic beads is comparable to that obtained with glass beads (of lower conductivity) experimentally. This confirms the suitability of the current solver for the pore-structure resolved simulations of the packed bed.

We use the numerical schemes as listed in Table 2.2 to solve the convective and diffusive terms[42] and to handle the pressure-velocity-coupling at each time step [48]. The adaptive time-stepping is carried out by limiting the maximum cell Courant number to 0.33.

Table 2.2: Numerical schemes for fully resolved simulations using OpenFOAM.

Settings	**Numerical scheme**
Time scheme	Backward (2^{nd} order)
Gradient scheme	Gauss linear, (2^{nd} order central)
Divergence scheme	Gauss limited linear
Laplacian scheme	Gauss linear corrected
Interpolation scheme	Linear
Pressure velocity coupling	PISO

For the D-F simulations in ANSYS-Fluent, the effect of porous medium is modelled by including the pressure drop in a porous medium due to the viscous and inertial effects as a source term **S** in the momentum equation, Eq.2.5 [20].

$$\nabla \cdot \phi \mathbf{u} = 0 \tag{2.4}$$

$$\left(\frac{\partial \mathbf{u}}{\partial t} + \mathbf{u} \cdot \nabla \mathbf{u}\right) = -\frac{1}{\rho_f}\nabla p + \nu \nabla^2 \mathbf{u} + \mathbf{g}\beta(T - T_{ref}) + \frac{1}{\rho_f}\mathbf{S} \tag{2.5}$$

$$(\rho c_p)^* \frac{\partial T}{\partial t} + (\rho c_p)_f \phi \mathbf{u} \cdot \nabla T = (\rho c_p)_f \alpha_{eff} \nabla^2 T \tag{2.6}$$

where,

- $(\rho c_p)^* = \phi(\rho c_p)_f + (1-\phi)(\rho c_p)_s$
- α_{eff} is calculated using an effective thermal conductivity, $\lambda_{eff} = \phi\lambda_f + (1-\phi)\lambda_s$, where λ_f and λ_s are the thermal conductivity of the fluid and solid (equal to zero in current simulations) respectively.

The source term, **S** in Eq.(2.5) is implemented as:

$$\mathbf{S} = -\frac{\mu}{C_0}\phi\mathbf{u} - C_1\frac{1}{2}\rho_f\phi\mathbf{u}\,|\,\phi\mathbf{u}\,| \tag{2.7}$$

For a packed bed cavity C_0 and C_1 are calculated using Ergun's equation as:

$$C_0 = \frac{d^2}{150}\frac{\phi^3}{(1-\phi)^2} \tag{2.8}$$

$$C_1 = \frac{3.5}{d}\frac{1-\phi}{\phi^3} \tag{2.9}$$

where d and ϕ are the diameter of the spherical beads and local porosity, respectively. For each packing scheme the packed bed section is substituted by a Darcy equivalent, both in position/size and properties. The porosity, ϕ is calculated for the porous layer using the porous layer height, L_H ($L_H = 0.2L, 0.4L$ etc. for 1 Layer packing, 2 Layer packing etc. respectively) and the diameter of the sphere d as:

$$\phi = \frac{V_T^{\text{porous}} - V_T^{\text{spheres}}}{V_T^{\text{porous}}} \tag{2.10}$$

where, V_T^{porous} and V_T^{spheres} is the total volume of the cavity of height L_H and volume occupied by the spherical beads, respectively. The Eq. (2.4)-(2.7) in ANSYS Fluent user manual (when re-arranged) are the same as reported in [20]. For the investigated d/L ratio and porosity, the permeability K is equal to 1.05×10^{-6} resulting in a Da varying between 2.62×10^{-3} and 1.05×10^{-4} for packing height varying from 1 Layer to 5 Layers.

The governing equations in ANSYS-Fluent are solved using the numerical schemes listed in Table 2.3.

Table 2.3: Numerical schemes for D-F simulations using Fluent.

Settings	**Numerical scheme**
Time scheme	2^{nd} order Implicit
Gradient	Least square Cell based
Momentum	Bounded Central differencing
Energy	Bounded Central differencing
Pressure	Second order
Pressure velocity coupling	PISO

The time step size determined using for D-F simulations also satisfy the condition of maximum cell Courant number ≤ 0.33.

2.2.3. MESH REQUIREMENT

The pore-structure resolved (P-R) simulations are carried out using polyhedral mesh (Fig.2.2(b)), generated by converting a fine tetrahedral mesh (Fig.2.2(a)). The function

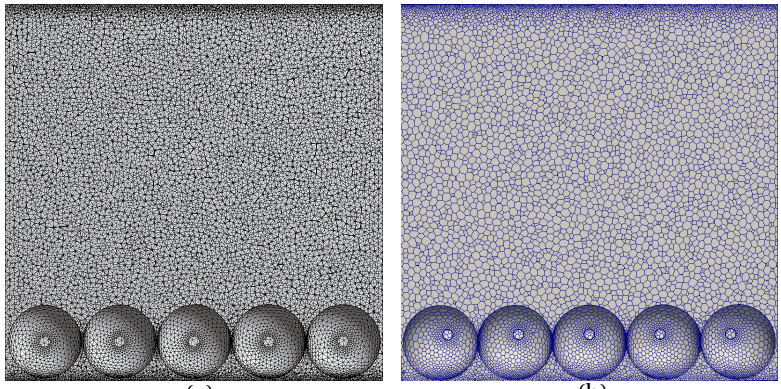

(a) (b)

Figure 2.2: Cubical cavity packed with 1 layer of adiabatic spherical beads meshed using (a) tetrahedral grids (b) polyhedral grids.

polyDualMesh available in OpenFOAM is used to carry out this conversion. The number of mesh cells is decreased using this approach. For example, it reduces a 30 million cell tetrahedral mesh to a polyhedral mesh with around 6 million cells. Initial estimates of the grid requirement close to the wall and the bulk of the cavity are made based on the correlations provided in [49] for Rayleigh-Bénard convection. Using the estimate for the highest $Ra = 2.3 \times 10^7$ as a base, a grid independence study is carried out using three different polyhedral meshes with 0.5 million, 4 million and 6 million cells for the cavity packed with 1 layer of spherical beads. The time-averaged integral Nusselt number (deviation less than 4%) and time- and plane- averaged non-dimensional temperature, θ_m along the vertical direction (Fig.2.3) are used to ensure that we get a grid-independent solution. Though the volume of the packed-cavity to be meshed decreases with an increase in the number of layers of spherical beads, we use $\sim$ 6 million polyhedral cells to account for the increase in curved surfaces in the domain.

For the fluid-only and Darcy-Forchheimer simulations, we use structured hexahedral grid cells, with a growth factor of 1.2 close to the horizontal isothermal walls. A grid independence study is carried out using 32^3, 64^3 and 128^3 and 167^3 hexahedral cells. The deviation of time- and wall- averaged integral Nusselt number between 128^3 and 167^3 cells is less than 0.5% for $Ra = 2.3 \times 10^7$. All the reported results are thus obtained with the 128^3 hexahedral cells.

2.3. RESULTS AND DISCUSSION

The influence of Rayleigh number, packing height and location of packing of spherical beads on the flow and heat transfer is discussed in this section. In the following sections, the ANSYS Fluent simulations with Darcy and Forchheimer terms are referred to as Darcy-Forchheimer (D-F) simulations. All the D-F simulations are carried with grid-size required to fully resolve the flow in the porous media free region. In the porous region we find the flow velocities to be very low such that the Reynolds number calculated with maximum flow velocity as the velocity scale and square root of permeability

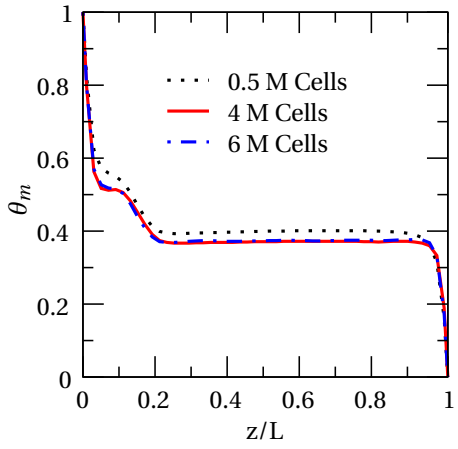

Figure 2.3: Time- and plane- averaged mean temperature variation along Z direction in a cavity filled with 1 layer of spherical adiabatic beads for different mesh sizes at $Ra = 2.3 \times 10^7$.

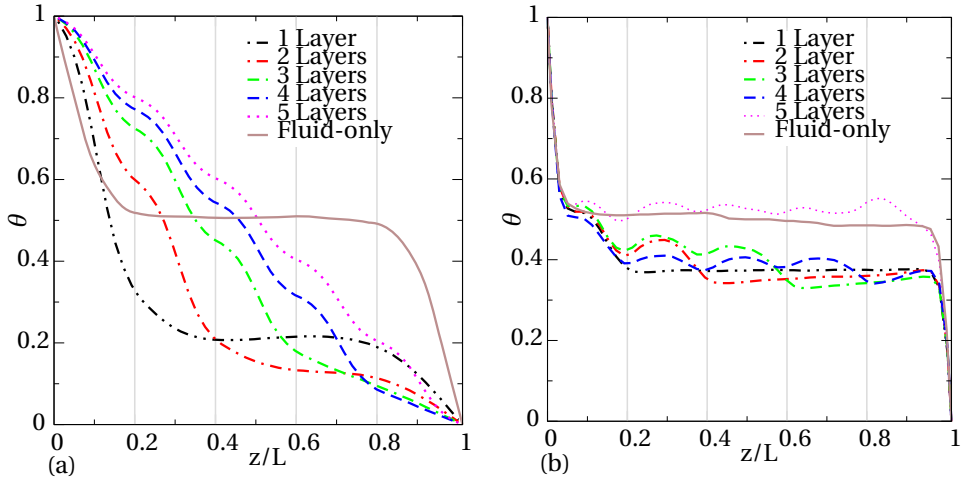

Figure 2.4: Time- and plane- averaged non-dimensional temperature for cavities filled with different layers of spherical bead packing at (a) $Ra = 1.16 \times 10^5$, (b) $Ra = 2.3 \times 10^7$. Plane-averaging along planes with adiabatic spheres results in the wavy temperature distribution. The deviation in mean temperature from $\theta = 0.5$ for 5 layer packing indicates the need of time averaging for longer period.

$\sqrt{K}$ as the length scale is ≈ 3 within the porous region. Thus laminar models are used for the simulations.

The pore-scale resolved simulations are compared to D-F simulations to better understand the suitability and applicability of D-F assumptions to simulate the flow and heat transfer in fully and partially packed porous domains. The results obtained with D-F simulations are also reported in terms of intrinsic velocity **u**. All the results reported below are expressed in non-dimensional form. The instantaneous temperature is non-

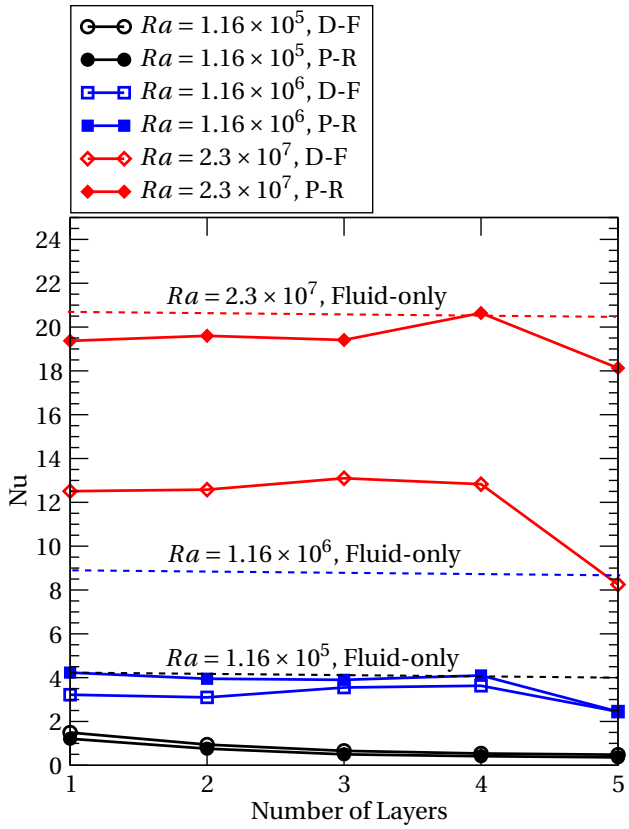

Figure 2.5: Variation of time- and wall- averaged Nusselt number with number of layers of packing at different Rayleigh numbers. A comparison of pore-structure resolved (P-R) simulations is made with that from Darcy-Forchheimer (D-F) simulations and fluid-only filled cavity.

dimensionalised using the temperature difference between the top and bottom wall as in $\theta = \frac{T - T_c}{T_h - T_c}$. The instantaneous intrinsic velocities, $\mathbf{u}$ are non-dimensionalized with the characteristic velocity scale $U_0 = \frac{{Ra_f}^{3/7}\alpha}{L}$ [50], such that the non-dimensional velocity vector $\mathbf{u}^*$ equals

$$\mathbf{u}^* = \frac{\mathbf{u}}{U_0} \tag{2.11}$$

The time- and wall- averaged global heat transfer is expressed in terms of Nusselt number defined as:

$$Nu = -\frac{L}{\Delta T}\left(\frac{\partial T}{\partial z}\right)_{wall} \tag{2.12}$$

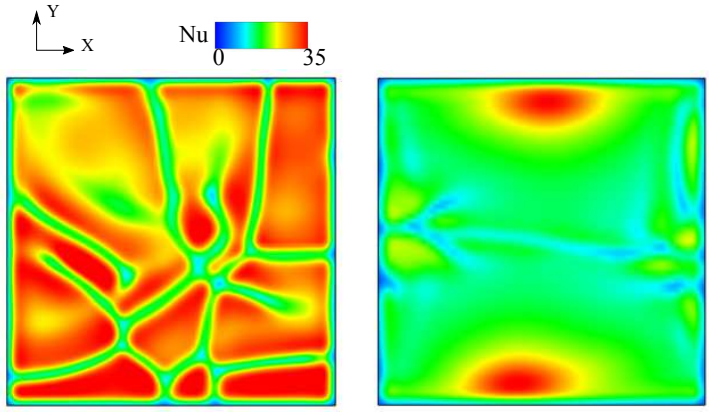

Figure 2.6: Instantaneous Nusselt number distribution (top view) at the bottom wall, in a cavity with porous media filled to a height equivalent to (a)1 layer (b) 5 layers of spherical beads at $Ra = 2.3 \times 10^7$ obtained with Darcy-Forchheimer (D-F) simulations.

2.3.1. INFLUENCE OF Ra AND PACKING HEIGHT

We compare the heat transfer and flow features in P-R cavities with 1-5 layers of spherical beads stacked from the bottom to the top. The results from P-R simulations are compared with the D-F simulation results with the same local Darcy number Da and ϕ. We also compare the heat transfer obtained with P-R and D-F simulations to that in a fluid-only filled cavity. In Fig.2.4 we plot the time- and plane-averaged (averaged along XY plane) non-dimensional temperature of pore-structure resolved (P-R) simulations with 1 Layer to 5 Layer of spherical beads. The vertical lines indicate the packing height, for e.g. $z/L = 0.2$ and $z/L = 1$ represent the height of 1Layer packing and 5 Layer packing, respectively. At low $Ra = 1.16 \times 10^5$ (Fig.2.4(a)), the temperature distribution becomes conduction-dominated with the increase in the number of layers of spherical beads i.e. from 1Layer to 5Layer packing. The "close to linear" temperature in fully-packed cavity (5 Layer) indicates the absence of convection in the cavity. The flow resistance imposed by the adiabatic spherical beads results in this behaviour.

In contrast to the above, at $Ra = 2.3 \times 10^7$ (Fig.2.4(b)) the slope of time- and plane-averaged temperature close to the wall ($z/L = 0$ and $z/L = 1$) is comparable to that in a fluid-only filled cavity, indicating a convection dominated heat transfer. The presence of multi-layered adiabatic spherical beads results in an asymmetry in the temperature distribution, which vanishes in the cavity with 5 layers of packing.

From Fig.2.5 we observe that the inclusion of spherical beads in the cavity, adversely affects the convective flow and thus the heat transfer is lower than in the fluid-only cavity, especially at low Ra. The non-dimensional heat transfer Nu in P-R cavities and in cavities with the D-F assumption are comparable at lower Rayleigh numbers ($Ra = 1.16 \times 10^5, 1.16 \times 10^6$). At $Ra = 1.16 \times 10^5$ the heat transfer is much lower than in a fluid-only filled-cavity, and decreases with an increase in the number of layers of packing. At $Ra = 1.16 \times 10^6$, though the heat transfer is much lower than in fluid-only cavity, it is

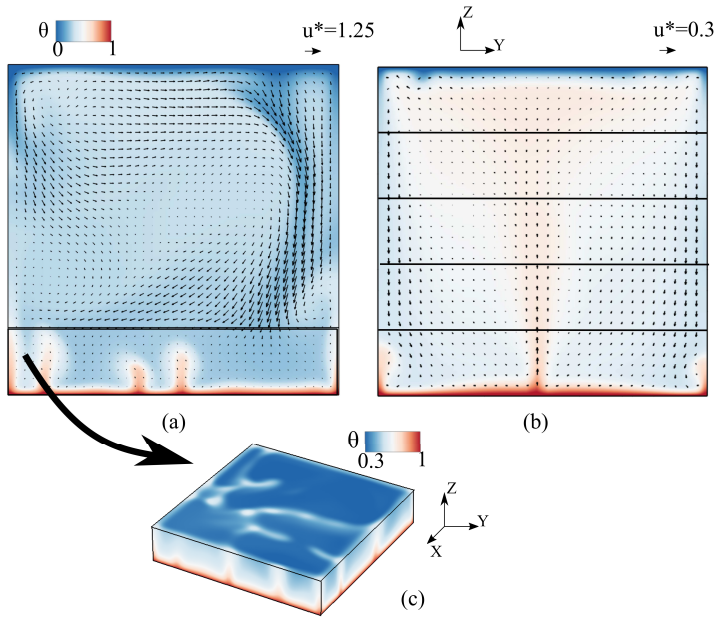

Figure 2.7: Instantaneous non-dimensional temperature distribution and velocity vectors at $x/L = 0.43$, in a cavity with (a) 1 layer (layer height highlighted with a box) (b) 5 layers at $Ra = 2.3 \times 10^7$ simulated using Darcy-Forchheimer assumption. The velocity vectors are visualized by projecting them to a 32×32 grid along the vertical plane. The enlarged 3D view of the temperature distribution in the porous region of cavity with 1 Layer of packing is depicted in (c) with a different colour scale.

practically independent of the layers of packing (1 Layer-4 Layer). However, when the spherical beads are introduced close to the top cold wall (5 Layer), the heat transfer reduces further.

With the increase in Ra ($Ra = 2.3 \times 10^7$), the heat transfer in P-R cavities are slightly lower than (1 Layer-3 Layer, 5 Layer) or comparable (4 Layer) to that in fluid-only filled cavities, while the heat transfer obtained from simulations with D-F assumption is observed to be much lower than in the fluid-only cavities. The results from the P-R simulations are qualitatively similar to that obtained experimentally for partially filled [23] and fully-filled cavities [21]. Unlike the P-R simulations, the D-F simulations cannot capture this behaviour and thus significantly under-predict the heat transfer.

To understand the difference in heat transfer (Nu) between P-R and D-F simulations we analyse the instantaneous local Nusselt number, local non-dimensional temperature and the local non-dimensional velocity magnitude in cavities with 1 Layer and 5 Layer packing, at $Ra = 2.3 \times 10^7$.

DARCY-FORCHHEIMER SIMULATIONS

In simulations with D-F assumption, the local Nusselt number (Fig.2.6) at the bottom hot wall significantly decreases with the increase in the height of packing. In the D-F cavity with porous layer equivalent to the height of 1 Layer of spherical bead packing (Fig.2.6(a)), the instantaneous heat transfer is high throughout the surface of the bottom

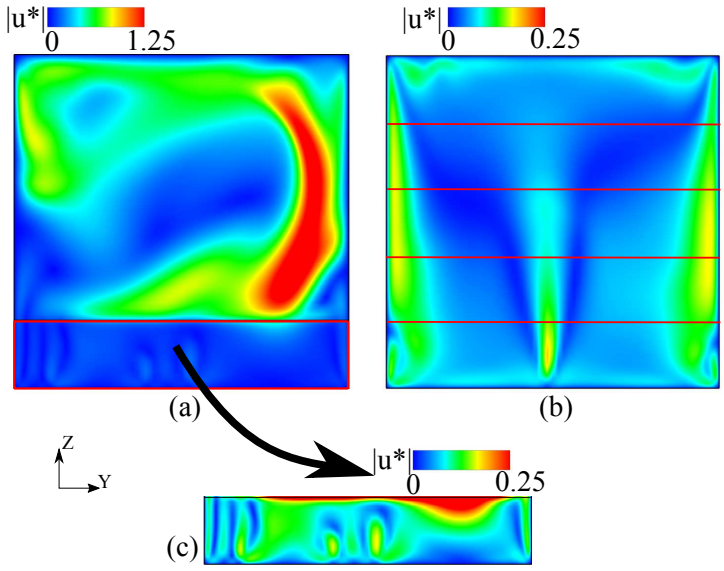

Figure 2.8: Instantaneous non-dimensional velocity magnitude distribution at $x/L = 0.43$, in a cavity with (a) 1 layer (b) 5 layers at $Ra = 2.3 \times 10^7$ simulated using Darcy-Forchheimer assumption. The legend of (c) has a different scale from (a).

wall. However, when the cavity is fully filled with porous media (Fig.2.6(b)), the surface area with high local Nusselt number is smaller when compared to that in the cavity with 1 Layer of packing.

The reason for the reduction in heat transfer with the increase in porous layer height, becomes clear from the local non-dimensional instantaneous temperature (Fig.2.7) and velocity magnitude (Fig.2.8) along a plane ($X/L = 0.43$) in the configurations with 1 Layer and 5 Layers of packing. From Fig.2.7(a) we see that the cold thermal plumes erupting from the top cold wall moves downward (as indicated by the velocity vectors) towards the bottom wall. From the velocity vectors we see that the flow in the porous region is lower when compared to the fluid-only region above the porous layer (Fig.2.7(a)). The temperature at the interface of the fluid-only and porous region (Fig.2.7(c)) is close to the cold fluid temperature. The fluid region above this interface thus behaves like a fluid only cavity.

When the cavity is fully packed with porous media the asymmetry in temperature distribution (Fig.2.7(b)) observed above, vanishes.The velocity vectors suggest the flow velocity to be much lower than that in the cavity with 1 Layer of packing (Fig.2.7(a)). The contours of non-dimensional velocity magnitude confirm the reduction in flow velocity when the cavity is fully packed with porous media (Fig.2.8(b)) when compared to the cavity with 1 Layer of packing (Fig.2.8(a)). From Fig.2.7 and Fig.2.8 we find that the convective contribution to the heat transfer in the cavity decreases when the cavity is fully packed. The fluid-only region in the partially filled cavity dictates the total heat transfer thus resulting in a higher heat transfer (Fig.2.6(a)) than in the fully-packed cavities (Fig.2.6(b)).

PORE-STRUCTURE RESOLVED SIMULATIONS

As observed in Fig.2.5, the heat transfer obtained with pore-structure resolved simulations are comparable to that in fluid-only filled cavities and is higher than in D-F simulations, at high Ra. This is also evident from the local Nusselt number distribution of heat transfer at the bottom hot wall in P-R simulations, obtained in cavities with 1 Layer and 5 Layer of packing (Fig.2.9). The local Nusselt number in P-R simulations (Fig.2.9) are higher than in D-F simulations (Fig.2.6). Unlike the Nusselt number distribution with D-F simulations, the heat transfer in P-R simulations are high in the regions close to the pore-space and are close to 0 at regions very close to the point of contact of the spherical beads with the bottom wall. To explain this behaviour, we look at the local flow and temperature in the plane $X/L = 0.43$, where the spherical beads and the pore-space are comparable in size. In Fig.2.10 we compare configurations with 1 Layer (Fig.2.10(a)) and 5 Layer (Fig.2.10(b)) of spherical bead packing, at $Ra = 2.3 \times 10^7$. The instantaneous non-dimensional temperature contours also have the non-dimensional velocity vectors to give an indication of the direction and strength of the in-plane (ZY plane) flow. At the top right corner of the temperature contours we have the non-dimensional out-of plane velocity (u_x^*) contours.

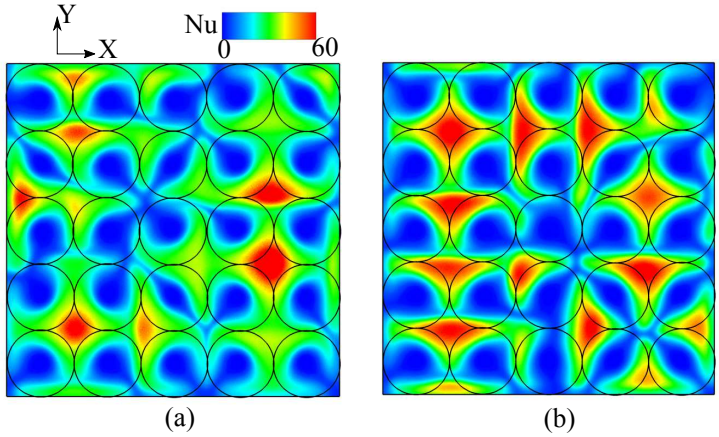

Figure 2.9: Instantaneous Nusselt number distribution (top view) at the bottom wall, in a cavity with (a)1 layer (b) 5 layers of spherical beads at 2.3×10^7 obtained with pore-structure resolved (P-R) simulations.

From the temperature contours we observe that the thermal plumes erupting from the isothermal walls are thinner than the pore-space size (discussed later in next section), resulting in a flow-dominated heat transfer. This results in the heat transfer in spherical bead filled cavities to be comparable to that in a fluid-only filled cavity. Unlike the cavity with 1 Layer packing in which the flow is 3-dimensional with high value of out of plane velocity u_x^* (Fig.2.10(a)), in the cavity with 5 Layer packing (Fig.2.10(b)), we observe a channeled (2D planar) flow with negligible out of plane velocity. The slight increase in heat transfer observed with 4 Layer packing (Fig.2.5) could be due to the dominance of the channeled flow in which the thin hot and cold plumes move through the pore-space and directly impinge on the cold and hot walls. However, a slight reduction in heat transfer occurs when the 5^{th} layer of spherical beads is placed close to the cold

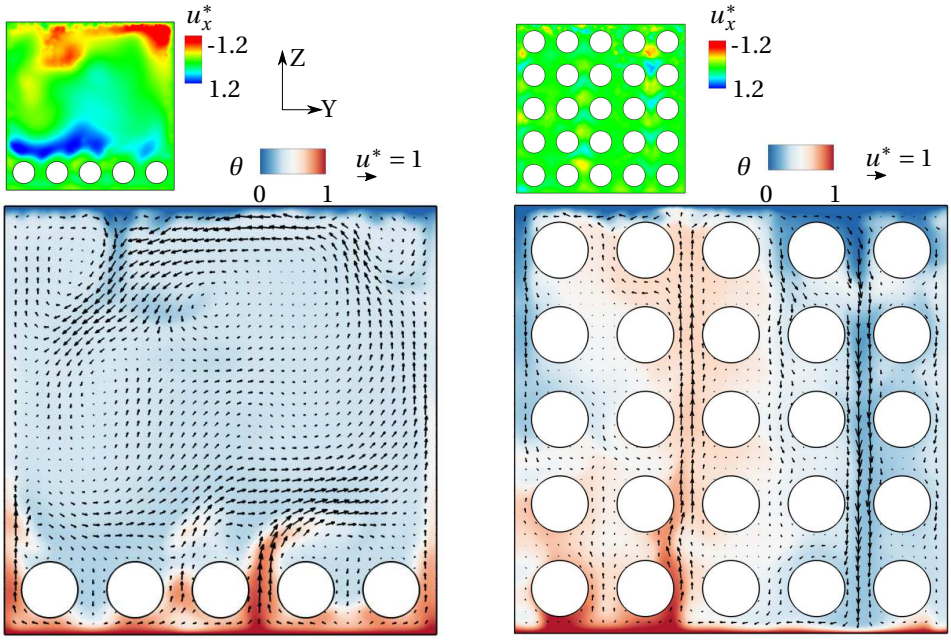

(a) (b)

Figure 2.10: Instantaneous non-dimensional temperature distribution and velocity vectors at $x/L = 0.43$, in a cavity with (a) 1 layer, (b) 5 layers of spherical beads at $Ra = 2.3 \times 10^7$. The smaller figure to the left of temperature contour depicts the non-dimensional out of plane velocity. The velocity vectors are visualized by projecting them to a 32×32 grid along the vertical plane.

wall. Losing the area for the eruption of cold plumes in the cavity with 5 layers of packing results in this reduction, the effect of which is expected to diminish at higher Ra [21, 37].

To understand the local flow in P-R simulations, we look at the frequency spectra of thermal and kinetic energy at $Ra = 2.3 \times 10^7$ (of vertical velocity u_z) at the probe location ($y/L = 0.5$, $x/L = 0.6$, $z/L = 0.6$) in cavities with 1 Layer, 3Layer and 5 Layer packing. The probe is far from the spherical beads in cavity with 1Layer packing, close to the beads in 3Layer packing and within the pore-space in 5Layer packing. We also compare the spectra with that in a fluid-only cavity (same probe location) to understand the influence of spherical beads on local flow and thermal features.

The frequency spectra of thermal and kinetic energy at $Ra = 2.3 \times 10^7$ (of vertical velocity u_z) is turbulent in a fluid-only cavity following $E_T(f) \sim f^{-7/5}$ and $E_{u_z}(f) \sim f^{-11/5}$ comparable to that reported in [51] and [52], respectively. From the P-R simulations of the spherical bead filled cavities, we observe that the temporal flow and temperature fluctuations (Fig.2.11) dies out with the addition of layers of spherical beads. When we increase the number of the packing layers, the flow is still turbulent and thus the energy spectra follow the turbulent scaling for 1 Layer and 3 Layer packing, while the flow becomes oscillatory in the cavity with 5 Layer packing. This indicates that the flow becomes less turbulent as the relative distance of the probe with the spherical beads decreases, because of the increased resistance imposed by the spheres.

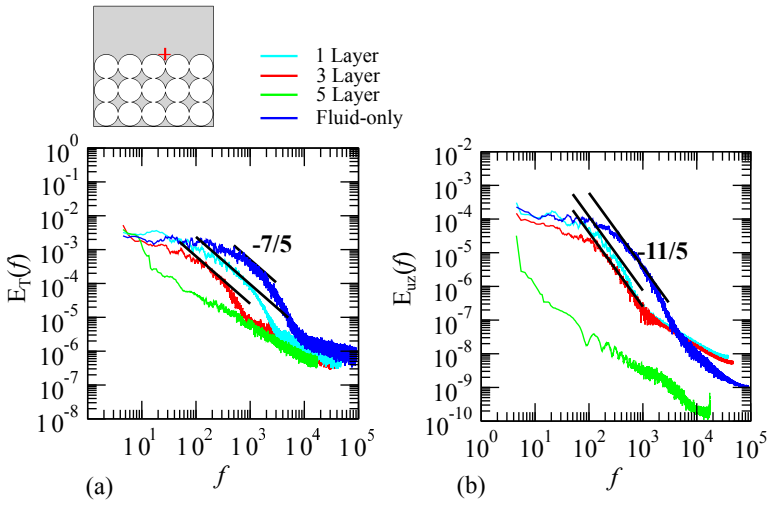

Figure 2.11: Power-laws for the frequency (a) thermal energy spectra and (b) kinetic energy spectra of the vertical velocity u_z at $Ra = 2.3 \times 10^7$, $y/L = 0.5, x/L = 0.6, z/L = 0.6$.

2

2.3.2. INFLUENCE OF SHIFT OF PACKING

In contrast to the cavities with spherical beads touching the hot wall (Fig.2.5), the suppression in heat transfer is comparatively lower when the spherical beads are shifted away from the hot wall (Fig.2.12), both in P-R and D-F simulations.

PORE-STRUCTURE RESOLVED SIMULATIONS

With P-R simulations, at $Ra = 1.16 \times 10^5$, for both 1 Layer and 2 Layer cases (Fig.2.12), when the packing is away from the wall i.e for 1L/2L Quarter/Middle (P-R), the suppression in heat transfer varies significantly from that in cavities with the spherical beads touching the wall 1L/2L Bottom (P-R), for e.g. $Nu_{\text{1 Layer Middle}} > Nu_{\text{1 Layer Quarter}} > Nu_{\text{1 Layer Bottom}}$. At higher Ra ($Ra = 1.6 \times 10^6, 2.3 \times 10^7$), the heat transfer in porous media filled cavities with the packing away from the isothermal walls becomes comparable to or even slightly higher than that in fluid-only filled cavities, unlike the cavities in which the spherical beads touch the hot wall (1L Bottom (P-R)). To understand this difference in heat transfer behaviour, we look at the thermal plume (boundary layer) thickness defined as:

$$\delta_{th} = \frac{L}{2Nu}. \tag{2.13}$$

When the thermal plume size δ_{th} is scaled with the diameter of the pore-space d_p (Fig.2.13), we observe that the thermal plumes are thicker than the pore-space ($\delta_{th}/d_p > 1$) at low Ra ($Ra = 1.16 \times 10^5$). While with the increase in Ra, thermal plumes become comparable to pore-size ($Ra = 1.16 \times 10^6$) and even gets smaller than the pore-size ($Ra = 2.31 \times 10^7$). At the lowest Ra ($Ra = 1.16 \times 10^5$), as the thermal plumes are thicker than the pore-space, the inclusion of the spherical beads leads to a considerable suppression in heat transfer as the thermal plumes cannot meander through the pore-space. The inclusion of spher-

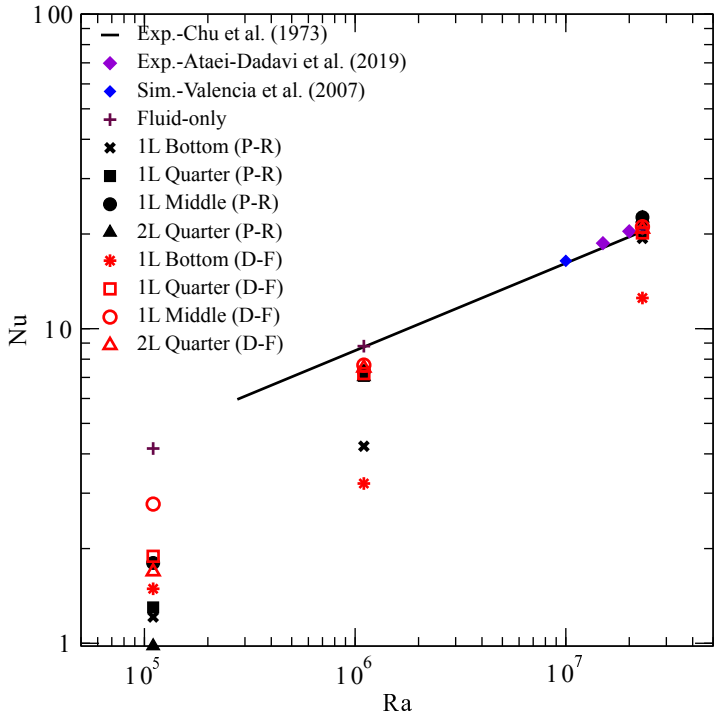

Figure 2.12: Variation of Nu with Ra in pore-structure resolved (P-R) and Darcy-Forchheimer (D-F) simulations for different packing arrangement. The results are compared with heat transfer in fluid-only cavities reported in literature [21, 45, 46]. For naming convection of packing arrangement refer to Table 2.1.

ical beads thus increases the resistance offered to the thermal plumes and even makes them thicker (Fig.2.13).

A comparison of the cavities with 1 Layer of packing (Fig.2.12) shows that the suppression in heat transfer is minimum when the porous layer is at the center of the cavity (1L Middle (P-R)). This indicates that the influence of the packing on heat transfer decreases with the increase in its distance from the hot isothermal wall.

At $Ra = 1.16 \times 10^6$, as the thermal plume thickness of the fluid-only cavity is comparable to the pore-space (Fig.2.13) and thus the reduction in heat transfer with the inclusion of spherical beads away from the isothermal walls is minimal (Fig.2.12). This is also evident from the small change in the δ_{th}/d_p ratio in the cavities with spherical beads, when compared to the fluid-only filled cavity (Fig.2.13). With the increase in Ra ($Ra = 2.31 \times 10^7$), the thermal plumes become much thinner than the pore-space (Fig.2.13). The inclusion of layers of packing irrespective of their location, thus does not significantly obstruct the flow as the plumes meander through the pore-space. Thus at high Ra, the heat transfer in cavities with spherical beads are comparable to that in a fluid-only cavity (Fig.2.12).

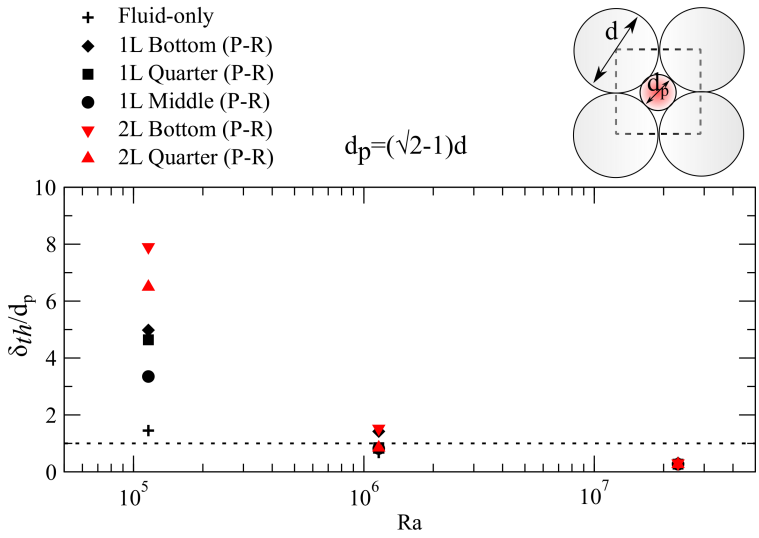

Figure 2.13: Ratio of boundary layer thickness to pore-size at different *Ra*, for pore-scale resolved simulations. The boundary layer thickness of fluid-only cavity is also scaled with pore-size of the porous media filled-cavity for reference.

DARCY-FORCHHEIMER SIMULATIONS

At the lowest $Ra = 1.16 \times 10^5$, when the porous media touches the bottom hot wall, the heat transfer with with D-F and P-R simulations are comparable, for e.g. $Nu_{1\text{ Layer Bottom}}$(D-F)$\approx Nu_{1\text{ Layer Bottom}}$(P-R) (Fig.2.12).

However, the heat transfer obtained with the D-F simulations are lower than the P-R simulations at higher *Ra*, for e.g. at $Ra = 2.31 \times 10^7$, $Nu_{1\text{ Layer Bottom}}$(D-F)$< Nu_{1\text{ Layer Bottom}}$(P-R). When the porous media is away from the isothermal hot wall, we observe a different behaviour.

- At $Ra = 1.16 \times 10^5$, *Nu* with D-F simulations are higher than with the P-R simulations (Fig.2.12). This indicates that the flow within the pore-space of the spherical bead packing in P-R simulations is blocked as the thermal plumes are thicker than the pore-space (Fig.2.13). While in the D-F simulations of the cavities with porous media not touching the isothermal walls, the convective flow is not fully choked as in P-R simulations, thus resulting in comparatively higher heat transfer (Fig.2.12).
- At $Ra = 1.16 \times 10^6$ and $Ra = 2.31 \times 10^7$, the D-F and P-R simulations gives us comparable heat transfer, irrespective of the number of layers (Fig.2.12).

We also observe that the resistance to the convective flow imposed by the porous media in D-F simulations is higher when it touches the isothermal wall when compared to the cavity with the porous media located away from it, thus resulting in lower heat transfer (Fig.2.12), i.e. $Nu_{1\text{ Layer Bottom}}$(D-F)$< Nu_{1\text{ Layer Quarter}}$(D-F).

To understand the difference in the behaviour of the D-F simulations when the porous media touches the wall and when it is away from the wall, we look at the instantaneous

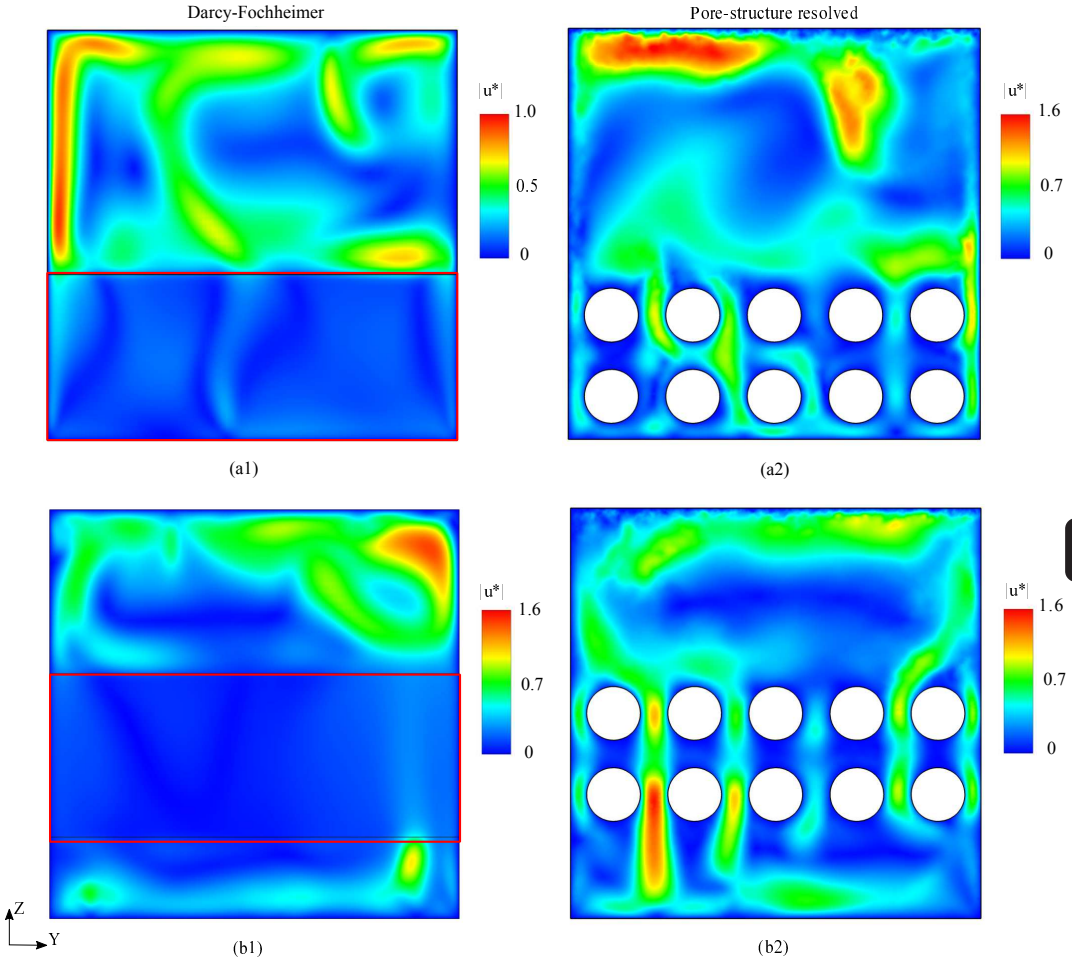

Figure 2.14: Instantaneous non-dimensional velocity magnitude distribution at $x/L = 0.43$, in a cavity with 2 layers of spherical beads at $Ra = 2.3 \times 10^7$ in Darcy-Forchheimer (a1,b1) and pore-structure resolved (a2,b2) simulations. (a1,a2) has porous media from $z/L = 0$ to 0.4 and (b1, b2) has porous media from $z/L = 0.2$ to 0.6.

non-dimensional velocity magnitude and temperature distribution along the plane, $X/L = 0.43$ in cavities with 2 Layer of porous media packing touching the isothermal wall (Fig.2.14(a1), Fig.2.15(a1)) and away from it (Fig.2.14(b1), Fig.2.15(b1)). We also compare it with the P-R simulations of the respective cavities (Fig.2.14(a2,b2), Fig.2.15(a2,b2)).

Since the thermal boundary layer is thinner than the pore-space at $Ra = 2.31 \times 10^7$ (Fig.2.13), the pore-space flow velocity in the P-R simulation of the cavity with 2 Layer packing touching the bottom wall (Fig.2.14(a2)), is less influenced by the spherical beads, resulting in hot thermal plumes at high velocity meandering through the pore-space (Fig.2.15(a2)). In the cavities with porous media touching the isothermal hot wall, the flow velocity in the porous region obtained with D-F simulation (Fig.2.14(a1)) is much

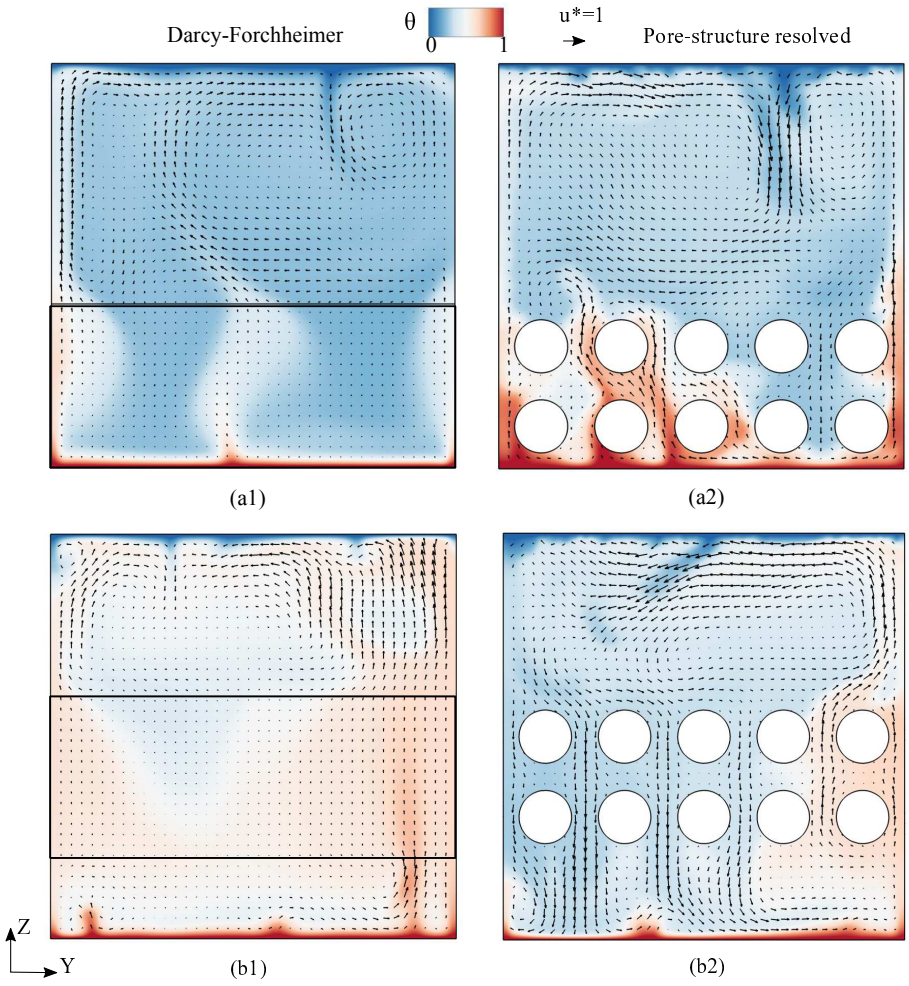

Figure 2.15: Instantaneous non-dimensional temperature distribution and velocity vectors at $x/L = 0.43$, in a cavity with 2 layers of spherical beads at $Ra = 2.3 \times 10^7$ in Darcy-Forchheimer (a1,b1) and pore-scale resolved (a2,b2) simulations. (a1,a2) has porous media from $z/L = 0$ to 0.4 and (b1, b2) has porous media from $z/L = 0.2$ to 0.6.

lower than with the P-R simulation (Fig.2.14(a2)). We also observe that in the simulation with D-F assumption, hot thermal plumes of comparatively lower temperature (Fig.2.15(a1)) erupt from the bottom hot wall. Unlike the D-F simulation, the temperature and flow velocity of the hot thermal plumes (erupting from the bottom wall) within the pore-space is higher in the P-R simulation (Fig.2.15(a2)). The combined effect of the thermal plume temperature and flow velocity results in lower convective heat transfer in the simulation with D-F assumption (Fig.2.5).

However, in the D-F simulation with porous-media defined away from the wall (Fig.2.14(b1)),

the flow velocity close to the isothermal walls is less influenced by the porous media and is comparable to that in the P-R simulation (Fig.2.14(b2)). Thus, comparable flow velocity close to the isothermal walls results in comparable heat transfer with D-F (2L Quarter (D-F)) and P-R (2L Quarter (P-R)) simulations (Fig.2.12).

2.4. SUMMARY AND CONCLUSION

A detailed study on the validity and applicability of Darcy-Forchheimer assumption to simulate convective heat transfer in flow dominated porous media filled-cavity is reported. The Darcy-Forchheimer simulations of cavities with porous media touching the isothermal walls and away from them are compared with the pore-structure resolved simulations at different Ra. Major findings of this work can be summarized as:

(i) In cavities with porous media touching the isothermal wall, the heat transfer in simulations with Darcy-Forchheimer assumption is comparable to that in pore-structure resolved simulations at low Ra. With an increase in Ra, the Darcy- Forchheimer simulations under-predict the heat transfer. At high Ra, the temperature and velocity of the thermal plumes impinging the hot wall are higher in the pore-structure resolved simulations resulting in heat transfer comparable to fluid-only cavities.

(ii) In cavities with porous media not touching the isothermal wall, Darcy-Forchheimer simulations and pore-structure resolved simulations report comparable heat transfer irrespective of the number of layers of packing and its location, for $Ra \geq 1.16 \times 10^6$. However, at low $Ra = 1.16 \times 10^5$ D-F simulations over-predict the heat transfer. This shows that the laminar model for porous-media simulations predicts heat transfer comparable to the pore-structure resolved simulations, when the non-porous regions are fully resolved.

(iii) Heat transfer in a porous medium filled-cavity decreases when the porous medium is close to the isothermal walls. A slight enhancement in heat transfer with porous media over the fluid-only cavity occurs when the channeling effect dominates over the effect due to the reduction in the area available for plume impingement when the packings are away from the isothermal walls.

(iv) From pore-structure resolved simulations, we observe that when the thermal boundary layer thickness (thermal plume size) is larger than the pore-space (of a pore-structure resolved cavity), the location and the number of layers of packing influence the heat transfer ($Ra = 1.16 \times 10^5$) for all packing configurations. However, it is practically independent of the porous packing when the boundary layer thickness is considerably smaller than the pore-size and when the porous media does not touch the wall (($Ra = 2.31 \times 10^7$). When the porous media touches the isothermal wall, the heat transfer is however reduced by the adiabatic spherical beads close to the wall. The reduction in heat transfer compared to fluid-only cavity is due to the comparatively lower flow velocity close to the wall.

REFERENCES

[1] O. Laguerre, S. B. Amara, G. Alvarez, and D. Flick, *Transient heat transfer by free convection in a packed bed of spheres: Comparison between two modelling approaches and experimental results,* Applied Thermal Engineering **28**, 14 (2008).

[2] O. Laguerre, S. B. Amara, M.-C. Charrier-Mojtabi, B. Lartigue, and D. Flick, *Experimental study of air flow by natural convection in a closed cavity: Application in a domestic refrigerator,* Journal of Food Engineering **85**, 547 (2008).

[3] F. Torriano, H. Campelo, M. Quintela, P. Labbé, and P. Picher, *Numerical and experimental thermofluid investigation of different disc-type power transformer winding arrangements,* International Journal of Heat and Fluid Flow **69**, 62 (2018).

[4] A. Shams, F. Roelofs, E. Komen, and E. Baglietto, *Large eddy simulation of a randomly stacked nuclear pebble bed,* Computers & Fluids **96**, 302 (2014).

[5] M. A. Fazilati, A. Sedaghat, and A. A. Alemrajabi, *Natural induced flow due to concentration gradient in a liquid desiccant air dehumidifier,* Applied Thermal Engineering **105**, 105 (2016).

[6] X. Li, J. Cai, F. Xin, X. Huai, and J. Guo, *Lattice boltzmann simulation of endothermal catalytic reaction in catalyst porous media,* Applied Thermal Engineering **50**, 1194 (2013).

[7] I. Thiagalingam, M. Dallet, I. Bennaceur, S. Cadalen, and P. Sagaut, *Exact non local expression for the wall heat transfer coefficient in tubular catalytic reactors,* International Journal of Heat and Fluid Flow **54**, 97 (2015).

[8] A. Babich and D. Senk, *Recent developments in blast furnace iron-making technology,* in *Iron Ore* (Elsevier, 2015) pp. 505–547.

[9] K. Boomsma, D. Poulikakos, and F. Zwick, *Metal foams as compact high performance heat exchangers,* Mechanics of materials **35**, 1161 (2003).

[10] D. Missirlis, K. Yakinthos, P. Storm, and A. Goulas, *Modeling pressure drop of inclined flow through a heat exchanger for aero-engine applications,* International Journal of Heat and Fluid Flow **28**, 512 (2007).

[11] Z.-Q. Zhu, Y.-K. Huang, N. Hu, Y. Zeng, and L.-W. Fan, *Transient performance of a PCM-based heat sink with a partially filled metal foam: Effects of the filling height ratio,* Applied Thermal Engineering **128**, 966 (2018).

[12] D. A. Nield, A. Bejan, *et al.*, *Convection in porous media*, Vol. 3 (Springer, 2006).

[13] Y. Katto and T. Masuoka, *Criterion for the onset of convective flow in a fluid in a porous medium,* International Journal of Heat and Mass Transfer **10**, 297 (1967).

[14] I. Catton and T. Jonsson, *Prandtl Number Dependence of Natural Convection in Porous Media,* Journal of Heat Transfer **109**, 371 (1987).

[15] N. Kladias and V. Prasad, *Natural Convection in Horizontal Porous Layers: Effects of Darcy and Prandtl Numbers,* Journal of Heat Transfer **111**, 926 (1989).

[16] C. Y. Zhao, T. J. Lu, and H. P. Hodson, *Natural convection in metal foams with open cells,* International Journal of Heat and Mass Transfer **48**, 2452 (2005).

[17] I. Ataei-Dadavi, N. Rounaghi, M. Chakkingal, S. Kenjereš, C. R. Kleijn, and M. J. Tummers, *An experimental study of flow and heat transfer in a differentially side heated cavity filled with coarse porous media,* International Journal of Heat and Mass Transfer **143**, 118591 (2019).

[18] N. Seki, S. Fukusako, and H. Inaba, *Heat transfer in a confined rectangular cavity packed with porous media,* International Journal of Heat and Mass Transfer **21**, 985 (1978).

[19] D. J. Keene and R. Goldstein, *Thermal convection in porous media at high Rayleigh numbers,* Journal of Heat Transfer **137**, 034503 (2015).

[20] P. Nithiarasu, K. Seetharamu, and T. Sundararajan, *Effect of porosity on natural convective heat transfer in a fluid saturated porous medium,* International Journal of Heat and Fluid Flow **19**, 56 (1998).

[21] I. Ataei-Dadavi, M. Chakkingal, S. Kenjereš, C. R. Kleijn, and M. J. Tummers, *Flow and heat transfer measurements in natural convection in coarse-grained porous media,* International Journal of Heat and Mass Transfer **130**, 575 (2019).

[22] V. Kathare, F. Kulacki, and J. H. Davidson, *Buoyant convection in superposed metal foam and water layers,* in *ASME 2008 Heat Transfer Summer Conference collocated with the Fluids Engineering, Energy Sustainability, and 3rd Energy Nanotechnology Conferences* (American Society of Mechanical Engineers, 2008) pp. 217–223.

[23] V. Prasad, K. Brown, and Q. Tian, *Flow visualization and heat transfer experiments in fluid-superposed packed beds heated from below,* Experimental Thermal and Fluid Science **4**, 12 (1991).

[24] V. Prasad, *Flow instabilities and heat transfer in fluid overlying horizontal porous layers,* Experimental thermal and fluid science **6**, 135 (1993).

[25] M. Fahs, A. Younes, and T. A. Mara, *A new benchmark semi-analytical solution for density-driven flow in porous media,* Advances in Water Resources **70**, 24 (2014).

[26] M. Fahs, A. Younes, and A. Makradi, *A reference benchmark solution for free convection in a square cavity filled with a heterogeneous porous medium,* Numerical Heat Transfer, Part B: Fundamentals **67**, 437 (2015).

[27] Q. Shao, M. Fahs, H. Hoteit, J. Carrera, P. Ackerer, and A. Younes, *A 3-d semianalytical solution for density-driven flow in porous media,* Water Resources Research **54** (2018), 10.1029/2018wr023583.

[28] F. J. Guerrero-Martínez, P. L. Younger, N. Karimi, and S. Kyriakis, *Three-dimensional numerical simulations of free convection in a layered porous enclosure,* International Journal of Heat and Mass Transfer **106**, 1005 (2017).

[29] K. Vafai, *Convective flow and heat transfer in variable-porosity media,* Journal of Fluid Mechanics **147**, 233 (1984).

[30] T. Basak, S. Roy, and H. S. Takhar, *Effects of nonuniformly heated wall(s) on a natural-convection flow in a square cavity filled with a porous medium,* Numerical Heat Transfer, Part A: Applications **51**, 959 (2007).

[31] D. Das, M. Roy, and T. Basak, *Studies on natural convection within enclosures of various (non-square) shapes – a review,* International Journal of Heat and Mass Transfer **106**, 356 (2017).

[32] D. Das, P. Biswal, M. Roy, and T. Basak, *Role of the importance of 'forchheimer term' for visualization of natural convection in porous enclosures of various shapes,* International Journal of Heat and Mass Transfer **97**, 1044 (2016).

[33] A. Bagchi and F. Kulacki, *Natural convection in fluid–superposed porous layers heated locally from below,* International Journal of Heat and Mass Transfer **54**, 3672 (2011).

[34] D. Poulikakos, *Buoyancy-driven convection in a horizontal fluid layer extending over a porous substrate,* The Physics of fluids **29**, 3949 (1986).

[35] Y. Su, A. Wade, and J. H. Davidson, *Macroscopic correlation for natural convection in water saturated metal foam relative to the placement within an enclosure heated from below,* International Journal of Heat and Mass Transfer **85**, 890 (2015).

[36] H. Karani and C. Huber, *Role of thermal disequilibrium on natural convection in porous media: insights from pore-scale study,* Physical Review E **95**, 033123 (2017).

[37] M. Chakkingal, S. Kenjereš, I. Ataei-Dadavi, M. Tummers, and C. R. Kleijn, *Numerical analysis of natural convection with conjugate heat transfer in coarse-grained porous media,* International Journal of Heat and Fluid Flow **77**, 48 (2019).

[38] M. Chakkingal, S. Kenjereš, I. A. Dadavi, M. Tummers, and C. R. Kleijn, *Numerical analysis of natural convection in a differentially heated packed bed with non-uniform wall temperature,* International Journal of Heat and Mass Transfer **149**, 119168 (2020).

[39] M. Chakkingal, J. de Geus, S. Kenjereš, I. Ataei-Dadavi, M. Tummers, and C. R. Kleijn, *Assisting and opposing mixed convection with conjugate heat transfer in a differentially heated cavity filled with coarse-grained porous media,* International Communications in Heat and Mass Transfer **111**, 104457 (2020).

[40] I. Ataei-Dadavi, M. Chakkingal, S. Kenjeres, C. R. Kleijn, and M. J. Tummers, *Experiments on mixed convection in a vented differentially side-heated cavity filled with a coarse porous medium,* International Journal of Heat and Mass Transfer **149**, 119238 (2020).

[41] D. D. Gray and A. Giorgini, *The validity of the Boussinesq approximation for liquids and gases,* International Journal of Heat and Mass Transfer **19**, 545 (1976).

[42] H. G. Weller, G. Tabor, H. Jasak, and C. Fureby, *A tensorial approach to computational continuum mechanics using object-oriented techniques,* Computers in Physics **12**, 620 (1998).

[43] A. Zenklusen, S. Kenjereš, and P. R. von Rohr, *Vortex shedding in a highly porous structure,* Chemical Engineering Science **106**, 253 (2014).

[44] A. Zenklusen, S. Kenjereš, and P. R. von Rohr, *Mixing at high schmidt number in a complex porous structure,* Chemical Engineering Science **150**, 74 (2016).

[45] T. Y. Chu and R. J. Goldstein, *Turbulent convection in a horizontal layer of water,* Journal of Fluid Mechanics **60**, 141 (1973).

[46] L. Valencia, J. Pallares, I. Cuesta, and F. X. Grau, *Rayleigh-bénard convection of water in a perfectly conducting cubical cavity: effects of temperature-dependent physical properties in laminar and turbulent regimes,* Numerical Heat Transfer, Part A: Applications **47**, 333 (2005).

[47] M. Chakkingal, R. Voigt, C. R. Kleijn, and S. Kenjereš, *Effect of double-diffusive convection with cross gradients on heat and mass transfer in a cubical enclosure with adiabatic cylindrical obstacles,* International Journal of Heat and Fluid Flow (Accepted) (2020).

[48] R. Issa, *Solution of the implicitly discretised fluid flow equations by operator-splitting,* Journal of Computational Physics **62**, 40 (1986).

[49] O. Shishkina, R. J. Stevens, S. Grossmann, and D. Lohse, *Boundary layer structure in turbulent thermal convection and its consequences for the required numerical resolution,* New Journal of Physics **12**, 075022 (2010).

[50] B. Castaing, G. Gunaratne, F. Heslot, L. Kadanoff, A. Libchaber, S. Thomae, X.-Z. Wu, S. Zaleski, and G. Zanetti, *Scaling of hard thermal turbulence in Rayleigh-Bénard convection,* Journal of Fluid Mechanics **204**, 1 (1989).

[51] S.-Q. Zhou and K.-Q. Xia, *Scaling properties of the temperature field in convective turbulence,* Physical review letters **87**, 064501 (2001).

[52] X.-D. Shang and K.-Q. Xia, *Scaling of the velocity power spectra in turbulent thermal convection,* Physical Review E **64**, 065301 (2001).

3

PORE-SCALE ANALYSIS OF HEAT TRANSFER IN A PACKED BED CAVITY HEATED FROM THE BOTTOM AND COOLED FROM THE TOP

We report numerical simulations of fluid natural convection with conjugate heat transfer in a bottom-heated, top-cooled cubical cavity packed with relatively large ($d/L = 0.2$) solid spheres in a Body Centered Tetragonal (BCT) configuration. We study largely varying solid-to-fluid thermal conductivity ratios between 0.3 and 198, for a fluid Prandtl number of 5.4 and fluid Rayleigh numbers between 1.16×10^6 and 1.16×10^8 and compare global heat transfer results from our present simulations to our previously published experimental results. The interplay between convection suppression due to the solid packing, and conductive heat transfer in the packing leads to three different regimes, each with a distinct impact of the solid packing on the flow and heat transfer. At low Rayleigh numbers $\approx 10^6$, all packings suppress convective flow. Compared to fluid only Rayleigh-Bénard convection, heat transfer is therefore reduced in low conductivity packings, whereas for high conductivity packings it is increased due to significant conductive heat transfer. At intermediate Rayleigh numbers $\approx 10^7$, low conductivity packings no longer suppress convection, whereas flow is still suppressed in high conductivity packings due to the thermal stratification imposed on the fluid by the solid. Consequently, heat transfer is lower compared to fluid only Rayleigh-Bénard convection, even in high conductivity packings. With a further increase of Rayleigh number $\gtrsim 10^8$, convection starts to be the dominant heat transfer mechanism in all packings, and convective heat transfer is close to that for fluid only Rayleigh-Bénard convection. The contribution of solid conduction in high conductivity packings causes the overall heat transfer to be above that for Rayleigh-Bénard convection [1].

[1] This Chapter is published in IJHFF with DOI: https://doi.org/10.1016/j.ijheatfluidflow.2019.03.008

NOMENCLATURE

Greek Symbols

α Thermal diffusivity,$(\lambda/\rho c_p)$, m^2/s

β Coefficient of volume expansion of fluid, K^{-1}

λ Thermal conductivity, W/m.K

ν Kinematic viscosity of fluid, m^2/s

ϕ Porosity

ρ Density of fluid, kg/m^3

Other symbols and Abbreviations

$\mathbf{u}^*$ non-dimensional pore-scale velocity, $\dfrac{\mathbf{u}}{U_0}$

$\mathbf{u}$ Pore-scale velocity, m/s

$\mathbf{g}$ accel. due to gravity (acts along Z axis), m/s^2

Θ^* Non-dimensional temperature, $\dfrac{T-T_c}{T_h-T_c}$

c_p Specific heat capacity, J/kg.K

d Diameter of sphere, m

Da Darcy number, K/L^2

E Effective heat transfer *w.r.t* RB convection

E_{conv} Effective convective heat transfer *w.r.t* RB convection

K Permeability

L Height of cavity, m

Nu_f Nusselt number based on fluid properties

Nu_c Non-dimensional heat transfer due to conduction in the porous media filled cavity

Nu_{RB} Nusselt number Rayleigh-Bénard convection

p Pressure, N/m^2

Pr Prandtl Number

Ra_f Rayleigh Number based on fluid properties, $\dfrac{\mathbf{g}\beta_f \Delta T L^3}{\nu_f \alpha_f}$

T Temperature, K

T_{ref} Reference temperature, $\dfrac{T_h+T_c}{2}$, K

t_0 characteristic time scale, $\frac{L}{U_0}$, s

U_0 characteristic velocity scale, $\frac{Ra_f{}^{3/7}\alpha}{L}$, m/s

X, Y, Z represents the rectangular coordinate system

PP Polypropylene

RB Fluid only Rayleigh-Bénard convection

Subscripts

c Cold

f Fluid

h Hot

n Normal to the surface

s Solid

3.1. INTRODUCTION

The study of convective heat transfer in porous media has been mostly based on Darcy's model for porous media, i.e. an approach in which porosity is accounted for in a volume-averaged sense. It assumes that the porous length scales are small compared to the flow and thermal length scales. In various practical applications, such as convection in gravel embankments [1], in heat exchangers [2], in packed bed reactors [3], in fins to enhance heat transfer [4] or in the hearth of blast furnaces [5], however, the porous material is coarse-grained, i.e. the porous length scales are not small compared to the dimensions of e.g. hydrodynamic and thermal boundary layers and thermal plumes.

Detailed studies on the approaches and challenges in modelling variable density flows in porous media reported in [6, 7] explain the use of the standard Darcy model and various extended Darcy models (such as the Darcy-Forscheimer model, which accounts for high-Reynolds number effects). All these models are based on the volume averaging approach, and, although not providing information on flow and thermal features at the pore-scale, these studies help us in understanding the global flow and heat transfer in porous media.

Numerical studies with both standard [8] and extended [9] Darcy models using a local thermal equilibrium assumption, where a single equation is used to describe the temperature in the fluid, as well as the porous medium, discuss the effects of particle size and thermal properties in heat transfer. They suggest that the critical Rayleigh number for the onset of convection predicted with the Darcy-Forscheimer model decreases from the value predicted by the standard Darcy flow model, as the particle diameter and/or the liquid-to-solid conductivity ratio is increased. The intensity of the convective flow is also reported to depend on the Darcy number Da and the fluid Prandtl number Pr_f. A Da independent asymptotic convective heat transfer regime is reported at higher Ra_f . Using separate energy equations for the solid and fluid regions have been reported [10] to lead to better predictions of overall heat transfer compared to the local equilibrium approach.

Whereas solid conduction may play an important role in the heat transfer in porous media at low Ra_f, convective heat transfer becomes increasingly dominant with increasing fluid Rayleigh number Ra_f [11, 12]. These experimental results calculate the thermal boundary layer thickness from the Nusselt number. The increase in Nusselt number with the thinning of thermal boundary layer hints at the increased contribution of convective flow in the heat transfer process. Considerable scatter in experimental data, however, is reported at moderate Ra_f. Visualization of the flow at the upper boundary of a porous media filled, bottom-heated cavity [13] shows an increase in lateral spread of the fluid velocity, suggesting an increase in the 3-dimensionality of the flow within the pore-space at higher Ra_f. Indeed, our recent particle image velocimetry experiments [14] in a bottom heated cavity packed with optically transparent hydrogel beads show an increase in flow velocities within the pore-space with an increase in Ra_f. However, the results from the experiments are limited to a 2D plane due to the complex geometry.

Studies on convection in cavities filled with comparatively coarse-grained porous media, such as packed beads [15], suggest the use of effective (i.e. volume averaged, combined for fluid and solid) medium properties to explain the heat transfer mechanism. Heat transfer measurements in different fluids and in porous media consisting of

beads of different conductivity and size, for instance, could be adequately quantified in terms of the effective Prandtl number of the porous medium. The overall heat transfer is reported to be independent of the fluid Prandtl number Pr_f when the effective Prandtl number of the medium is high. Similar studies on heat transfer in metal foams also report the influence of Ra_f and Da on heat transfer [16, 17].

However, in contrast to what is found in [15], for porous media like metal foams, it is reported [10, 18] that non-dimensional numbers calculated from effective medium properties are insufficient to fully characterize natural convective heat transfer. Studies on the influence of the shape and morphology of the solid structures in porous media [19] show that heat transfer depends on the specific surface area of the porous medium, further illustrating the need to analyse convective heat transfer in (coarse-grained) porous media while addressing local, 3-dimensional, pore-scale effects, rather than effective media properties alone. Such local information helps in understanding global heat transfer mechanisms [12], and is essential for the development and evaluation of Volume Averaged Navier Stokes (VANS) closure models for convective flow in such media [20, 21].

At present, a detailed study accounting for pore-scale flow and thermal effects in coarse-grained porous media is missing in the literature. In this paper, we present a detailed 3D numerical study, resolving the local convective flow and temperature distributions in coarse-grained porous media with conjugate heat transfer. This paper aims at understanding the heat transfer process in a bottom heated cubical cavity filled with a structured packing of relatively large spheres of varying conductivity, and teaches that the interplay between convection suppression due to the solid packing, and conductive heat transfer in the packing, leads to three different convection regimes, each with a distinct impact of the solid packing on the flow and heat transfer.

3.2. MATHEMATICAL FORMULATIONS AND NUMERICAL METHODS

3.2.1. PHYSICAL PROBLEM

Natural convection in porous media is analysed in a bottom-heated, top-cooled cubical cavity with dimensions $L\times L\times L$ at fluid Rayleigh numbers, in the range $1.16\times10^6 \leq Ra_f \leq 1.16\times10^8$. The porous medium is composed of spherical beads arranged in structured Body Centred Tetragonal (BCT) Packing. The ratio of the diameter of the beads, d to the length of the cavity, L is chosen to be 0.2. Due to the finite dimensions of the cavity, the average porosity is $\phi = 0.41$ (as opposed to $\phi = 0.302$ for an infinite BCT packing) and estimating the permeability from the Kozeny–Carman equation, $K = \frac{\phi^3 d^2}{180(1-\phi)^2}$ [22], we get $Da \sim 4\times10^{-5}$. Water is used as the fluid ($Pr_f = 5.4$). Various materials are studied as packing materials, resulting in solid-to-fluid thermal conductivity ratios between 0.3 and 198. As will be discussed later, the cases studied in this paper lead to stationary or slightly oscillatory laminar flows in the porous media filled cavity. With $\beta \sim 2\times10^{-4}\mathrm{K}^{-1}$ and $\Delta T < 10\mathrm{K}$, it is ensured in all our simulations that $\beta\Delta T << 1$ and thus the Boussinesq approximation is valid. Using the Boussinesq approximation [23], we numerically solve the transient Navier-Stokes and thermal energy transport equations for Newtonian flow and conjugate heat transfer in and between the fluid and the solid.

Fluid phase:

$$\nabla \cdot \mathbf{u} = 0 \tag{3.1}$$

$$\frac{\partial \mathbf{u}}{\partial t} + \mathbf{u} \cdot \nabla \mathbf{u} = -\frac{1}{\rho} \nabla p + \nu \nabla^2 \mathbf{u} + \mathbf{g}\beta(T_f - T_{ref}) \tag{3.2}$$

$$\frac{\partial T_f}{\partial t} + \mathbf{u} \cdot \nabla T_f = \alpha_f \nabla^2 T_f \tag{3.3}$$

Solid phase:

$$\frac{\partial T_s}{\partial t} = \alpha_s \nabla^2 T_s \tag{3.4}$$

For used symbols, we refer to the List of Nomenclature.
The solid and fluid regions are coupled via Dirichlet–Neumann Partitioning. The fluid region is solved with the Dirichlet boundary condition $T_f = T_s$ at the coupled interface, while the solid region is solved with Neumann boundary condition:

$$\lambda_f \frac{\partial T_f}{\partial n} = \lambda_s \frac{\partial T_s}{\partial n} \tag{3.5}$$

calculated locally. The fluid and solid regions are solved iteratively.

3.2.2. NUMERICAL METHOD

In order to perform numerical simulations in our present complex geometry, we make use of the capabilities of the OpenFOAM finite volume CFD solver [24]. We use unstructured tetrahedral grids to carry out numerical simulations for the packed bed cavities and structured grids for the reference (fluid only) Rayleigh-Bénard convection simulations (further referred to as RB convection). The application and accuracy of OpenFOAM in using arbitrary tetrahedral meshes has been scrutinized in [25], who conclude that differences between the solutions with unstructured tetrahedral grid cells and non-body conforming cartesian grids are small, but with additional computational costs for simulations with tetrahedral grids. The capability of OpenFOAM to accurately simulate momentum and mass transfer using unstructured grids are also discussed in [26, 27].

The above set of equations, Eq.(3.1)-(3.4) are thus discretized and fully resolved numerical simulations are carried out, using a conjugate heat transfer solver that we developed in OpenFOAM 2.4.0 [24]. The standard solver "chtMultiRegionFoam" in OpenFOAM is modified to account for the Boussinesq approximation as implemented in the standard solver "buoyantBoussinesqPimpleFoam". The temperature equation for the solid phase is treated as a passive scalar equation. In the simulations reported below, we use a 2nd order backward differencing time marching scheme and a 2nd order central differencing scheme defined as "backward scheme" and "limitedLinear" respectively in OpenFOAM to solve the convective and diffusive terms for both the solid and fluid phase [24]. The pressure-velocity-coupling at each time step is handled by the iterative PISO algorithm [28]. The energy transport equation (Eq.(3.3)) is solved with the divergence-free velocity obtained in each time step.

3.2.3. GEOMETRY AND BOUNDARY CONDITIONS

We use water as the working fluid and study a range of fluid Ra_f ($1.16\times10^6 \leq Ra_f \leq 1.16\times 10^8$) . The material of the BCT packed beads is varied to realize a large variation in solid-to-fluid thermal conductivity ratios, viz. $\lambda_s/\lambda_f = 0.3$ for polypropylene, 1.0 for hydrogel, 70 for steel and 198 for brass, respectively. The coordinate system is chosen such that gravity, **g** acts along Z axis. The bottom and top walls are isothermal at temperatures T_h and T_c ($T_h > T_c$) respectively. All vertical walls of the cavity are adiabatic. No-slip boundary conditions are applied at all walls.

A grid independence study is carried out using three different meshes. In all the simulations reported, the flow was found to be in the laminar regime, with slight oscillations at the highest Ra_f reported. Thus the global non-dimensional heat transfer at the walls, defined by the Nusselt number, was chosen as the criterion to check grid independence. On the coarsest mesh 1, a fixed tetrahedral grid cell size $h \approx d/8 \approx L/40$ was used in the solid phase and in the core of the cavity, and consequently also at the interfaces between the fluid and the solid spheres. Along the isothermal walls, the grid cell size was gradually refined to $h_{BL} \approx d/16 \approx L/80$. For the medium mesh 2 we used $h \approx d/12 \approx L/60$ and $h_{BL} \approx d/16 \approx L/80$, whereas for the finest mesh 3 we used $h \approx d/16 \approx L/80$ and $h_{BL} \approx d/32 \approx L/160$. At the highest studied Rayleigh number $Ra_f = 1.16\times10^8$, the deviation in overall Nusselt number obtained between mesh 2 and mesh 3 is found to be less than 3%. Consequently, the mesh 3 is used for all presented simulations, i.e. with a base grid size $h \approx d/16$, refined to $h_{BL} \approx d/32$ in the thermal boundary layers along the isothermal walls. The latter is in line with the recommendation $h_{BL}/L \approx 0.75 Nu_f^{-3/2}$ [29] and experimentally obtained values for Nu_f [14], and ensures a minimum number of 5-6 cells in the wall thermal boundary layers. The resulting mesh consists of $\sim 5\times10^6$ non-uniform tetrahedral grid cells. Because of the laminar flow characteristics varying from pure steady to slightly oscillatory, an adaptive time stepping is specified such that the Courant-Friedrichs-Lewy number is below 0.33. In practice, this led to a fixed simulation time step once a quasi-steady state had been reached.

3.3. RESULTS AND DISCUSSION

3.3.1. INSTANTANEOUS THERMAL FIELD FEATURES

To illustrate the influence of the solid-to-fluid thermal conductivity ratio on the temperature distribution in the cavity, Fig.3.1 shows side views of the thermal plumes (projected in the XZ-plane) at $t/t_0 = 20$ for a cavity packed with hydrogel (top) and brass beads (bottom) (solid-to-fluid thermal conductivity ratio of 1 and 198, respectively). The thermal plumes are identified as the isosurfaces of the instantaneous non-dimensionalized temperature $\Theta^* = 0.8$ [hot (red)] and 0.2 [cold (blue)] at $t/t_0 = 20$. In the brass packed cavity, at $Ra_f = 1.16\times10^7$, the thermal plumes are confined to a height less than the first layer thickness of the beads. In a cavity packed with hydrogel beads, on the other hand, cold and hot plumes meandering through the void space in the packing result in convective flow throughout the domain. At $Ra_f = 1.16\times10^8$, the thermal plumes meander and penetrate the pore spaces within the bulk of the porous medium as well as along the side walls, for both brass and hydrogel packings. Compared to $Ra_f = 1.16\times10^7$, we see a thinning of the thermal plumes at $Ra_f = 1.16\times10^8$. Such plume thinning at higher Ra_f

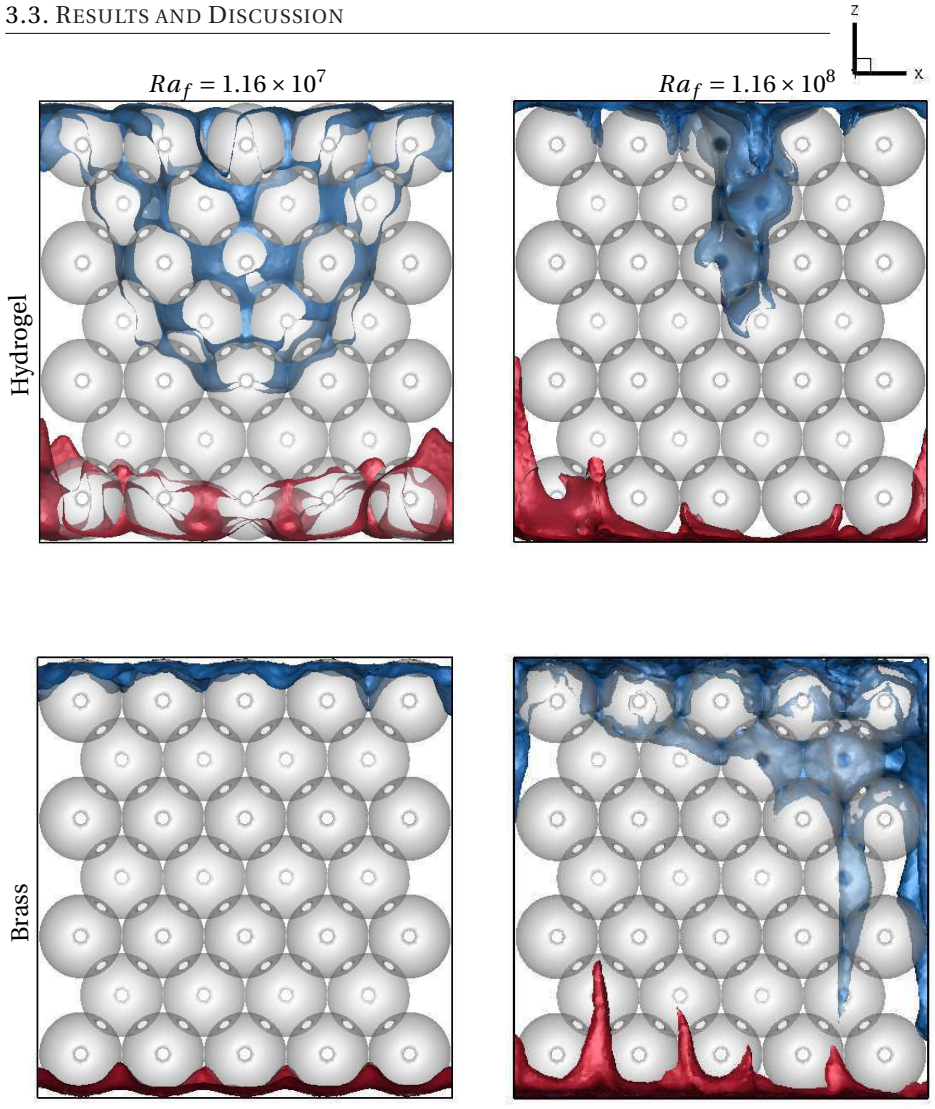

Figure 3.1: A side-view of the instantaneous non-dimensional temperature isosurfaces at $t/t_0 = 20$, in a cavity filled with hydrogel (top) and brass (bottom) beads at $Ra_f = 1.16 \times 10^7$ (left) and $Ra_f = 1.16 \times 10^8$ (right) ($\Theta^* = 0.2$,Blue; $\Theta^* = 0.8$,Red)

was also observed in our experimental study [14].

The nature of the flow structures is visible in Fig.3.2, showing instantaneous $u - w$ velocity vectors at $t/t_0 = 20$, in a characteristic vertical plane located at $Y/L = 0.62$. At $Ra_f = 1.16 \times 10^7$ (Fig.3.2), the flow is mainly localized along the side walls for brass packing. The horizontally stratified temperature distribution confirms the absence of prominent flow in core of the cavity. The flow structures change with the conductivity of the solid packing material. For low conductivity hydrogel packing, the flow is no longer localized along the side walls, but also prevalent throughout the cavity, with a

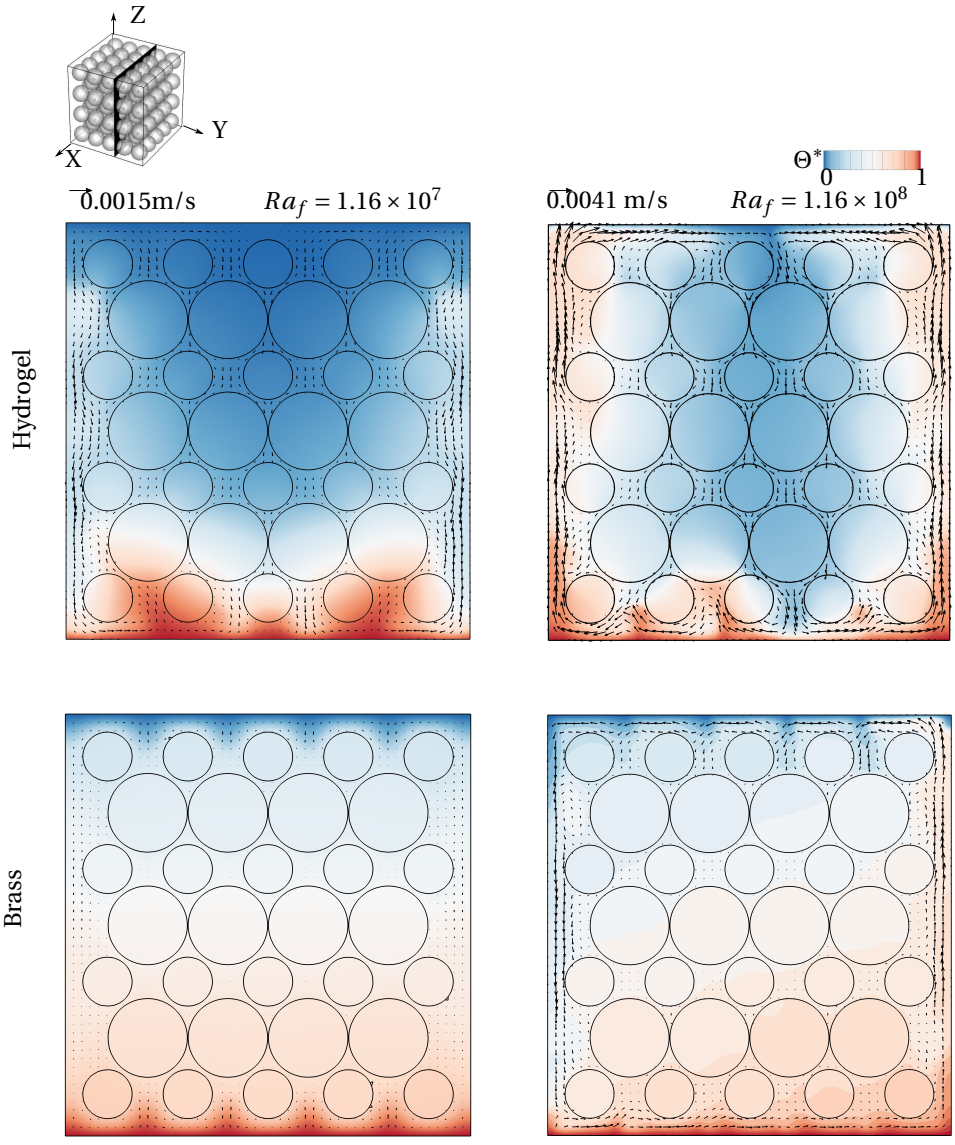

Figure 3.2: Instantaneous velocity vectors and temperatures at $t/t_0 = 20$, in a characteristic vertical plane at $Y/L = 0.62$ at $Ra_f = 1.16 \times 10^7$ (left) and $Ra_f = 1.16 \times 10^8$ (right), for a cavity packed with hydrogel (top) and brass (bottom) beads.

comparatively weaker flow in the core of the cavity. This has a strong impact on the temperature distribution. At $Ra_f = 1.16 \times 10^8$ (Fig.3.2), on the other hand, fluid flow is present throughout the cavity for both brass and hydrogel packings, as reflected in the temperature contours.

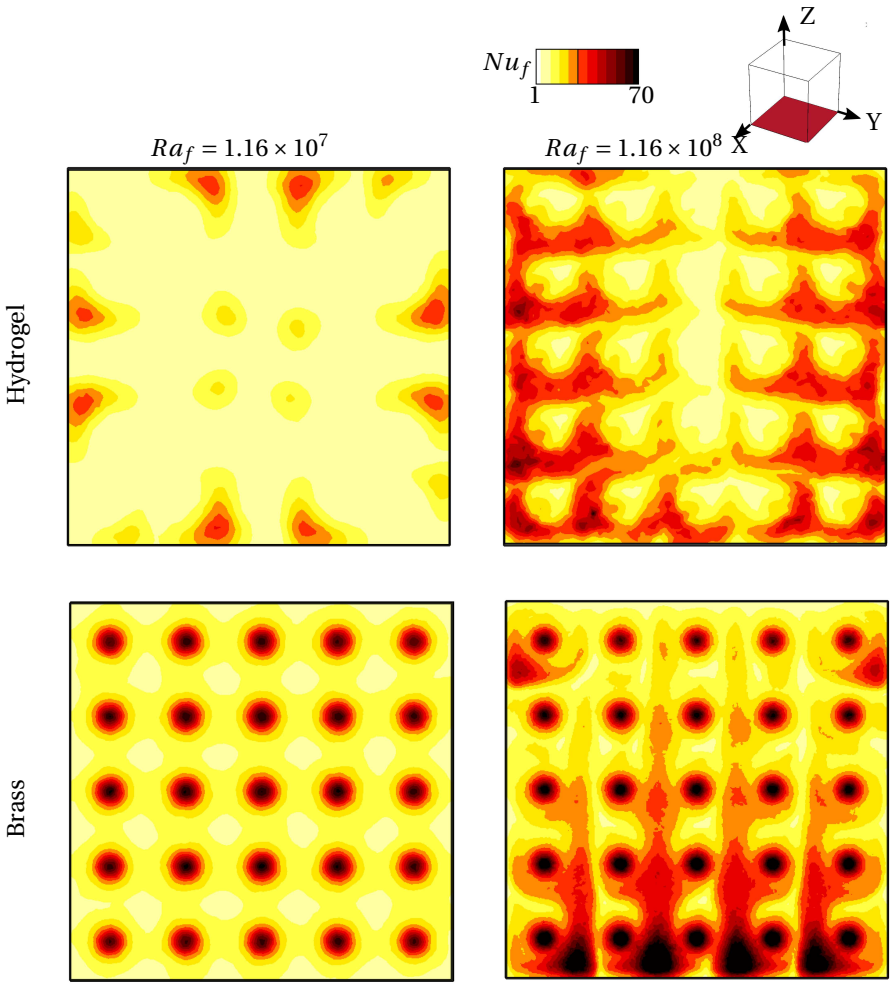

Figure 3.3: Instantaneous Nusselt number Nu_f distributions at the hot wall at $t/t_0 = 20$, in a cavity packed with hydrogel (top) and brass (bottom) beads, at $Ra_f = 1.16 \times 10^7$ (left) and 1.16×10^8 (right).

The local Nusselt number, Nu_f calculated as:

$$Nu_f = -\frac{L}{\Delta T}\left(\frac{\partial T}{\partial y}\right)_{wall} \tag{3.6}$$

where, ΔT and L are the temperature difference and distance between the hot and cold walls respectively, is analyzed at the hot wall to understand the influence of the packing material on heat transfer. The presence of coarse-grained porous media results in strong local variations of the (instantaneous) Nusselt number Nu_f along the isothermal walls, depending on the thermal conductivity of the packing material (Fig.3.3). For a high con-

ductivity brass packing and low $Ra_f = 1.16 \times 10^7$, local high Nu_f spots occur close to the point of contact of the spheres with the wall, due to the dominance of solid conduction over convective heat transfer in these points. At higher $Ra_f = 1.16 \times 10^8$, the contribution of convective heat transfer relative to solid conduction increases, and heat transfer becomes more uniform and higher on average.

For a low conductivity hydrogel packing and low $Ra_f = 1.16 \times 10^7$, high Nu_f regions occur mostly close to the side walls, due to the dominance of convective heat transfer in these regions. On average, however, heat transfer is lower than for brass packing. At higher $Ra_f = 1.16 \times 10^8$, convective heat transfer enhancement is no longer limited to the near wall regions, and heat transfer is more uniform along the entire isothermal wall. Although distributed differently along the wall, at $Ra_f = 1.16 \times 10^8$ the average heat transfer is dominated by convection and similar for both low and high conductivity packing.

3.3.2. INSTANTANEOUS FLOW FEATURE ANALYSIS

The instantaneous velocities ($\mathbf{u}$) are non-dimensionalized with characteristic velocity scale (U_0) [2] [30], such that the non-dimensional velocity vector $\mathbf{u}^*$ equals

$$\mathbf{u}^* = \frac{\mathbf{u}}{U_0}$$

In Fig.3.4, the vertical flow in the packed cavity is visualized by means of isosurfaces of the non-dimensional vertical velocity w^* being 0.2 (red) and -0.2 (blue) at $t/t_0 = 20$. At $Ra_f = 1.16 \times 10^7$, vertical flow is virtually absent in the case of a brass packed cavity, while in the hydrogel packed cavity a relatively strong vertical flow is present close to the side walls, with a weaker flow in the core of the cavity. At $Ra_f = 1.16 \times 10^8$, relatively strong vertical flows are present along the side walls as well as in the core of the cavity, both in brass and in hydrogel packed cavities. The flow in the core of the cavity is stronger in the case of a hydrogel packed cavity, compared to the brass packed cavity.

What was observed for the vertical velocity component, is also generally seen for the lateral velocity components. Fig.3.5 shows isosurfaces of the scaled lateral velocity v^*, i.e. the velocity component in the Y-direction at $t/t_0 = 20$. At low $Ra_f = 1.16 \times 10^7$, lateral flow is almost absent in the brass packed cavity, and mostly concentrated along the walls for the hydrogel packed cavity. At higher $Ra_f = 1.16 \times 10^8$, lateral flow in the core of the hydrogel packed cavity has strongly increased compared to $Ra_f = 1.16 \times 10^7$, resulting in significant lateral velocities throughout the cavity. In the brass filled cavity, even at higher $Ra_f = 1.16 \times 10^8$, lateral flows are concentrated along the walls and mostly absent in the core of the cavity.

The increased vertical and lateral flow velocities, along the walls and in the core of the cavity, as observed at higher Ra_f, cause convective heat transfer by the fluid to dominate over heat conduction in the solid, diminishing the difference of overall Nu_f for low and high conductivity packing materials, with increase in Ra_f.

[2] The convective velocity scale is calculated as:

$$U_0 = \frac{{Ra_f}^{3/7}\alpha}{L}$$

which follows from, $U_0 = \frac{\mathbf{g}\beta\Delta\mathbf{T_f}\delta_\theta^2}{\nu_f}$ where, $\delta_\theta = Ra_f^{-2/7}L$

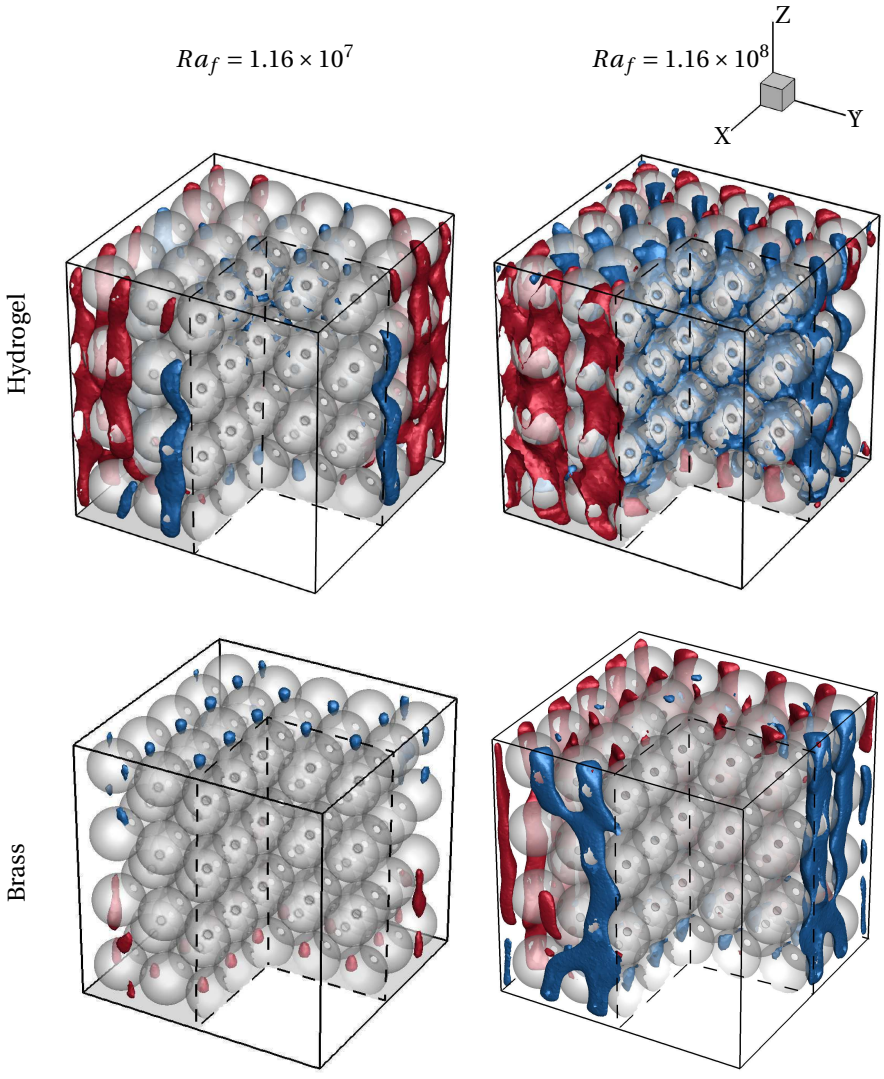

Figure 3.4: Instantaneous normalized vertical velocity isosurfaces, $w^* = 0.2$ (red) and $w^* = -0.2$ (blue) at $t/t_0 = 20$, in a cavity packed with hydrogel (top) and brass (bottom) at $Ra_f = 1.16 \times 10^7$ (left) and 1.16×10^8 (right).

3.3.3. PLANE AVERAGED FEATURES

In Fig.3.6(a) we show instantaneous scaled velocity magnitudes $U^* = (u^{*2} + v^{*2} + w^{*2})^{0.5}$ averaged over the XY-plane at $t/t_0 = 20$, as a function of Z/L, for both brass packed and hydrogel packed cavities at $Ra_f = 1.16 \times 10^7$ and $Ra_f = 1.16 \times 10^8$. Also included are the same plane averaged velocities for pure Rayleigh-Bénard (RB) convection in a water filled cavity at the same values of Ra_f. Due to the applied scaling, scaled velocities in RB convection are roughly independent of Ra_f. In the packed cavity, however, the

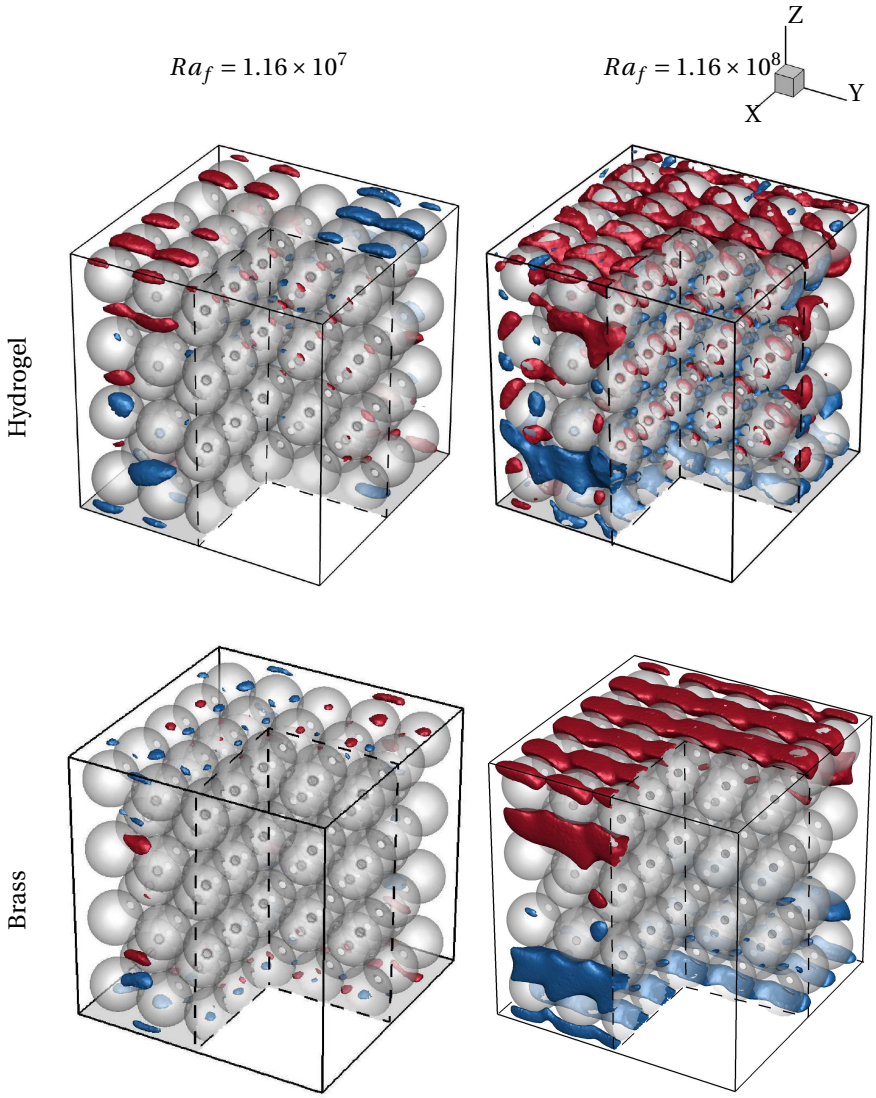

Figure 3.5: Instantaneous normalized lateral velocity isosurfaces, $v^* = 0.2$ (red) and $v^* = -0.2$ (blue) at $t/t_0 = 20$, in a cavity packed with hydrogel (top) and brass (bottom) beads at $Ra_f = 1.16 \times 10^7$ (left) and 1.16×10^8 (right).

scaled velocities strongly depend on Ra_f. At $Ra_f = 1.16 \times 10^7$, the scaled velocities in the hydrogel packed cavity are about an order of magnitude smaller compared to the RB convection, whereas they are yet another order of magnitude smaller in the brass packed cavity. This indicates that, at low Rayleigh numbers, convective heat transfer is small compared to that in RB convection in the hydrogel packed cavity, whereas it is negligible in the brass packed cavity dominated by conduction. At $Ra_f = 1.16 \times 10^8$, the average velocity magnitudes in the hydrogel and brass packed cavities are similar, and

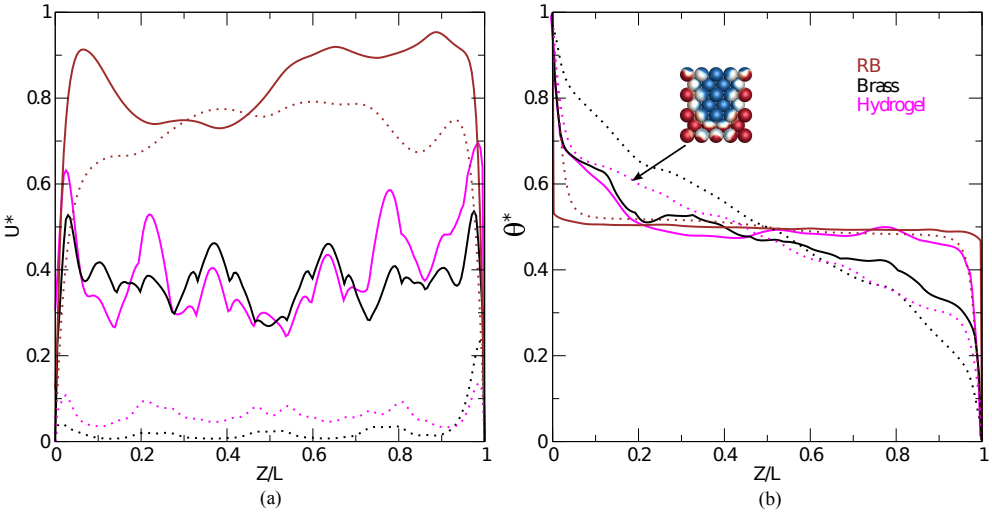

Figure 3.6: Instantaneous scaled velocity magnitudes U^* (a) and normalized temperatures Θ^* (b) at $t/t_0 = 20$, averaged over XY-planes as a function of Z/L, in RB convection (brown), hydrogel packed (pink) and brass packed (black) cavities at Ra_f=1.16×10^7 ($\cdots$) and 1.16×10^8(—). An example of the temperature distribution on the surface of the solid spheres is depicted in the inset.

only a factor two lower than in RB convection, confirming that convection starts to dominate the overall heat transfer in packed cavities at higher Rayleigh numbers, causing it to become independent of the packing material and to approach that of RB convection.

In Fig.3.6(b) we show instantaneous normalized temperatures, averaged over the XY-plane at $t/t_0 = 20$, as a function of Z/L, for both brass packed and hydrogel packed cavities at $Ra_f = 1.16 \times 10^7$ and $Ra_f = 1.16 \times 10^8$. Also included are the same plane averaged temperatures for pure Rayleigh-Bénard (RB) convection at the same values of Ra_f. At $Ra_f = 1.16 \times 10^7$, the plane averaged temperature in the brass packed cavity varies almost linearly with height, again indicating the dominance of solid conduction heat transfer over convection. In the hydrogel packed cavity on the other hand, the vertical temperature profile is strongly nonlinear due to the significance of convection, exhibiting thermal boundary layers at the isothermal walls that are similar to those in RB convection. In the core of the cavity, however, the temperature varies much more gradually in the hydrogel packed cavity, compared to RB convection. At $Ra_f = 1.16 \times 10^8$, the plane averaged temperatures close to the isothermal walls in the both packed cavities become similar to those in RB convection, whereas in the core of the cavity the temperature profile is still strongly influenced by the presence of the solid packing.

3.3.4. THE TIME EVOLUTION OF WALL-AVERAGED HEAT TRANSFER

In Fig.3.7 we show the time evolution of the instantaneous, bottom wall-averaged, Nusselt number for cavities packed with brass, steel and hydrogel beads ($\lambda_{brass} > \lambda_{steel} > \lambda_{hydrogel}$) at $Ra_f = 1.16 \times 10^7$ and 1.16×10^8, as well as for RB convection.

At the lower $Ra_f = 1.16 \times 10^7$, the solid packing suppress all flow and thermal fluctuations and the wall heat transfer is steady for all packing materials. In RB convection, on

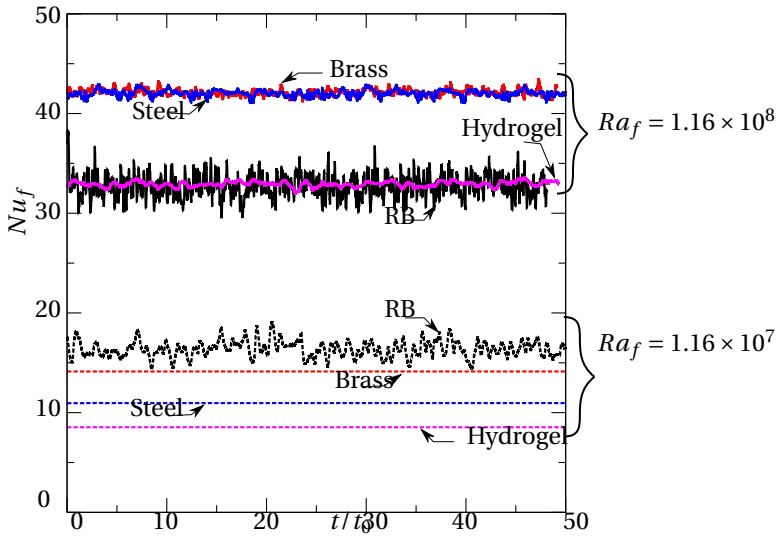

Figure 3.7: Time evolution of instantaneous, bottom wall-averaged, Nusselt number for cavities packed with brass (red), steel (blue) and hydrogel (magenta) beads, as well as for RB convection (black) at $Ra_f = 1.16 \times 10^7$ (dashed) and 1.16×10^8 (solid).

3

the other hand, significant (~ 10% peak-peak) fluctuations in heat transfer are being observed. In the packed cavities, the wall-averaged heat transfer increases with increased solid conductivity, but is always lower than for RB convection, due to the highly suppressed convection.

At the higher $Ra_f = 1.16 \times 10^8$, flow and heat transfer exhibit oscillatory behaviour, with peak-peak oscillations ~ 12% in RB convection to ~ 3% in the brass bead packed cavity. In all cases, however, the wall-averaged heat transfer is statistically steady. Due to the increased role of convection, heat transfer in the hydrogel packed cavity is almost equal to that in RB convection. For the high conductivity brass and steel packing, the conductive heat transfer along with the convective heat transfer, results in wall-averaged Nusselt numbers which are 30% higher than for the RB convection and hydrogel packed cavities.

3.3.5. ANALYSIS LONG-TERM TIME-AVERAGED WALL HEAT TRANSFER MECHANISMS

To understand the influence of thermal properties of the solid packing on heat transfer, we focus on the analysis of time and wall-averaged Nusselt numbers in Fig.3.8, in which Nusselt numbers obtained from the present simulations and from our experiments in [14] are compared for cavities packed with different materials, as well as fluid only RB convection, at different Ra_f. In Fig.3.8, the $Nu_f = 0.118 \times Ra_f^{0.3063}$ correlation obtained from our experiments for pure fluid RB convection at $10^7 < Ra_f < 10^8$ is extrapolated towards $Ra_f = 10^6$ for comparison with the packed cavity results at $Ra_f < 10^7$. For the RB convection, and hydrogel and brass packed cavities, Nusselt numbers obtained

from simulations are in good agreement with experimental results at $1.16\times10^7 \le Ra_f \le 1.16\times10^8$. At very low $Ra_f \approx 10^6$, heat transfer in steel and brass packed cavities is higher, and in hydrogel and polypropylene (PP) packed cavities is lower, than for the RB convection. As will be discussed in more detail below, at this low Rayleigh number, convection is effectively suppressed due to wall friction in all packings, eliminating convective heat transfer. The addition of a significant amount of solid conduction heat transfer in steel and brass, however, causes overall heat transfer in these packings to be larger than for RB convection. Increasing Ra_f to 10^7 causes an onset of convection and increasing Nusselt numbers in the low conductivity (PP and hydrogel) packings. In the steel and brass packings, on the other hand, convection is still suppressed at $Ra_f \approx 10^7$. As a result, for steel and brass the Nusselt number is fully determined by solid conduction and independent of Ra_f up to $Ra_f \approx 10^7$.

Upon a further increase to $Ra_f \approx 10^8$, convective heat transfer starts to dominate the overall heat transfer in all packings, causing Nusselt numbers to be very similar for brass and steel packings. At $Ra_f \approx 10^8$, the influence of solid conduction can still be observed, causing Nusselt number in steel and brass packings to be higher, and in PP and hydrogel packings to be lower than for RB convection.

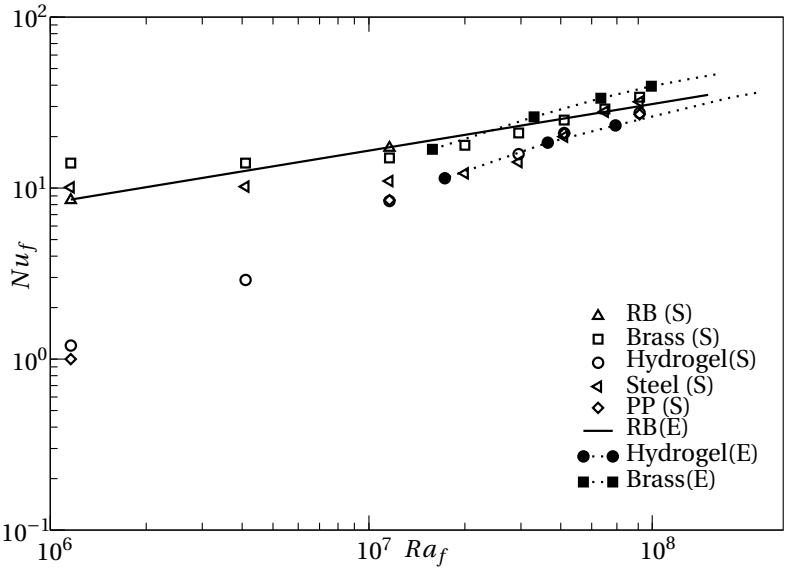

Figure 3.8: Simulated and experimental ([14]) long-term time-and-wall-averaged Nusselt numbers as a function of Rayleigh number for $1.16\times10^6 \le Ra_f \le 1.16\times10^8$ in cavities packed with polypropylene (PP), hydrogel, steel and brass, as well as in RB convection. The solid line represents the $Nu_f - Ra_f$ relation obtained experimentally for RB convection and the dotted lines connecting the symbols represent the asymptotic behavior of Nu_f with increase in Ra_f for different packing materials.

To further study the impact of coarse-grained solid packings on the overall heat transfer, the heat transfer enhancement factor E, defined as:

$$E = \frac{Nu_f}{Nu_{RB}} \tag{3.7}$$

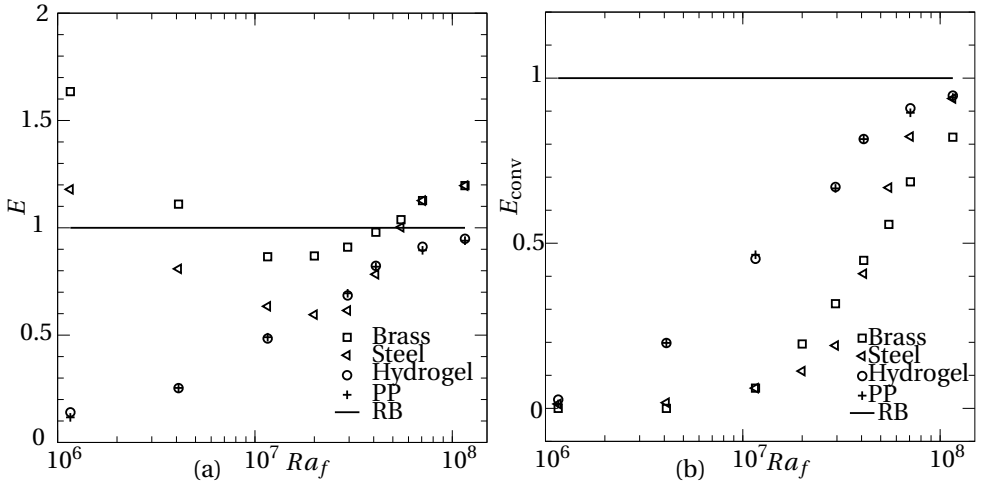

Figure 3.9: Heat transfer in a cavity packed with PP, hydrogel, steel and brass (a) scaled total heat transfer (b) scaled convective heat transfer.

is used to compare the overall heat transfer in packed cavities to that in an RB convection. When the enhancement factor $E > 1$, the coarse-grained solid packings enhances heat transfer compared to RB convection, whereas for $E < 1$ the coarse-grained solid packings reduces heat transfer.

For high thermal conductivity brass and steel packings, $E > 1$ at low $Ra_f \approx 10^6$. At increased Ra_f, E decreases, reaching a minimum around $Ra_f = 1-2\times10^7$, after which it increases with increasing Nu_f. For both materials, E appears to approach an asymptotic value around $E = 1.2$ for large Ra_f.

For the low thermal conductivity packings PP and hydrogel, $E < 1$ for the entire range of studied Ra_f. At very low $Ra_f \approx 10^6$, heat transfer is reduced by an order of magnitude compared to RB convection, due to the suppression of flow and the absence of significant conductive heat transfer. With increasing Ra_f, convective heat transfer increases and the total heat transfer seems to asymptotically approach that for RB convection ($E \to 1$ for $Ra_f \to \infty$).

From the above it is clear that conduction heat transfer plays a dominant role in high conductivity packings at low Rayleigh numbers, whereas convective heat transfer dominates at higher Rayleigh numbers and in low conductivity packings. In order to more precisely quantify the relative contribution of (solid and stagnant fluid) conduction and fluid convection to the total heat transfer, we calculate the effective convective enhancement factor, E_{conv} :

$$E_{\text{conv}} = \frac{Nu_f - Nu_c}{Nu_{RB} - 1} \tag{3.8}$$

where, Nu_c is the contribution of solid and (stagnant) fluid conduction to the overall heat transfer in packed cavities. Nu_c was obtained from simulations in which gravity was set to zero, thus leaving solid and stagnant fluid conduction as the only heat transfer mechanisms.

Fig.3.9 shows that, at low Ra_f, the contribution E_{conv} of convection to the total heat transfer enhancement is almost zero for all packings materials. This may be understood from the fact that convective flow is effectively suppressed due to wall friction in the coarse-grained packings. Thus it is concluded that E being larger than 1 at low at $Ra_f \approx 10^6$ for brass and steel packings is due to the increased thermal conduction, as compared to the situation for a fluid-only filled cavity.

At $Ra_f \approx 10^7$, the contribution E_{conv} of convection to the heat transfer enhancement is significantly less for steel and brass packings, compared to PP and hydrogel packings, with the latter two being almost equal. This indicates that convective flow is very similar in PP and hydrogel packings, whereas it is almost absent in the high conductivity packings. The latter can be understood from the stabilizing effect that the high conductivity packings has on the (no-flow) stratified temperature distribution. For brass and steel packings, even though $E > 1$ at $Ra_f = 1.16 \times 10^8$, E_{conv} is less than 1, and even lower than E_{conv} for PP and hydrogel packings. Apparently, even at this high Rayleigh number, at which convection is the dominant heat transfer mechanism for all packings, the relative contribution of convection to the overall heat transfer is still slightly lower for brass and steel packings, compared to PP and hydrogel packings.

3.4. SUMMARY AND CONCLUSION

We performed numerical simulations of fluid natural convection in bottom-heated, top-cooled cubical cavities packed with relatively large ($d/L = 0.2$) solid spheres of largely varying thermal conductivities (solid-to-fluid thermal conductivity ratios between 0.3 and 198), focusing on the pore-scale flow and heat transfer, at $1.16 \times 10^6 \leq Ra_f \leq 1.16 \times 10^8$. At low Rayleigh numbers $\leq 10^6$, the packings effectively suppresses convective heat transfer, irrespective of the packings material. As a result, the overall heat transfer is strongly reduced in low conductivity packings, as compared to pure Rayleigh-Bénard convection in a fluid-only filled cavity. For high conductivity solid packings, however, the overall heat transfer is increased compared to RB convection, due to a significant contribution of conductive heat transfer. At intermediate Rayleigh numbers $\approx 10^7$, low conductivity coarse-grained packings no longer suppress convection. High conductivity packings, on the other hand, have a strongly stabilizing effect on the (stagnant) stratified temperature distribution that would be present in e.g. zero gravity, and as a result, convective flow is still highly suppressed. Consequently, at intermediate Rayleigh numbers, the total heat transfer is lower than for RB convection, even in high conductivity packings.

With an even further increase of Rayleigh number $> 10^8$, convection starts to be the dominant heat transfer mechanism in packed cavities, irrespective of the packings material. As a consequence, convective heat transfer for all packings is close to that for RB convection, although the contribution of solid conduction in high conductivity packings causes the overall heat transfer to be above that for RB convection. These results help us to understand the mechanism of heat transfer in a porous media filled cavity with different packing materials.

The results presented in this paper have been obtained for mono-sized, relatively large ($d/L = 0.2$) packings of solid spheres. For such coarse packings, the overall flow strongly deviates from Darcy flow. The influence of sphere size on the trends observed

in this paper, e.g. on the Rayleigh number at which the overall heat transfer is no longer influenced by the presence of the solid packing, yet remains to be further studied, as is the transition from non-Darcy to Darcy behavior at shrinking sphere sizes. The influence of a multi-sized distribution of the sphere sizes of the packing was also beyond the scope of the present paper, but is a very interesting topic for further study. A lower porosity, resulting from the presence of spheres of varying size, close to the vertical walls might lead to a lower heat transfer, especially at low and intermediate Rayleigh numbers at which the convective flow is concentrated along the vertical walls.

REFERENCES

[1] D. J. Goering and P. Kumar, *Winter-time convection in open-graded embankments,* Cold Regions Science and Technology **24**, 57 (1996).

[2] A. Mohamad, *Heat transfer enhancements in heat exchangers fitted with porous media part I: constant wall temperature,* International Journal of Thermal Sciences **42**, 385 (2003).

[3] D. J. Gunn, *Transfer of heat or mass to particles in fixed and fluidised beds,* International Journal of Heat and Mass Transfer **21**, 467 (1978).

[4] M. Mesgarpour, A. Heydari, and S. Saedodin, *Numerical analysis of heat transfer and fluid flow in the bundle of porous tapered fins,* International Journal of Thermal Sciences **135**, 398 (2019).

[5] S. Ueda, S. Natsui, H. Nogami, J.-I. Yagi, and T. Ariyama, *Recent progress and future perspective on mathematical modeling of blast furnace,* ISIJ International **50**, 914 (2010).

[6] H.-J. Diersch and O. Kolditz, *Variable-density flow and transport in porous media: approaches and challenges,* Advances in water resources **25**, 899 (2002).

[7] D. A. Nield and A. Bejan, *Convection in Porous Media* (Springer New York, 2013).

[8] N. Kladias and V. Prasad, *Natural Convection in Horizontal Porous Layers: Effects of Darcy and Prandtl Numbers,* Journal of Heat Transfer **111**, 926 (1989).

[9] N. Kladias and V. Prasad, *Flow Transitions in Buoyancy- Induced Non-Darcy Convection in a Porous Medium Heated From Below,* Journal of Heat Transfer **112**, 675 (1990).

[10] M. S. Phanikumar and R. L. Mahajan, *Non-Darcy natural convection in high porosity metal foams,* International Journal of Heat and Mass Transfer **45**, 3781 (2002).

[11] H. Sakamoto and F. A. Kulacki, *Buoyancy Driven Flow in Saturated Porous Media,* Journal of Heat Transfer **129**, 727 (2007).

[12] D. J. Keene, *Thermal Convection in Porous Media at High Rayleigh Numbers,* Journal of Heat Transfer **137**, 1 (2015).

[13] C. R. B. Lister, *An explanation for the multivalued heat transport found experimentally for convection in a porous medium,* Journal of Fluid Mechanics **214**, 287–320 (1990).

[14] I. Ataei-Dadavi, M. Chakkingal, S. Kenjeres, C. R. Kleijn, and M. J. Tummers, *Flow and heat transfer measurements in natural convection in coarse-grained porous media,* International Journal of Heat and Mass Transfer **130**, 575 (2019).

[15] T. Jonsson and I. Catton, *Prandtl number dependence of natural convection in porous media,* Journal of Heat Transfer **109**, 371 (1987).

[16] V. Kathare, J. H. Davidson, and F. A. Kulacki, *Natural convection in water-saturated metal foam,* International Journal of Heat and Mass Transfer **51**, 3794 (2008).

[17] H. Xu and Z. Xing, *The lattice Boltzmann modeling on the nanofluid natural convective transport in a cavity filled with a porous foam,* International Communications in Heat and Mass Transfer **89**, 73 (2017).

[18] C. Y. Zhao, T. J. Lu, and H. P. Hodson, *Natural convection in metal foams with open cells,* International Journal of Heat and Mass Transfer **48**, 2452 (2005).

[19] C. Zhao, L. Dai, G. Tang, Z. Qu, and Z. Li, *Numerical study of natural convection in porous media (metals) using lattice boltzmann method (LBM),* International Journal of Heat and Fluid Flow **31**, 925 (2010).

[20] B. Blais and F. Bertrand, *On the use of the method of manufactured solutions for the verification of CFD codes for the volume-averaged Navier-Stokes equations,* Computers and Fluids **114**, 121 (2015).

[21] I. Thiagalingam, M. Dallet, I. Bennaceur, S. Cadalen, and P. Sagaut, *Exact non local expression for the wall heat transfer coefficient in tubular catalytic reactors,* International Journal of Heat and Fluid Flow **54**, 97 (2015).

[22] R. W. Johnson, *Handbook of fluid dynamics* (Crc Press, 2016).

[23] D. D. Gray and A. Giorgini, *The validity of the Boussinesq approximation for liquids and gases,* International Journal of Heat and Mass Transfer **19**, 545 (1976).

[24] H. G. Weller, G. Tabor, H. Jasak, and C. Fureby, *A tensorial approach to computational continuum mechanics using object-oriented techniques,* Computers in Physics **12**, 620 (1998).

[25] J. Finn and S. V. Apte, *Relative performance of body fitted and fictitious domain simulations of flow through fixed packed beds of spheres,* International Journal of Multiphase Flow **56**, 54 (2013).

[26] A. Zenklusen, S. Kenjereš, and P. R. von Rohr, *Vortex shedding in a highly porous structure,* Chemical Engineering Science **106**, 253 (2014).

[27] A. Zenklusen, S. Kenjereš, and P. R. von Rohr, *Mixing at high schmidt number in a complex porous structure,* Chemical Engineering Science **150**, 74 (2016).

[28] R. Issa, *Solution of the implicitly discretised fluid flow equations by operator-splitting,* Journal of Computational Physics **62**, 40 (1986).

[29] O. Shishkina, R. J. A. M. Stevens, S. Grossmann, and D. Lohse, *Boundary layer structure in turbulent thermal convection and its consequences for the required numerical resolution,* New Journal of Physics **12**, 075022 (2010).

[30] B. Castaing, G. Gunaratne, F. Heslot, L. Kadanoff, A. Libchaber, S. Thomae, X.-Z. Wu, S. Zaleski, and G. Zanetti, *Scaling of hard thermal turbulence in Rayleigh-Bénard convection,* Journal of Fluid Mechanics **204**, 1 (1989).

4

INFLUENCE OF NON-UNIFORM WALL TEMPERATURE ON HEAT TRANSFER IN A POROUS MEDIA FILLED DIFFERENTIALLY HEATED CAVITY

We report numerical simulations of natural convection and conjugate heat transfer in a differentially heated cubical cavity packed with relatively large hydrogel beads ($d/L = 0.2$) in a Simple Cubic Packing configuration. We study the influence of a spatially non-uniform, sinusoidally varying, wall temperature on the local flow and heat transfer, for a solid-to-fluid conductivity ratio of 1, a fluid Prandtl number of 5.4, and fluid Rayleigh numbers between 10^5 and 10^7. We present local and overall flow and heat transfer results for both sphere packed and water-only filled cavities, when subjected to variations of the wall temperature at various combinations of the amplitude and characteristic phase angle of the imposed wall temperature variations. It is found that imposing a sinusoidal spatial variation in the wall temperature may significantly alter the local flow and heat transfer, and consequently the overall heat transfer. At identical average temperature difference, applying a spatial variation in wall temperature at well-chosen phase angle can lead to significant heat transfer enhancement when compared to applying uniform wall temperatures. However, this is achieved at the cost of increased entropy generation, thus requiring a higher energy input to maintain the sinusoidal wall temperature [1].

[1] This Chapter is published in IJHMT with DOI: https://doi.org/10.1016/j.ijheatmasstransfer.2019.119168

NOMENCLATURE

Greek Symbols

α Thermal diffusivity,$(k/\rho c_p)$, m^2/s

β Coefficient of volume expansion of fluid, K^{-1}

ν Kinematic viscosity of fluid, m^2/s

ϕ Porosity

ρ Density of fluid, kg/m^3

ζ Fraction of maximum non-dimensional temperature, θ_{max}

k Thermal conductivity, W/m.K

Other symbols and Abbreviations

$<>_{Vf}$ Averaged over volume of fluid

$< Nu_f >$ Area-weighted average of the local Nusselt number on the left and right walls.

$\mathbf{u}^*$ Non-dimensional pore-scale velocity, $\dfrac{\mathbf{u}}{U_0}$

$\mathbf{u}$ Pore-scale velocity, m/s

ΔT Mean temperature difference between the left and right walls $T_r - \overline{T_l}$, K

$\mathbf{g}$ Accel. due to gravity (acts along Z axis), m/s^2

$\overline{T}$ Spatial mean temperature, K

Φ_{ph} Phase angle of the non-dimensional sinusoidal wall temperature at the left wall

Ψ Irreversibility coefficient, $\dfrac{\nu\rho T_{ref}}{k}\left(\dfrac{\alpha}{L(T_r-\overline{T_l})}\right)^2$

θ Non-dimensional temperature, $\dfrac{T-\overline{T_l}}{T_r-\overline{T_l}}$

θ_l^{amp} Amplitude of non-dimensional sinusoidal wall temperature at the left wall

θ_m Non-dimensional volume-averaged temperature of fluid

c_p Specific heat capacity, J/kg.K

d Diameter of sphere, m

L Height of cavity, m

Nu_f Local Nusselt number based on fluid properties, $-\dfrac{L}{\Delta T}\left(\dfrac{\partial T}{\partial y}\right)_{wall}$

p Pressure, N/m^2

Ra_f Rayleigh Number based on fluid properties, $\frac{g\beta_f \Delta T L^3}{\nu_f \alpha_f}$

$RMTD$ Root mean sq.deviation of temperature.

T Temperature, K

T_{ref} Average temperature between the walls $\frac{T_r + \overline{T_l}}{2}$, K

$Vol(f)_{CD}$ Cumulative distribution of fraction of fluid volume

$\dot{S_\theta}$ Total volumetric non-dimensional entropy generation representation

U_0 Characteristic velocity scale, $\frac{{Ra_f}^{1/2}\alpha}{L}$, m/s

X, Y, Z Represents the rectangular coordinate system

CWT Constant wall temperature

SWT Sinusoidal wall temperature

Subscripts

f Fluid

l Left wall

m Volume-weighted average

r Right wall

s Solid

4.1. INTRODUCTION

Natural convective heat transfer in porous-media is extensively studied owing to its occurrence in various industrial and technological applications like packed-bed reactors [1–3], solar air heaters [4], greenhouses [5], energy storage [6], solid waste treatment [7] etc. In most of these applications, the temperature distribution at the walls is non-uniform. For example, in green houses and solar collectors, the angle at which the sun rays fall at the surface can result in non-uniform wall temperature. This can influence the convective flow and thus the effective heat transfer.

Several studies have been carried out to investigate the influence of non-uniform wall temperature on natural convection in fluid-only and porous-media filled cavities. Numerical simulations of bottom heated - top cooled fluid-only [8] and porous media-filled [9] cavities with non-uniform wall temperatures report an increase in heat transfer with increase in the magnitude of the non-uniformity of the wall temperature. Similarly, an enhancement in heat transfer occurs in a side-heated fluid-only filled-cavity with non-uniform wall temperature [10] along with a significant change in the flow pattern. Similar studies with porous media filled side-heated cavities also report changes in flow patterns and consequent change in Nusselt number with the change in amplitude [11, 12] and wavelength of sinusoidal wall temperature variations [13, 14]. The phase difference between the sinusoidal temperature variations at the hot and cold walls is observed to significantly affect the temperature distribution [15], especially at large wavelengths in the wall temperature variation. However, in contradiction to the above literature, a non-uniform heating of the bottom wall and cooling of the side walls in fluid-only [16] and porous-media filled-cavities [17] result in the lowering of overall heat transfer rate when compared to cavities with constant wall temperature.

To understand and quantify the loss and degradation of energy under various heating arrangements, various researchers have turned to use entropy generation [18] as a guiding pathway. Studies on entropy generation to optimize the heat transfer process in porous-media filled-cavities with different thermal boundary conditions [16, 19], suggest that heating at discrete locations is an effective strategy for optimal thermal processing of materials. Studies on temperature distribution and heat transfer optimization in fully and partially filled porous-media [20–22] indicate the strong influence of non-uniform temperature in entropy generation and pore-scale temperature distribution.

All the studies above on porous-media filled cavities are based on the Darcy assumption where one assumes that the porous length scales are small compared to flow and thermal scales, such that the detailed morphology of the porous medium does not influence the large scale flow and temperature distribution. However, in many real-life applications such as the ones reported above, the porous length scales are not small compared to their flow and thermal counterparts. Also, the variation in temperature distribution and the associated change in heat transfer demands for an in depth analysis of the influence of non-uniform temperature at the boundaries in systems where the flow and thermal scales are comparable to the pore-scale.

In our earlier work [23–25] we reported on the local flow and heat transfer in bottom-heated, top-cooled cavities with isothermal walls and filled with coarse grained porous media. In these studies we quantified the influence of material, packing, and size of coarse-grained porous-media on local flow and heat transfer at different Rayleigh num-

ber.

In the present work, we report detailed CFD simulations of a differentially heated coarse-grained porous-media filled-cavity with sinusoidal spatial variations in the wall temperature at different phase angles, to understand its influence on the local flow and temperature distribution and on entropy generation. We compare the flow and temperature distributions to those in a cavity with uniform wall temperatures. We also compare the results with water-only filled differentially heated cavities under similar conditions, to understand the influence of coarse-grained porous-media in enhancing/suppressing heat transfer.

4.2. MATHEMATICAL FORMULATIONS AND NUMERICAL METHODS

4.2.1. PHYSICAL PROBLEM

We analyze natural convection in a porous-media filled $L \times L \times L$ cubical cavity, with side-heated and side-cooled vertical walls. Water is used as the fluid ($Pr_f = 5.4$). The coarse-grained porous-media is composed of relatively large spherical hydrogel beads arranged in structured Simple Cubic Packing (SCP), resulting in a porosity, $\phi = 0.48$. A Simple Cubic Packing has pores that are geometrically similar to connected vertical and horizontal channels, facilitating flow channelling even at lower Rayliegh numbers and thus increasing the impact of the morphology of the coarse-grained packing on the thermal and flow behaviour. We choose the ratio of the diameter of the beads, d to the length of the cavity, L to be 0.2. The use of hydrogel beads results in a solid-to-fluid thermal conductivity ratio $k_s/k_f = 1$. The flow in differentially heated cavities at the Rayleigh numbers discussed later, is steady and laminar in nature. We numerically solve the steady-state incompressible Navier-Stokes equations and the energy equation for the fluid, and the energy equation for the solid. The heat transfer between the solid and the fluid domain results in a conjugate heat transfer problem. With the Boussinesq approximation ($\beta \Delta T << 1$)[26], all fluid properties are taken to be constant, except for the fluid density in the body-force term included in the Navier-Stokes equations.

Fluid phase:

$$\nabla \cdot \mathbf{u} = 0 \tag{4.1}$$

$$\mathbf{u} \cdot \nabla \mathbf{u} = -\frac{1}{\rho} \nabla p + \nu \nabla^2 \mathbf{u} + \mathbf{g} \beta (T - T_{ref}) \tag{4.2}$$

$$\mathbf{u} \cdot \nabla T_f = \alpha_f \nabla^2 T_f \tag{4.3}$$

Solid phase:

$$\alpha_s \nabla^2 T_s = 0 \tag{4.4}$$

For used symbols, refer to the List of Nomenclature.

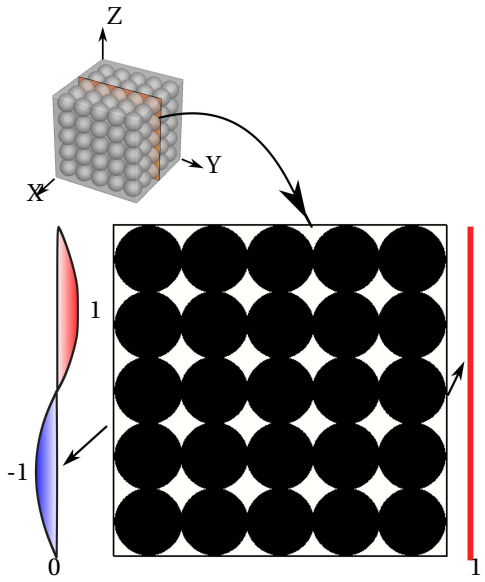

Figure 4.1: Geometrical representation of the differentially heated water filled cavity with hydrogel beads. The left wall has a sinusoidal non-dimensional temperature, $\theta_r = 1$, with $\overline{\theta_l} = 0$ and $\theta_l^{amp} = 1$.

4.2.2. NUMERICAL METHOD

For our porous media filled cavity simulations the above set of equations, Eq.(4.1)-(4.4) is discretized and steady-state numerical simulations [27] are carried using the conjugate heat transfer solver, "conjugateHeatSimpleFoam" available in foam-extend-4.0 [27], a fork of the OpenFOAM open source library for Computational Fluid Dynamics. We use unstructured tetrahedral grids to simulate the packed bed cavities. The capability of OpenFOAM to simulate flow using arbitrary tetrahedral meshes is discussed in [28–30]. The fluid temperature Eq.(4.3) and the solid temperature Eq.(4.4) of the conjugate heat transfer problem are combined into a combined matrix equation, by the method of block coupling [31, 32]. Thus the fluid flow equation is solved in the fluid region only, and the energy equation, discretised separately on the fluid and solid regions, is solved in a single linear solver call. This ensures a strong coupling between the solid and fluid regions. For water-only filled cavities we solve Eq.(4.1)-(4.3) using the OpenFOAM solver "BuoyantBoussinesqSimpleFoam", which is validated against the results reported in [33]. Here we use structured grids.

For both water-only and porous-media filled-cavities, a 2^{nd} order central differencing scheme, defined as "limitedLinear 1" in OpenFOAM, is used for the convective and diffusive terms [27]. The pressure-velocity-coupling at each iteration is handled by the iterative SIMPLE algorithm [34]. The energy transport equation Eq.(4.3), is solved with the divergence-free velocity obtained in each iteration.

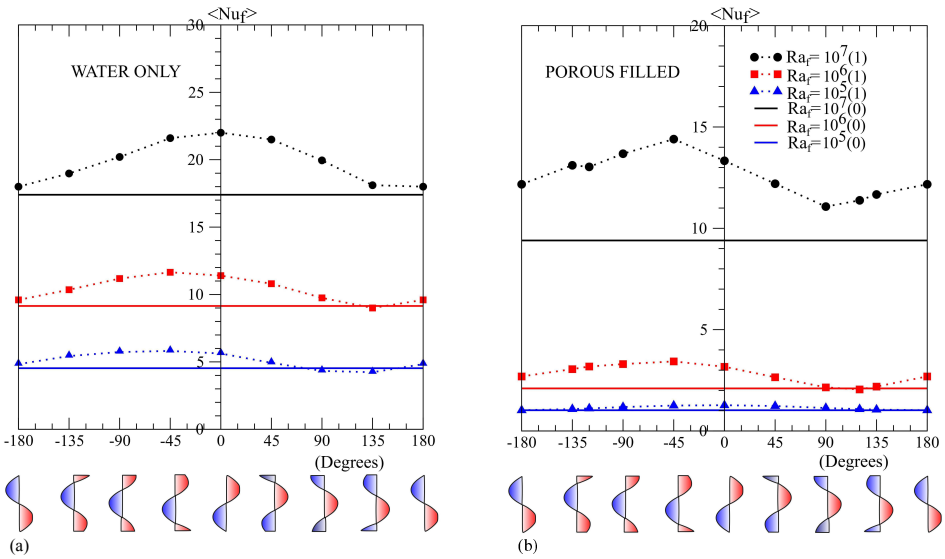

Figure 4.2: Variation of Nusselt number with phase angle at different Rayleigh numbers ($Ra_f = 10^5, 10^6, 10^7$) and different amplitudes, $\theta_l^{amp} = 0$(CWT), 1 in water-only (a) and porous media filled (b) cavity.

4.2.3. GEOMETRY AND BOUNDARY CONDITIONS

The simulations are carried out at Ra_f varying from 10^5 to 10^7. To analyze the data, the temperature and velocity are expressed in non-dimensionalized form (refer Nomenclature). The right wall of the cavities is maintained at a constant non-dimensional temperature, $\theta_r = 1$. The left wall of the cavity is maintained at:

1. a constant temperature (CWT), $\theta_l = 0$, or
2. a sinusoidally varying wall temperature (SWT):

$$\theta_l(z) = \theta_l^{amp} \sin\left(\frac{2\pi z}{L} + \Phi_{ph}\right) \tag{4.5}$$

with a mean temperature, $\overline{\theta_l} = 0$. The phase angle Φ_{ph} varies from $-180°$ to $180°$ (see Fig.4.1).

The influence of the amplitude of the sinusoidal temperature variation is studied by using two non-dimensional amplitudes, $\theta_l^{amp} = 0.5$ and 1. The phase angle, Φ_{ph} of the sinusoidal wall temperature variation is also varied. The system with CWT can also be visualized as a system with SWT, where $\theta_l^{amp} = 0$. All the other vertical and horizontal walls of the cavity are adiabatic. No-slip boundary condition is applied at all solid surfaces. Grid independence studies are carried out using three different unstructured tetrahedral grids with 1.9×10^6 (uniform grid size, $\Delta \approx d/16$), 5×10^6 (non-uniform grid size, $\Delta \approx d/16$ in the core and $\Delta \approx d/32$ at the walls of the cavity) and 1.03×10^7 cells (non-uniform grid size, $\Delta \approx d/16$ in the core and $\Delta \approx d/64$ at the walls of the cavity), at $Ra_f = 10^7$. Comparing the two finest meshes, a deviation in $< Nu_f >$ of $\sim 1\%$ is observed for the case

with maximum $< Nu_f >$ and a difference of ~ 0.8% in the case with minimum $< Nu_f >$. Therefore, the simulations at $Ra_f = 10^6$ and $Ra_f = 10^7$ are carried out with 5×10^6 and 1.9×10^7 cells respectively. We also confirm the quality of the mesh by comparing the degree of uniformity of temperature distribution $RMTD_m$ (as defined later in Eq.4.8) in the porous-media-filled cavity with the highest Nusselt number ($Ra_f = 10^7$,$\theta_l^{amp} = 1$, $\Phi_{ph} = -45°$) in which $RMTD_m$ changes by 2.2% when the mesh is refined from 5×10^6 to 1.9×10^7 cells. For the water-only filled cavity simulations, a grid independence study is carried out using 3 different structured grids; 32^3, 64^3 and 128^3 with a grid expansion ratio of 1.2. The deviation in maximum Nusselt number and $RMTD_m$ obtained with 64^3 and 128^3 are ~ 0.15% and ~ 0.5% respectively. Thus, the water-only filled-cavity simulations are carried out with the finest grid, 128^3.

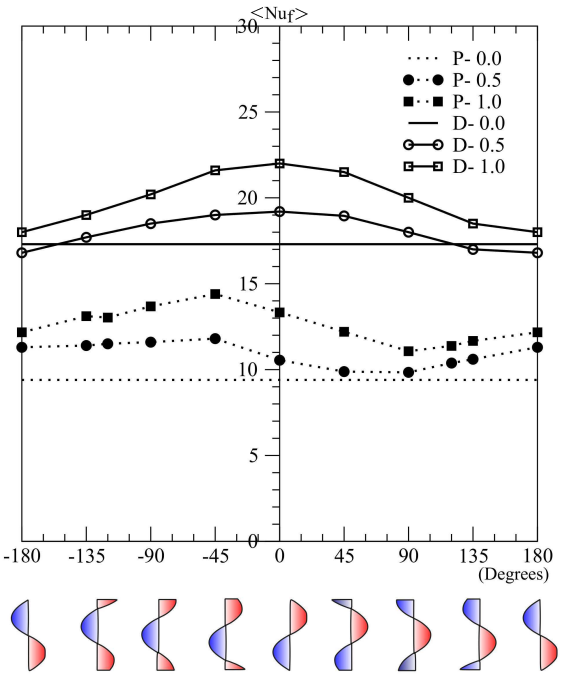

Figure 4.3: Variation of Nusselt number with phase angle at $Ra_f = 10^7$ and different amplitudes, θ_l^{amp} (0, 0.5, 1) of cold wall temperature variation in a differentially heated water-only cavity (**D**) and porous media filled-cavity (**P**).

4.3. RESULTS AND DISCUSSION

The heat transfer, flow and temperature distributions in the porous-media filled-cavities are compared to the results from water-only filled-cavities with CWT and SWT arrangements at various phase angles Φ_{ph}, three different $Ra_f = (10^5, 10^6, 10^7)$ and temperature variation amplitudes $\theta_l^{amp} = \{0.5, 1\}$.

4.3.1. WALL AVERAGED HEAT TRANSFER

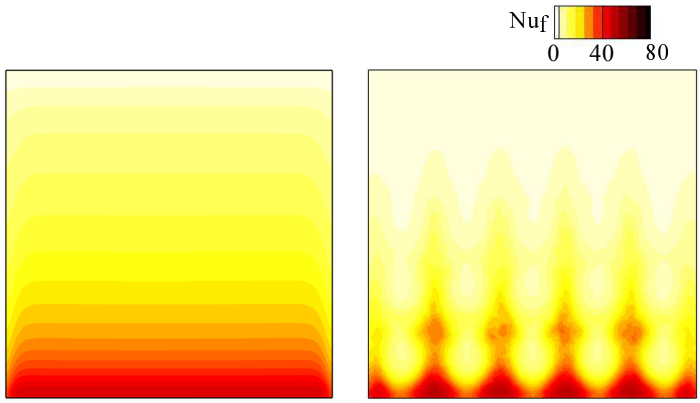

(a) Water only (b) Porous filled

Figure 4.4: Nusselt number contour on the right wall in a water-only (a) and porous media filled (b) cavity, with constant temperature of $\theta_l = 0$ and $\theta_r = 1$, at $Ra_f = 10^7$. The contours are represented using a linear scale with 30 contour levels.

To understand the influence of a sinusoidal wall temperature variation and its phase angle at different Ra_f, we focus on the wall averaged Nusselt numbers, $< Nu_f >$ (Fig.4.2). The wall-averaged Nusselt number is defined as the area-weighted value of the local Nusselt Number on the left and right walls.

The Nusselt numbers in water-only and porous-media filled cavities with SWT at $\theta_l^{amp} = 1$ and different phase angles, are compared with the cavities at CWT. For both CWT and SWT, the Nusselt number in water-only filled-cavity (Fig.4.2(a)) and porous-media filled-cavity (Fig.4.2(b)) increases with an increase in Ra_f. The wall-averaged Nusselt numbers obtained for water-only filled cavities with CWT follow the correlations [33]:

$$Nu_f = \begin{cases} 0.136 \times {Ra_f}^{0.305} & 700 < Ra_f \leq 10^6 \\ 0.236 \times {Ra_f}^{0.265} & 10^6 > Ra_f \end{cases}$$

with less than 2% deviation. Lower heat transfer is found in porous media filled CWT cavities.

With SWT non-uniform wall temperatures, the Nusselt number not only depends on Ra_f, but also on the amplitude θ_l^{amp} and the phase change Φ_{ph} of the sinusoidal temperature variations. In water-only filled cavities (Fig.4.2(a) and Fig.4.3), an amplitude $\theta_l^{amp} = 1$ leads to a maximum heat transfer enhancement of approximately 30% at $\Phi_{ph} = -45°$ for $Ra_f = 10^5 - 10^6$, and at $\Phi_{ph} = 0°$ for $Ra_f = 10^7$. This maximum heat transfer enhancement decreases with decreasing θ_l^{amp} (Fig.4.3). At some values of the phase changes Φ_{ph}, the application of varying wall temperatures may lead to a decrease in heat transfer, for instance at $Ra_f = 10^7$, $\theta_l^{amp} = 0.5$ and $\Phi_{ph} = 180°$ (Fig.4.3). In porous medium filled cavities, (Fig.4.2(b) and Fig.4.3), an amplitude $\theta_l^{amp} = 1$ leads to

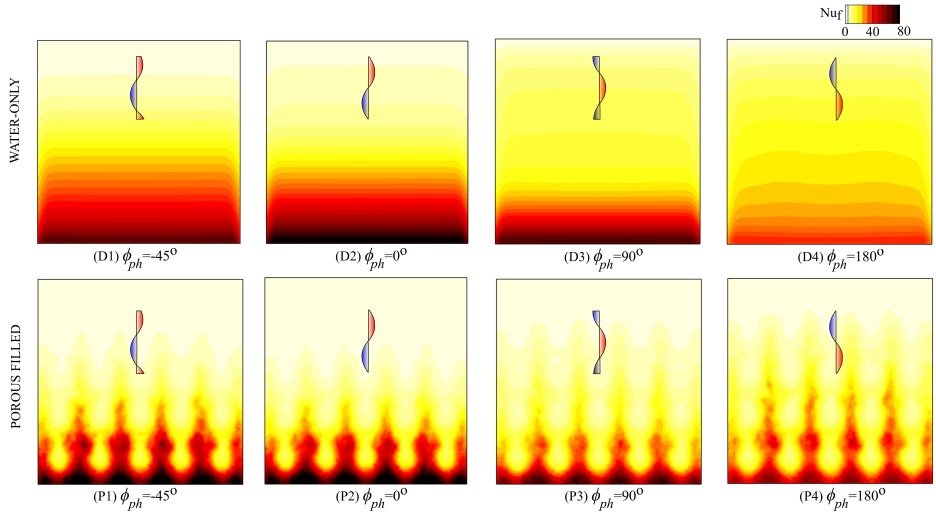

Figure 4.5: Nusselt number contour at the right wall in a water-only (**top row**) and porous media filled (**bottom row**) cavity, with the left wall having sinusoidal temperature distribution of amplitude $\theta_l^{amp} = 1$ and varying phase angle Φ_{ph}, at $Ra_f = 10^7$. The contours are represented using a linear scale with 30 contour levels.

a maximum heat transfer enhancement of approximately 60% at $\Phi_{ph} = -45°$ for $Ra_f = 10^5 - 10^7$. Again, this maximum heat transfer enhancement decreases with decreasing θ_l^{amp} (Fig.4.3). A decrease in heat transfer due to the application of non-uniform wall temperatures is not observed for porous medium filled cavities.

4

4.3.2. LOCAL NUSSELT NUMBER DISTRIBUTION

At first, we analyze the local Nu_f distribution at the right wall of both fluid-only and porous-media filled cavities (Fig.4.4) with CWT. The maximum heat transfer in a water-only cavity (Fig.4.4(a)) is uniformly distributed along the horizontal direction at the bottom of the right wall. In a porous-media filled cavity (Fig.4.4(b)) the maximum heat transfer is limited to the pore-space close to the bottom of the right wall resulting in a non-uniform heat transfer along the horizontal direction.

The heat transfer at the right wall in the porous-filled cavity is very low over a large fraction of the wall area, with heat transfer at the top being close to that due to pure conduction. The hydrogel beads obstructing the flow result in lower flow velocities in the porous-filled cavity (Fig.4.6(b)) when compared to the fluid-only cavity (Fig.4.6(a)). The obstructed flow at the top of the porous-filled cavity results in a conduction dominated temperature distribution near the top of the right wall, unlike the water-only filled cavity in which the temperature distribution is governed by convection.

To understand the influence of varying temperature distribution, a sinusoidal wall temperature with $\theta_l^{amp} = 1$ and different phase angle, Φ_{ph} is applied at the left wall. We analyze its influence on the Nu_f distribution at the right wall (which has a constant wall temperature $\theta_r = 1$) of water-only filled cavities and porous-media filled cavities in

Fig.4.5.

In both the cavities, the Nusselt number distribution at the right wall is influenced by the phase angle of the sinusoidal left wall temperature. In water-only cavities (Fig.4.5(D1-D4)), the maximum increase in heat transfer is observed at $\Phi_{ph} = 0°$ (D2) while a maximum heat transfer in porous-media filled cavities is observed at $\Phi_{ph} = -45°$ (Fig.4.5(P1)). Similar to the porous-media filled cavities with CWT (Fig.4.4), the Nusselt number distribution at the top of the right wall in porous-media filled cavities with SWT (Fig. 4.7(P1-P4)) is low owing to the hydrogel beads obstructing the flow, which again results in a conduction dominated temperature distribution near the top of the right wall.

4.3.3. LOCAL THERMAL AND FLOW FEATURES

The difference in local heat transfer between CWT and SWT, and its dependence on the phase angle in the latter, hints at variations in local temperature and flow features, which are further discussed in this section. The flow velocities **u** are non-dimensionalized with a characteristic velocity scale, U_0 (refer nomenclature) [35], such that:

$$\mathbf{u}^* = \frac{\mathbf{u}}{U_0} \tag{4.6}$$

Similarly, the temperature is non-dimensionalized with the right wall and average left wall temperature (refer nomenclature). In Fig.4.6 we analyze the flow and temperature distribution at $Ra_f = 10^7$, in a characteristic vertical plane at $X/L = 0.41$, in a water-only and porous medium filled-cavity at CWT. In the water-only cavity, large flow velocities are found in the thin boundary layers adjacent to the vertical walls. In the porous media filled cavity, the flow velocity is low resulting in comparatively thicker thermal boundary layers.

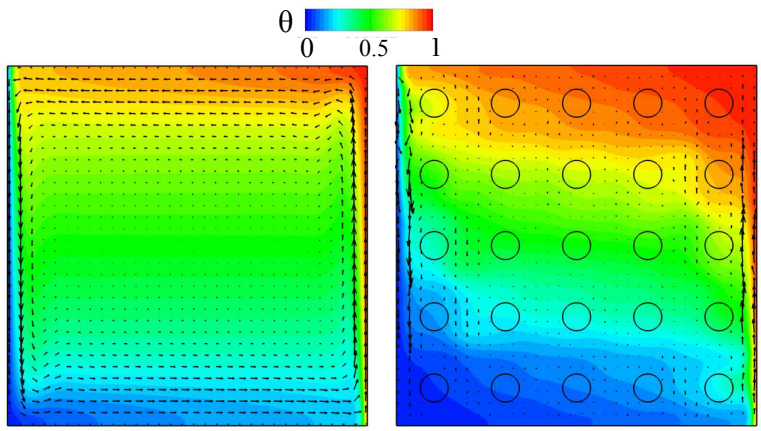

(a) Water only (b) Porous filled

Figure 4.6: Non-dimensional temperature contours and velocity vectors in a vertical plane at $X/L = 0.41$ in a water-only (a) and porous media filled (b) cavity, with constant temperature $\theta_l = 0$ and $\theta_r = 1$, at $Ra_f = 10^7$. The contours are represented using a linear scale with 30 contour levels.

When a sinusoidal temperature distribution at different phase angles is applied at the

left wall, the flow and temperature distributions change considerably (Fig.4.7) varying from stable temperature stratification with virtually no flow at the top of the cavity for $\Phi_{ph} = -45°$ (Fig.4.7 (D1,P1)) to flow penetrating into the core of the cavities at $\Phi_{ph} = 90°$ and 180° (Fig.4.7(D3-D4, P3-P4)). In the water-only cavity (Fig.4.7(D3-D4)), a large difference in the flow along the left and right wall is observed. However, no significant enhancement in heat transfer is obtained owing to the fluid impinging the right wall at a higher temperature (when compared to Fig.4.6(a)). In a porous media filled cavity (Fig.4.7(P1)), the colder fluid moving down the left wall is deviated to the right wall by the porous media, resulting in fluid at lower temperature to impinge the right wall and thus leading to an enhanced heat transfer when compared to the cavity at CWT, as observed in Fig.4.2(b). However, the heat transfer is lower than in a fluid-only cavity with similar wall temperature distribution (Fig.4.2(b)) owing to a lower flow velocity. The current observation indicates that the combined effect of variations in local porosity close to the wall and the local wall temperature can result in strong local and overall variations in heat transfer.

As discussed earlier, the integral heat transfer varies with the wall temperature distribution in both the water-only (Fig.4.2(a)) and porous media (Fig.4.2(b)) filled cavities. To understand this behaviour, we look at the local pore-scale temperature and horizontal flow velocity in both water-only and porous-media filled cavities close to the right wall, at $Ra_f = 10^7$. We already see from the Nusselt number contours that the maximum heat transfer from the right wall occurs at the bottom, and varies with the local temperature distribution at the left wall. The local pore-scale temperature along the vertical line $Y/L = 0.8$ in the plane $X/L = 0.41$ in both water-only (Fig.4.8(a)) and porous media filled (Fig.4.8(b)) cavties, close to the bottom of the right wall also varies strongly with the change in ϕ_{ph} of the SWT distribution. In the water-only filled cavities, the temperature at the bottom is lower in cavities with SWT than in the cavity with CWT (Fig.4.8(a)). The non-dimensional horizontal velocity u_y^*, with which the fluid impinges on the right wall, is higher in the cavity with SWT at $\phi_{ph} = -45°$ (Fig.4.9(a)), resulting in higher heat transfer (among the cases considered in the line plot) followed by the cavities with SWT at $\phi_{ph} = 90°$ and CWT. While in the porous media filled cavities, the combination of lower fluid temperature (Fig.4.8(b)) and higher non-dimensional horizontal velocity u_y^* (Fig.4.9(b)) (with which the fluid impinges on the right wall) is observed in the cavity with SWT at $\phi_{ph} = -45°$ followed by the cavities with SWT at $\phi_{ph} = 90°$ and CWT. Thus the combined effect of local temperature and velocity of the fluid results in the variation in heat transfer in both water-only and porous media filled cavities. Since the influence of the packing varies with the location of the plane, the effect of the variation in the local wall temperature of the left wall can be better understood from the domain averaged features.

4.3.4. DOMAIN AVERAGED THERMAL AND FLOW FEATURES

To understand the reason for the variation in heat transfer with amplitude and phase angle of SWT in the water-only and porous-media-filled cavity, we focus on volume-averaged temperature as discussed in the literature [36, 37]. The volume-averaged tem-

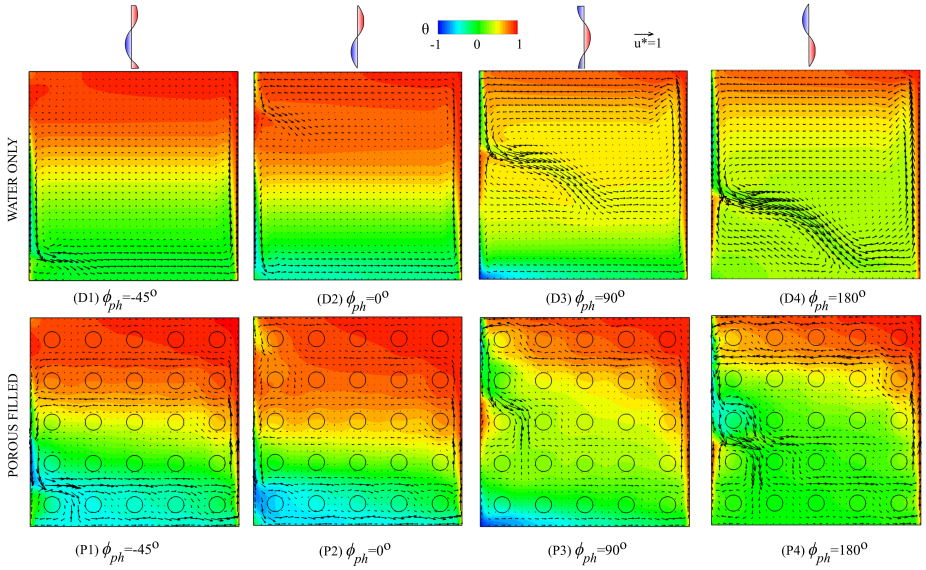

Figure 4.7: Non-dimensional temperature contours and velocity vectors in a vertical plane at $X/L = 0.41$ in a water-only (**top row**) and porous media filled (**bottom row**) cavities, with the left wall having a sinusoidal temperature distribution with amplitude $\theta_l^{amp} = 1$ and varying phase angle Φ_{ph}, at $Ra_f = 10^7$. The contours are represented using a linear scale with 30 contour levels.

perature of the fluid region θ_m defined as:

$$\theta_m = \frac{\int\int\int \theta_f d\Omega_f}{\int\int\int d\Omega_f} \tag{4.7}$$

varies in water-only and porous media filled cavities with Ra_f (Fig.4.10). In water-only filled-cavities and porous media-filled cavities at constant wall temperature $\theta_m = 0.5$ (Fig.4.10(D1,P1)) for all Ra_f. However, with a sinusoidal wall temperature, a variation in θ_m occurs with the change in phase angle and Rayleigh number, with a strong variation in porous-media filled cavities (Fig.4.10(P1)). The degree of uniformity of temperature distribution in the cavities is quantified by calculating $< RMTD >_m$ defined as:

$$RMTD_m = \sqrt{\frac{\int\int\int (\theta_f - \theta_m)^2 d\Omega_f}{\int\int\int d\Omega_f}} \tag{4.8}$$

The value of $RMTD_m$ ranges between 0 and 1, with a low of $RMTD_m$ indicating higher degree of uniformity in the fluid temperature.

In a water-only filled-cavity with constant wall temperature ($\theta_l^{amp} = 0$), the $RMTD_m$ (Fig.4.10(D2)) decreases with an increase in Ra_f. When a sinusoidal wall temperature is applied at the left wall, a variation in the $RMTD_m$ with phase angle Φ_{ph}, is observed. We observe the highest degree of temperature non-uniformity at $\Phi_{ph} = 0°$, and the smallest

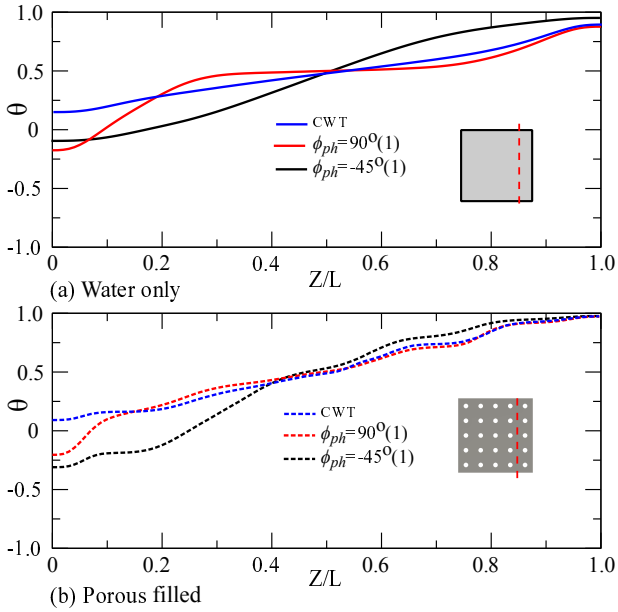

Figure 4.8: Non-dimensional temperature along the vertical line $Y/L = 0.8$, in a vertical plane at $X/L = 0.41$ in water-only (a) and porous media filled (b) cavities, with the left wall having a sinusoidal temperature distribution with amplitude $\theta_l^{amp} = 1$ at $\phi_{ph} = 90°$ (red) and $-45°$ (black), at $Ra_f = 10^7$. The results are compared with the respective cavities at constant wall temperature (blue).

4

at $\Phi_{ph} = 180°$. The minimum is less than the value in the cavity with constant wall temperature, indicating an increase in temperature uniformity with SWT at $\Phi_{ph} = 180°$ over the uniformity with constant wall temperature.

Unlike in a water-only cavity, in a porous-media filled-cavity with constant wall temperature, we observe a decrease in thermal uniformity with an increase in Ra_f. The increased flow close to the wall of the cavity results in a higher temperature difference between the regions close to the wall and core of the porous-media filled-cavity, eventually resulting in the increase in thermal non-uniformity with an increase in Ra_f. Strong variation in thermal uniformity with phase angle and Rayleigh number is visible in porous media filled cavities (Fig.4.10(P2)). The $RMTD_m$ in porous-media filled cavities at different phase angles and Rayleigh numbers are always higher than in a cavity with constant wall temperature.

The $RMTD_m$ gives an indication of uniformity in the cavities, but still doesn't completely explain the trend we observe in the Nusselt number (Fig.4.2). We can better understand the trend from the cumulative distribution of the fluid-volume of the cavity with the non-dimensional temperature ranging between $\theta_r = 1$ and $\overline{\theta_l} = 0$ (Fig.4.11) at a SWT amplitude of 1 and $Ra_f = 10^7$. In water-only cavities (Fig.4.11(a)) the fraction of fluid volume at temperatures close to 1 (right wall temperature) is higher at $\phi_{ph} = 0°$ and $-45°$ and so is the fluid at temperatures below 0 (mean left wall temperature). While in the cavity with SWT at $\phi_{ph} = 180°$ and in the cavity with CWT, the fraction of fluid-

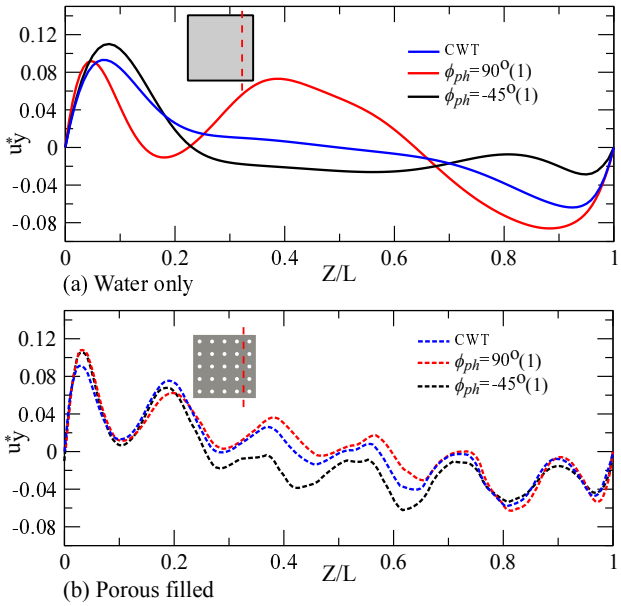

Figure 4.9: Non-dimensional horizontal velocity (u_y^*) along the vertical line $Y/L = 0.8$, in a vertical plane at $X/L = 0.41$ in water-only (a) and porous media filled (b) cavities, with the left wall having a sinusoidal temperature distribution with amplitude $\theta_l^{amp} = 1$ at $\phi_{ph} = 90°$ (red) and $-45°$ (black), at $Ra_f = 10^7$. The results are compared with the respective cavities at constant wall temperature (blue).

4

volume with temperature close to 1 is comparatively lower and no fraction of fluid volume has a temperature below 0. We obtain higher heat transfer in cavities with higher fraction of volume at temperature close to 1 and below 0 ($\phi_{ph} = 0°$ and $-45°$), and heat transfer comparable to cavity at constant wall temperature in the cavity with SWT at $\phi_{ph} = 180°$. Similar behaviour is observed in porous media filled cavities (Fig.4.11(b)). However, the heat transfer in the cavity at $\phi_{ph} = 180°$ is greater than in the cavity with CWT (Fig. 4.2(b)), due to the increased fraction of fluid at temperature lower than 0.

The increased values in $RMTD_m$ indicate the presence of strong temperature gradients which can result in the production of thermal entropy and thus increased thermodynamic irreversibility. In the current study the irreversibility coefficient Ψ, the ratio between the viscous and thermal irreversibilities [18] defined as:

$$\Psi = \frac{\nu \rho T_{ref}}{k} \left(\frac{\alpha}{L(T_r - \overline{T_l})} \right)^2 \tag{4.9}$$

is << 1. Thus, unlike cases where the contribution by the viscous dissipation is significant (as for example [38, 39]) the contribution of viscous dissipation to the total entropy generation is very low and is thus neglected in our analysis.

The local thermal entropy generated in the fluid, $\dot{S}_T'''$ is calculated as:

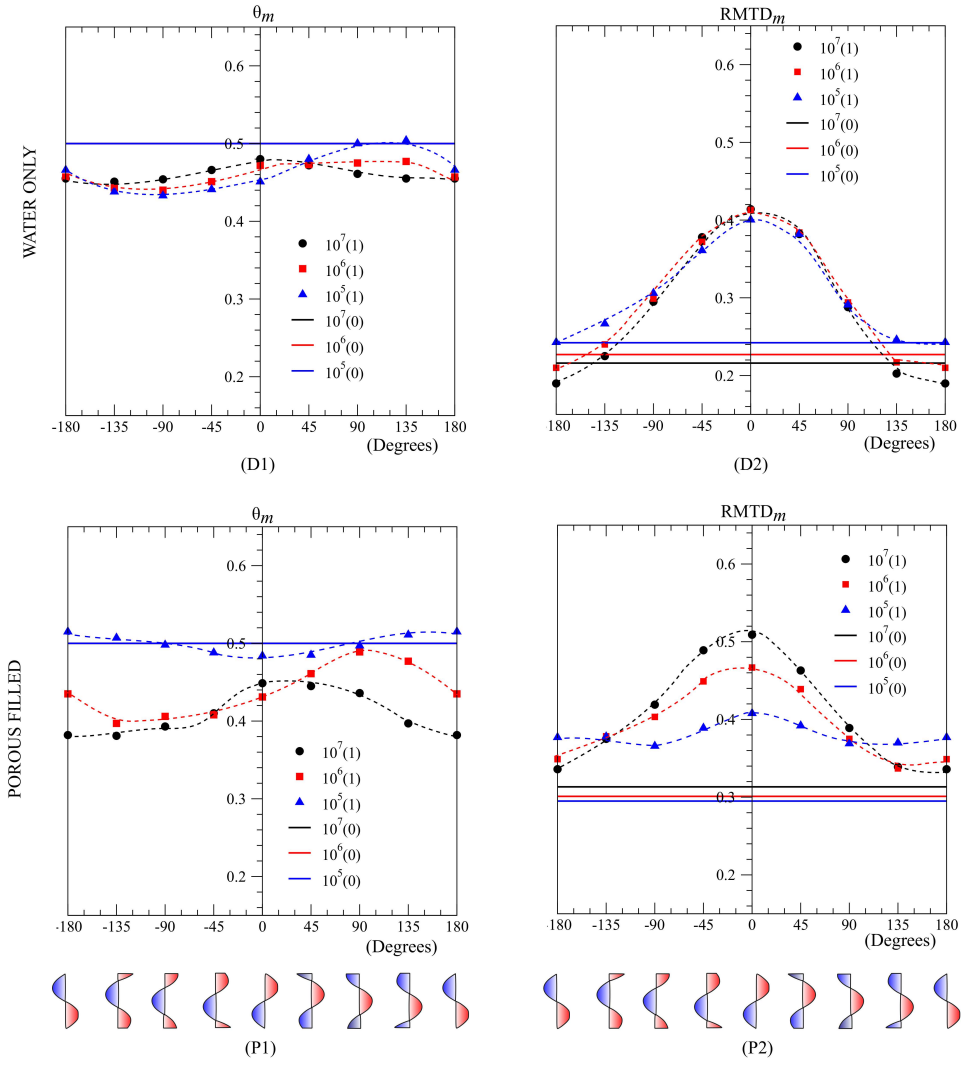

Figure 4.10: Variation of non-dimensional volume-averaged mean temperature (**D1, P1**) and $RMTD_m$ (**D2, P2**) of the fluid, with phase angle at different Rayleigh numbers ($Ra_f - 10^5, 10^6, 10^7$) and different amplitudes (0, 1) of sinusoidal wall temperature in a water-only (**top row**) and porous media filled (**bottom row**) cavity. The dotted lines are only to guide the eyes.

$$\dot{S}_T''' = \frac{k_f}{T_f^2} \nabla T_f \cdot \nabla T_f \tag{4.10}$$

It is scaled as:

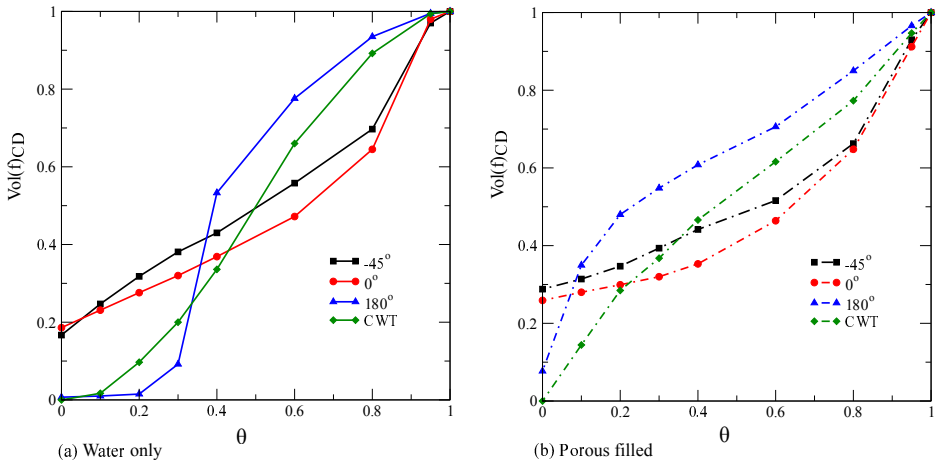

Figure 4.11: Cumulative distribution (discrete) of the fraction of fluid volume where $\theta \leq \zeta\theta_{max}$, in water-only (a) and porous media filled (b) cavities, with the left wall having a sinusoidal temperature distribution with amplitude $\theta_l^{amp} = 1$ at $\phi_{ph} = -45°$ (black), $\phi_{ph} = 0°$ (red), $\phi_{ph} = 180°$ (blue) at $Ra_f = 10^7$. The results are compared with the respective cavities at constant wall temperature (green).

$$\dot{S}'''_\theta = \frac{\dot{S}'''_T}{\frac{k_f}{T_{ref}^2}\left(\frac{\Delta T}{L}\right)^2} \tag{4.11}$$

for our visualizations reported in Fig.4.12 and Fig.4.13.

To compare the total entropy generated in the fluid region for different thermal configurations, we also define the total thermal entropy generated in the cavities as:

$$\dot{S_T} = \int\int\int \dot{S}'''_T d\Omega_f \tag{4.12}$$

where, the integration is carried out over the fluid volume only.
It is scaled as:

$$\dot{S_\theta} = \frac{\dot{S_T}}{\frac{k_f}{T_{ref}^2}\left(\frac{\Delta T}{L}\right)^2 L^3} \tag{4.13}$$

for the comparison of the different configurations reported in Fig.4.14.

In Fig.4.12(a, b), we observe that the non-dimensional thermal entropy generated in both fluid-only and porous medium filled cavities is higher close to the bottom and top of the vertical walls, where the temperature gradient is higher. The presence of spherical beads results in a comparatively higher temperature gradient at the core of the cavity (Fig.4.12(b)) than in a water-only cavity (Fig.4.12(a)), resulting in higher entropy generation. However, the flow of fluid "close to saturated temperature" (Fig.4.6(b)), redirected

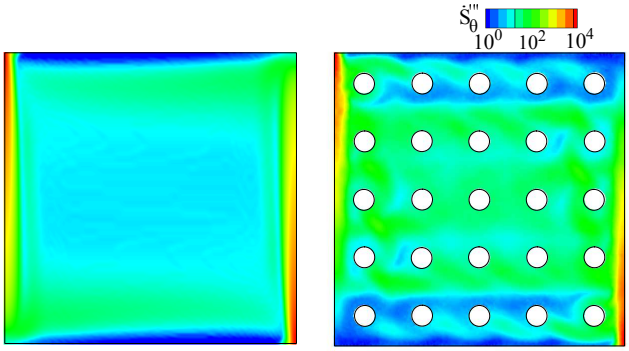

(a) Water-only (b) Porous filled

Figure 4.12: Entropy generated due to temperature gradient in the fluid region (log scale) in a characteristic vertical plane at $X/L = 0.41$ in a water-only (a) and porous media filled (b) cavity, with constant temperature left wall $\theta_l = 0$ and right wall temperature $\theta_r = 1$, at $Ra_f = 10^7$.

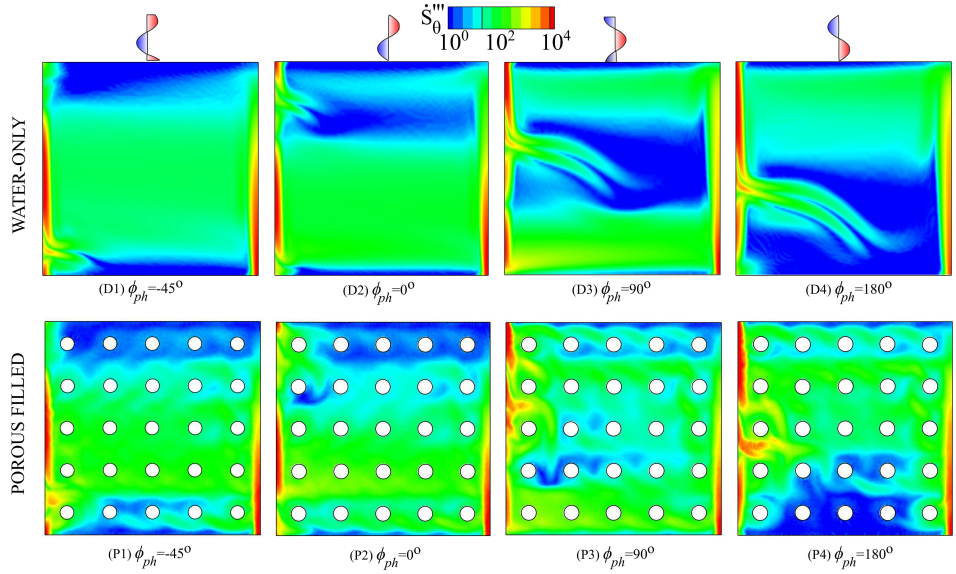

Figure 4.13: Entropy generated in the fluid region due to temperature gradient in a characteristic vertical plane at $X/L = 0.41$ in a water-only (**top row**) and porous media filled (**bottom row**) cavity, with the left wall having sinusoidal temperature distribution with amplitude $\theta_l^{amp} = 1$ and varying phase angle Φ_{ph}, at $Ra_f = 10^7$.

by the porous beads, results in lower temperature gradients at the pore-space close to the horizontal walls resulting in lower entropy generation (Fig.4.12(b)).

As expected, the influence of SWT on the local temperature distribution results in a change in entropy generated in both the cavities. The entropy generation in cavities with sinusoidal wall temperature variation (Fig.4.13(D1-D4, P1-P4)) is higher than in cavities

with constant wall temperature (Fig.4.12(a, b)). In a water-only filled-cavity with SWT at $\Phi_{ph} = -45°$, a decrease in the temperature gradient (Fig.4.7(D1)) close to the bottom and top of the cavity results in a lower entropy generation at these locations than in the cavity with constant wall temperature. However, the temperature gradient close to the vertical walls and in the core of the cavity increases, resulting in higher entropy generation at these locations than in the case with constant wall temperature. A shift in the regions with a lower entropy generation is evident from Fig.4.13(D1-D4). Close to the left wall of the water-only filled-cavity, we observe streaks of higher entropy generation which increase in size with increasing phase angle. With the change in phase angle, Φ_{ph} the locations at which maximum entropy is generated also changes. The presence of porous-media also results in an increase in entropy generation at all the phase angles (Fig.4.13(P1-P4)), when compared to the water-only cavities. The long streaks of entropy generation observed in the water-only cavities close to the left wall vanishes in the porous-media filled cavities.

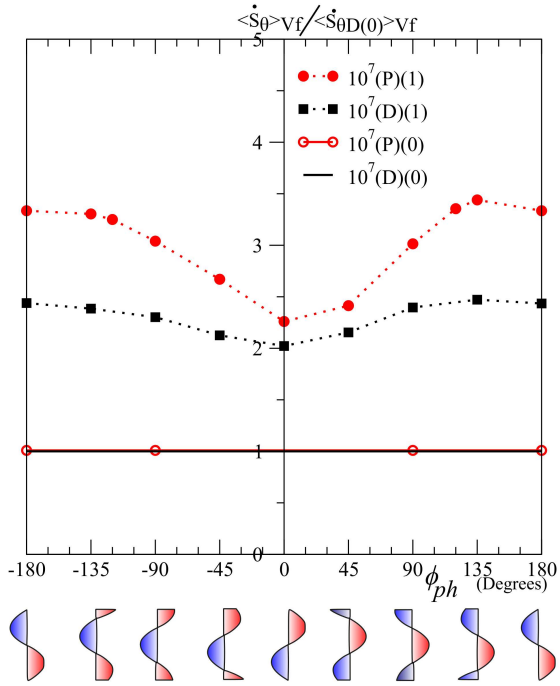

Figure 4.14: Variation of non-dimensional entropy generation of fluid due to temperature gradient with phase angle at $Ra_f = 10^7$, with SWT ($\theta_l^{amp} = 1$) and CWT ($\theta_l^{amp} = 0$) in a water-only **(D)** and porous media filled **(P)** cavity.

The spherical beads suppress and redirect the flow (Fig.4.7(P1-P4)), resulting in shorter/no streaks with high values of entropy generation. Instead of longer streaks of high entropy generation in the water-only cavity, the presence of spherical beads results in an increased entropy generation in the core of the cavity.

In Fig.4.14 we compare the average volumetric entropy generation (averaged over

fluid volume) at $Ra_f = 10^7$, with constant wall temperature and sinusoidal wall temperature at different phase angles. The average volumetric entropy generation, $< \dot{S}_\theta >_{Vf}$ in all the thermal configurations is scaled with the average volumetric entropy generated in a water-only filled-cavity with constant wall temperature, $< \dot{S}_{\theta D(0)} >_{Vf}$. From Fig.4.14, we observe that the total volumetric entropy generation in a water-only filled-cavity with sinusoidal wall temperature is roughly a factor 2 higher than in the water-only filled-cavity with constant wall temperature. The influence of the phase angle results in the maximum entropy generation at $\Phi_{ph} \approx \pm 135^\circ$ and a minimum entropy generation at $\Phi_{ph} \approx 0^\circ$. In a porous-media filled-cavity we see a similar effect of non-uniform wall temperatures on entropy production, but with an even larger increase.

4.4. SUMMARY AND CONCLUSION

We studied the influence that applying a spatially varying wall temperature to one of the thermally active vertical walls has on the flow and heat transfer in a differentially heated, water-filled, cubical cavity packed with relatively large spherical hydrogel beads. We showed that the phase angle and amplitude of sinusoidal wall temperature variations strongly influence the fluid flow and temperature distributions, and consequently the local and overall heat transfer. At identical average temperature difference, applying a spatial variation in wall temperature at well-chosen phase angle can lead to significant heat transfer enhancement when compared to applying uniform wall temperatures at the cost of increased entropy generation.

Both the presence of the sphere packing and the nature of the spatial temperature variations along the vertical walls were found to have a large impact on the velocity and temperature of the fluid impinging on the hot and cold walls. This indicates that a variation in the arrangement of the sphere packing and in the diameter of the spheres can result in different local and overall heat transfer. Also, the spatial distances at which we obtain maximum and minimum local heat transfer will vary with the amplitude, wave length and phase angle arrangement of the wall temperature variations, especially *w.r.t* the location of large porosity regions close to the wall.

A study on the influence of the spatial frequency of the sinusoidal wall temperature variations on the local flow and temperature distribution, and hence on the heat transfer, is recommended for future investigation. We expect that cavities with sinusoidal wall temperature variations will behave like the cavities with constant wall temperature in the limit of high spatial temperature variation frequencies, where the formation of local jet formation due to the interaction of the downward and upward flow close to the wall is expected to disappear.

REFERENCES

[1] D. J. Gunn, *Transfer of heat or mass to particles in fixed and fluidised beds,* International Journal of Heat and Mass Transfer **21**, 467 (1978).

[2] D. a. Nield and A. Bejan, *Springer*, Vol. 24 (2006) p. 640.

[3] D. B. Ingham and I. Pop, *Science* (2002) p. 449.

[4] A. Saxena, N. Agarwal, and G. Srivastava, *Design and performance of a solar air heater with long term heat storage,* International Journal of Heat and Mass Transfer **60**, 8 (2013).

[5] S. Reichrath and T. W. Davies, *Using CFD to model the internal climate of greenhouses: past, present and future,* Agronomie **22**, 3 (2002).

[6] H. Nazir, M. Batool, F. J. Bolivar Osorio, M. Isaza-Ruiz, X. Xu, K. Vignarooban, P. Phelan, Inamuddin, and A. M. Kannan, *Recent developments in phase change materials for energy storage applications: A review,* International Journal of Heat and Mass Transfer **129**, 491 (2019).

[7] J. Zhang, X. Kan, Y. Shen, K.-C. Loh, C.-H. Wang, Y. Dai, and Y. W. Tong, *A hybrid biological and thermal waste-to-energy system with heat energy recovery and utilization for solid organic waste treatment,* Energy **152**, 214 (2018).

[8] P. Chao, H. Ozoe, and S. W. Churchill, *The effect of a non-uniform surface temperature on laminar natural convection in a rectangular enclosure,* Chemical Engineering Communications **9**, 245 (1981).

[9] Y. Varol, H. F. Oztop, and I. Pop, *Numerical analysis of natural convection for a porous rectangular enclosure with sinusoidally varying temperature profile on the bottom wall,* International Communications in Heat and Mass Transfer **35**, 56 (2008).

[10] W.-s. Fu, C.-c. Tseng, and Y.-c. Chen, *Natural convection in an enclosure with non-uniform wall temperature,* International Communications in Heat and Mass Transfer **21**, 819 (1994), arXiv:0735-1933(94)00038-7 .

[11] Q.-h. Deng and J.-j. Chang, *Natural Convection in a Rectangular Enclosure with Sinusoidal Temperature Distributions on both Side Walls,* Numerical Heat Transfer, Part A: Applications **54**, 507 (2008).

[12] N. H. Saeid and Y. Yaacob, *Natural convection in a square cavity with spatial sidewall temperature variation,* Numerical Heat Transfer; Part A: Applications **49**, 683 (2006).

[13] N. H. Saeid and A. A. Mohamad, *Natural convection in a porous cavity with spatial sidewall temperature variation,* International Journal of Numerical Methods for Heat and Fluid Flow **15**, 555 (2005).

[14] S. Sivasankaran and M. Bhuvaneswari, *Natural convection in a porous cavity with sinusoidal heating on both sidewalls,* Numerical Heat Transfer; Part A: Applications **63**, 14 (2013).

[15] F. Wu, W. Zhou, and X. Ma, *Natural convection in a porous rectangular enclosure with sinusoidal temperature distributions on both side walls using a thermal non-equilibrium model,* International Journal of Heat and Mass Transfer **85**, 756 (2015).

[16] T. Basak, R. S. Kaluri, and A. R. Balakrishnan, *Effects of thermal boundary conditions on entropy generation during natural convection,* Numerical Heat Transfer; Part A: Applications **59**, 372 (2011).

[17] T. Basak, S. Roy, T. Paul, and I. Pop, *Natural convection in a square cavity filled with a porous medium: Effects of various thermal boundary conditions,* International Journal of Heat and Mass Transfer **49**, 1430 (2006).

[18] A. Bejan, *Entropy generation through heat and fluid flow* (Wiley, 1982).

[19] R. S. Kaluri and T. Basak, *Entropy generation due to natural convection in discretely heated porous square cavities,* Energy **36**, 5065 (2011).

[20] M. Torabi, K. Zhang, G. Yang, J. Wang, and P. Wu, *Heat transfer and entropy generation analyses in a channel partially filled with porous media using local thermal non-equilibrium model,* Energy **82**, 922 (2015).

[21] S. Du, M. J. Li, Q. Ren, Q. Liang, and Y. L. He, *Pore-scale numerical simulation of fully coupled heat transfer process in porous volumetric solar receiver,* Energy **140**, 1267 (2017).

[22] S. Bhardwaj, A. Dalal, and S. Pati, *Influence of wavy wall and non-uniform heating on natural convection heat transfer and entropy generation inside porous complex enclosure,* Energy **79**, 467 (2015).

[23] I. Ataei-Dadavi, M. Chakkingal, S. Kenjereš, C. R. Kleijn, and M. J. Tummers, *Flow and heat transfer measurements in natural convection in coarse-grained porous media,* International Journal of Heat and Mass Transfer **130**, 575 (2019).

[24] M. Chakkingal, S. Kenjereš, I. Ataei-Dadavi, M. Tummers, and C. R. Kleijn, *Numerical analysis of natural convection with conjugate heat transfer in coarse-grained porous media,* International Journal of Heat and Fluid Flow **77**, 48 (2019).

[25] I. Ataei-Dadavi, N. Rounaghi, M. Chakkingal, S. Kenjeres, C. R. Kleijn, and M. J. Tummers, *An experimental study of flow and heat transfer in a differentially side heated cavity filled with coarse porous media,* International Journal of Heat and Mass Transfer **143**, 118591 (2019).

[26] D. D. Gray and A. Giorgini, *The validity of the Boussinesq approximation for liquids and gases,* International Journal of Heat and Mass Transfer **19**, 545 (1976).

[27] H. G. Weller, G. Tabor, H. Jasak, and C. Fureby, *A tensorial approach to computational continuum mechanics using object-oriented techniques,* Computers in Physics **12**, 620 (1998).

[28] J. Finn and S. V. Apte, *Relative performance of body fitted and fictitious domain simulations of flow through fixed packed beds of spheres,* International Journal of Multiphase Flow **56**, 54 (2013).

[29] A. Zenklusen, S. Kenjereš, and P. R. von Rohr, *Vortex shedding in a highly porous structure,* Chemical Engineering Science **106**, 253 (2014).

[30] A. Zenklusen, S. Kenjereš, and P. R. von Rohr, *Mixing at high schmidt number in a complex porous structure,* Chemical Engineering Science **150**, 74 (2016).

[31] H. Rusche and H. Jasak, *Implicit solution techniques for coupled multi-field problems – Block Solution , Coupled Matrices,* Presentation , 22 (2010).

[32] I. Clifford, *Block-Coupled Simulations Using OpenFOAM,* Presentation , 1 (2011).

[33] A. M. Lankhorst, *Laminar and turbulent convection in cavities: Numerical modeling and experimental validation,* Ph.D. thesis, Technische Univ., Delft (Netherlands). (1991).

[34] S. V. Patankar, *Numerical heat transfer and fluid flow* (Hemisphere Pub. Corp. ; McGraw-Hill Washington : New York, 1980).

[35] J. Patterson and J. Imberger, *Unsteady natural convection in a rectangular cavity,* Journal of Fluid Mechanics **100**, 65 (1980).

[36] T. Basak, P. Gunda, and R. Anandalakshmi, *Analysis of entropy generation during natural convection in porous right-angled triangular cavities with various thermal boundary conditions,* International Journal of Heat and Mass Transfer **55**, 4521 (2012).

[37] T. Basak, R. S. Kaluri, and A. R. Balakrishnan, *Entropy generation during natural convection in a porous cavity: Effect of thermal boundary conditions,* Numerical Heat Transfer, Part A: Applications **62**, 336 (2012).

[38] G. Yang, J. Wu, and L. Yan, *Flow reversal and entropy generation due to buoyancy assisted mixed convection in the entrance region of a three dimensional vertical rectangular duct,* International Journal of Heat and Mass Transfer **67**, 741 (2013).

[39] G. Yang and J. Wu, *Entropy generation in a rectangular channel of buoyancy opposed mixed convection,* International Journal of Heat and Mass Transfer **86**, 809 (2015).

5

ASSISTING AND OPPOSING MIXED CONVECTION WITH CONJUGATE HEAT TRANSFER IN A DIFFERENTIALLY HEATED CAVITY FILLED WITH COARSE-GRAINED POROUS MEDIA

We report numerical simulations of assisting and opposing mixed convection in a side-heated, side-cooled cavity packed with relatively large solid spheres. The mixed convection is generated by imposing a movement on the isothermal vertical walls. For a fluid Prandtl number of 5.4 and fluid Rayleigh numbers of 10^6 *and* 10^7*, we varied the modified Richardson number from 0.025 to 500. As in fluids-only mixed convection, we find that the mutual interaction between forced and natural convection, leading to a relative heat transfer enhancement in assisting - and a relative heat transfer suppression in opposing - mixed convection, is most prominent at a Richardson number of approximately one, when the Richardson number is modified with the Darcy number* Da *and the Forcheimer coefficient* $C_f = 0.1$ *as* $Ri_m = Ri \times Da^{1/2}/C_f$*. We found that the ratio between the thermal boundary layer thickness at the isothermal walls and the average pore size plays an important role in the effect that the grain and pore size have on the heat transfer. When this ratio is relatively large, the thermal boundary layer is locally disturbed by the solid objects and these objects cause local velocities and flow recirculation perpendicular to the walls, resulting in significant differences in the wall-averaged heat transfer.* [1].

[1] This Chapter is published in ICHMT with DOI: https://doi.org/10.1016/j.icheatmasstransfer.2019.104457

NOMENCLATURE

Greek Symbols

α Thermal diffusivity,$(k/\rho c_p)$, m^2/s

β Coefficient of volume expansion of fluid, K^{-1}

λ Thermal conductivity ratio of solid to fluid, k_s/k_f

ν Kinematic viscosity of fluid, m^2/s

ϕ Porosity

ρ Density of fluid, kg/m^3

Other symbols and Abbreviations

ΔT Temperature difference between the left and right walls, K

$\mathbf{g}$ accel. due to gravity (acts along Z axis), m/s^2

$\mathbf{u}^*$ non-dimensionalized velocity

$\mathbf{u_w}$ moving wall velocity, m/s

$\mathbf{u}$ Pore-scale velocity, m/s

θ Non-dimensional temperature, $\dfrac{T-T_c}{T_h-T_c}$

c_p Specific heat capacity, J/kg.K

D Darcy only

d Diameter of sphere, m

$D+F$ Darcy and Forchheimer

Da Darcy number, K/L^2

FC Forced convection

K Permeability

k Thermal conductivity, W/m.K

k_m Stagnant thermal conductivity of porous medium, $k_m = 0.6$ for water-hydrogel bead system, W/m.K

L Height of cavity, m

MC Mixed convection

NC Natural convection

Nu_f Nusselt number based on fluid properties, $-\dfrac{L}{\Delta T}\left(\dfrac{\partial T}{\partial y}\right)_{wall}$

Nu_{eff} Relative strength of mixed convective heat transfer to that in natural and forced convection

p Pressure, N/m^2

Pr_f Prandtl Number based on fluid properties

Pr_m Modified porous medium Prandtl Number, $Pr_f Da^{-1/2} C_f \times (k_f/k_m)$

Ra_f Rayleigh Number based on fluid properties, $\dfrac{\mathbf{g}\beta_f \Delta T L^3}{\nu_f \alpha_f}$

Ra_m Porous medium Rayleigh Number, $Ra_f Da(k_f/k_m)$

Re_m Reynolds number porous medium, $\dfrac{u_w L}{\nu_f}\sqrt{Da}$

Ri Richardson number, $\dfrac{Ra_f}{Pr_f Re_L^2}$

Ri_m Modified Richardson number, $\dfrac{Ra_m}{Pr_m Re_m^2}$

T Temperature, K

T_p Combined temperature of the porous and fluid medium in Darcy simulation, K

T_{ref} Reference temperature, $\dfrac{T_h + T_c}{2}$, K

VAM volume averaged method

t_0 characteristic time scale, $\dfrac{L}{U_0}$, s

U_0 characteristic velocity scale, $\dfrac{{Ra_f}^{1/2}\alpha}{L}$, m/s

X, Y, Z represents the rectangular coordinate system

Subscripts

a Assisting

c Cold

f Fluid

h Hot

n Normal to the surface

o Opposing

s Solid

5.1. INTRODUCTION

In many real-life applications with forced convective heat transfer, the simultaneous effect of natural convection cannot be neglected. Several reported studies on this so-called mixed convection demonstrated the importance of considering natural convection effects along with imposed forced convection in the laminar [1, 2], laminar-turbulent transition and turbulent flow [3] regimes. The heat transfer mechanism of mixed convection differs from that of natural convection and forced convection because of the strong coupling between the externally imposed flow and the flow induced by density gradients as a result of temperature gradients. Thus, in addition to the fluid's Prandtl number (Pr), mixed convection heat transfer is generally governed by two dimensionless numbers, viz. the Rayleigh number (Ra) – which is a measure for the strength of natural convection heat transfer - and the Péclet number (Pe) – which is a measure for the strength of forced convection heat transfer. The ratio between the strengths of these two heat transfer mechanisms is determined by the so-called Richardson ($Ri = RaPr^2/Pe^2$) number, and mixed convection phenomena are particularly relevant for $0.1 < Ri < 10$.

In addition to numerous studies on mixed convection flow and heat transfer in fluid-only situations, mixed convective heat transfer in porous media is widely studied because of its practical relevance in for instance nuclear reactors [4], heat exchangers [5, 6], solar collectors [7, 8], geophysical systems [9] and electronic cooling [10]. Compared to fluid-only configurations, the presence of the porous medium significantly alters the flow and corresponding heat transfer [11–13]. An additional dimensionless parameter which now comes into play is the Darcy number, characterizing the permeability of the porous medium.

In literature, the great majority of experimental and numerical studies on pure natural [11, 14, 15] and forced [16–18] convection in porous media focus on the average flow and heat transfer features. A detailed collection of literature on mixed convective heat transfer in porous media is reported in [19, 20]. Most of the reported modelling studies were performed using a so-called Volume Averaging Method (VAM) approach to solve the large scale flow and temperature distributions in fine-grained porous media, applying Darcy and extended Darcy-type models for the flow and energy equations [21, 22]. Such VAM-based numerical studies of so-called assisting mixed convection (i.e. mixed convection in which the induced natural convection flow is in the same direction as the imposed forced convection flow) in fine-grained porous media revealed a continuous enhancement of heat transfer with both increasing Rayleigh and Péclet numbers [23, 24]. In contrast, for opposing forced convection, heat transfer initially decreases when Péclet number is increased at fixed Rayleigh number, followed by a gradual increase of heat transfer when Péclet is further increased [23].

Parametric studies of non-Darcy mixed convection in a vertical channel filled with a porous medium were performed in [25–27]. It was shown that the resulting heat transfer was enhanced when the Rayleigh and-/or Darcy numbers were increased. Effects of the conductivity ratio between the solid and the fluid, as well as different values of Darcy number were investigated in [28–34]. In most of the studies reported the contribution by forced convection is induced by moving the walls [35–37]. Though the flow close to the walls would differ from that in a cavity with a velocity inlet and an outlet (with zero flow velocity at the walls) , a lid-driven cavity displays different phenomena like corner

eddies, vortices, transition etc. in a comparatively simpler geometry [38], which makes it suitable to understand these phenomena observed in various real-life engineering applications like the ones listed above.

Modelling based on Darcy and extended Darcy-type of equations in combination with a form of the VAM does not suffice for situations characterized by relatively large pore scales. In particular, in numerous industrial and technological applications, such as gravel embankments [39], packed bed reactors [40], and the hearth of blast furnaces [41], the porous medium is coarse-grained, which means that the characteristic pore length scales are comparable to flow and thermal length scales [13]. For these situations, detailed insights into the local flow and temperature distributions are of crucial importance to understand local wall heat transfer phenomena, such as hot spots. Such insights, which can be obtained from modelling studies that fully resolve the geometrical structure of the coarse-grained porous medium, will reveal basic mechanisms for efficient flow and heat transfer control and potential optimizations. In our recent work on *pure natural* convection in coarse-grained porous media, we have attempted to explain the integral heat-transfer behaviour in terms of the local velocities and temperature distributions [12, 13, 42]. We observe the heat transfer to be dependent on the material of packing at low Rayleigh numbers, the effect of which decreases with the increase in Rayleigh number. However, what is still lacking in literature is insight in local, pore scale, flow and heat transfer mechanisms in *mixed* convection in coarse-grained porous media. In the current work, we study combined effect of forced convection induced by the motion of the cavity walls and natural convection due to the density difference induced by a horizontal temperature gradient in a porous media filled cavity. The current work aims at understanding the difference in heat transfer between coarse-grained simulations and Darcy/ extended-Darcy simulations in a generic mixed convective environment, like that in a lid-driven cavity and explain the difference based on local flow and temperature distribution.

5

5.2. MATHEMATICAL FORMULATIONS AND NUMERICAL METHODS

5.2.1. PHYSICAL PROBLEM

We analyze mixed convection in a differentially heated cubical cavity with dimensions $L \times L \times L$, filled with water ($Pr_f = 5.4$) and packed with a coarse-grained porous medium (Fig.5.1), at fluid Rayleigh numbers, $Ra_f = 10^6$ and 10^7. Spherical beads made of hydrogel (and thus having the same thermal properties as the fluid), are arranged in structured Body Centered Tetragonal (BCT) packing inside the cavity, to model a porous media filled cavity. The properties of the beads are chosen to be that of the fluid to avoid the complexity associated with the calculation of effective conductivity of the medium for Darcy and extended-Darcy simulations discussed below [43], which is out of the scope of current work. The ratio of the diameter of the beads, d to the length of the cavity, L is chosen to be 0.2. Finite dimensions of the cavity results in an average porosity of $\phi = 0.41$ (as opposed to $\phi = 0.302$ for an infinite BCT packing). The Darcy number, $Da = K/L^2 = \frac{\phi^3}{180(1-\phi)^2}\left(\frac{d}{L}\right)^2$ estimated using Kozeny–Carman equation is $Da \sim 4 \times 10^{-5}$ [14].

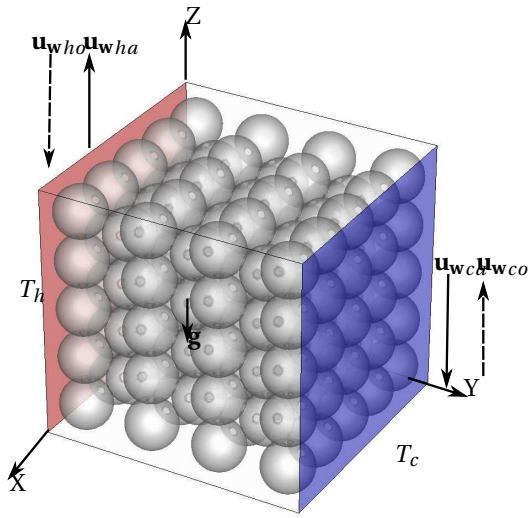

Figure 5.1: Schematic representation of a hydrogel bead filled side heated cavity with the side walls at temperature T_c and T_h. The arrows show the direction of moving wall.

The coordinate system is chosen such that gravity, **g** acts in the direction of the negative Z axis. The left and right walls are at isothermal temperatures T_h and T_c ($T_h > T_c$) respectively. All the other walls of the cavity are adiabatic. No-slip boundary conditions are applied at all walls. The hot and cold walls are given equal and opposite velocities in the vertical direction to induce forced convection, which assists or opposes the natural convection, depending on the direction of the wall velocities:

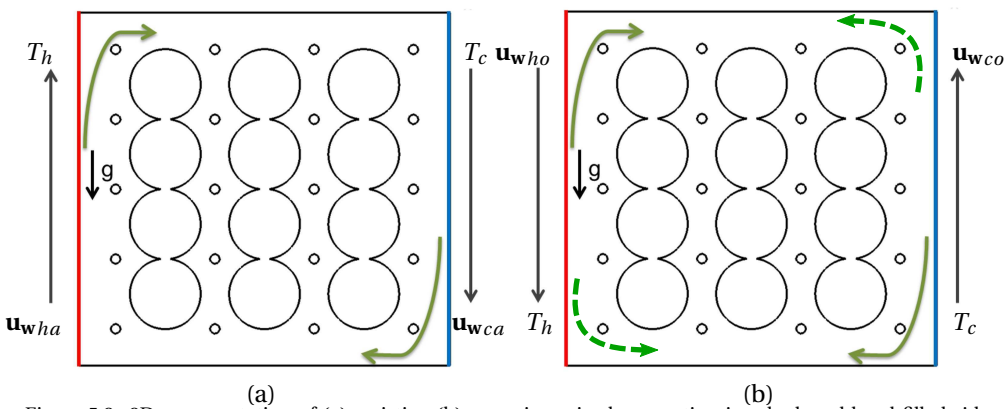

Figure 5.2: 2D representation of (a) assisting (b) opposing mixed convection in a hydrogel bead filled side heated cavity with the side walls at temperature T_c and T_h. In (a) solid arrows show the net flow due to forced and natural convection; in (b) dashed arrows and solid arrows show the direction of flow induced by forced convection and natural convection respectively.

1. **Assisting flow**: When the left hot wall moves in the upward direction ($\mathbf{u}_{\mathbf{w}ha}$) and the right cold wall moves in the downward direction ($\mathbf{u}_{\mathbf{w}ca}$) as shown by the solid vertical arrows, the forced convection assists the flow due to natural convection (Fig.5.2a).

2. **Opposing flow**: When the left hot wall moves in the downward direction ($\mathbf{u}_{\mathbf{w}ho}$) and the right cold wall moves in the upward direction ($\mathbf{u}_{\mathbf{w}co}$) as shown by the solid vertical arrows, the forced convection opposes the flow due to natural convection (Fig.5.2b).

The relative strength of natural convection over forced convection is expressed in terms of a modified Richardson number, Ri_m, based on a modified Rayleigh number, Ra_m, a modified Prandtl number Pr_m and a modified Reynolds number, Re_m, as introduced in [44] and defined in the Nomenclature of the present paper

$$Ri_m = \frac{Ra_m}{Pr_m Re_m^2} \tag{5.1}$$

A pre-multiplication factor, $C_f = 0.1$ is used in the calculation of Pr_m as discussed in [44]. For $Ri_m << 1$ forced convection is dominant, whereas for $Ri_m >> 1$ the flow is dominated by natural convection.

In all studied cases, $\beta\Delta T << 1$, and thus we ensure that the Boussinesq approximation [45] is valid. Thus assuming all the fluid properties, except the fluid density in the body forcing term of the Navier-Stokes (N-S) equations to be constant, the transient Navier-Stokes Eq.(5.2),(5.3) and thermal energy transport equations Eq.(5.4),(5.5) are solved numerically. The solid and fluid regions are thermally coupled at the interface using Dirichlet–Neumann Partitioning, to account for the conjugate heat transfer between the solid and the fluid region.

Fluid phase:

$$\nabla \cdot \mathbf{u} = 0 \tag{5.2}$$

$$\frac{\partial \mathbf{u}}{\partial t} + \mathbf{u} \cdot \nabla \mathbf{u} = -\frac{1}{\rho_f} \nabla p + \nu \nabla^2 \mathbf{u} + \mathbf{g}\beta(T_f - T_{ref}) \tag{5.3}$$

$$\frac{\partial T_f}{\partial t} + \mathbf{u} \cdot \nabla T_f = \alpha_f \nabla^2 T_f \tag{5.4}$$

Solid phase:

$$\frac{\partial T_s}{\partial t} = \alpha_s \nabla^2 T_s \tag{5.5}$$

At the coupled interface, we use Dirichlet and Neumann boundary conditions

$$T_f = T_s \tag{5.6}$$

to solve the fluid region.

$$k_f \frac{\partial T_f}{\partial n} = k_s \frac{\partial T_s}{\partial n} \tag{5.7}$$

to assure continuity of both the temperature and the heat flux at the fluid-solid interface.

The results from fully resolved coarse-grained media simulations are compared with Darcy-type VAM simulations (relative velocity resistance formulation). Here, the porous medium is modelled by taking the porosity, ϕ into account and by adding a momentum source term to the N-S equation [46]. A single thermal equation is used to model the energy transport.

$$\nabla \cdot \mathbf{u} = 0 \tag{5.8}$$

$$\frac{\partial \phi \mathbf{u}}{\partial t} + \mathbf{u} \cdot \nabla \mathbf{u} = -\frac{1}{\rho_f} \nabla p + \nu \nabla^2 \mathbf{u} + \mathbf{g}\beta(T_p - T_{ref}) + \frac{1}{\rho_f}\mathbf{S} \tag{5.9}$$

$$(\rho c_p)^* \frac{\partial T_p}{\partial t} + (\rho c_p)_f \phi \mathbf{u} \cdot \nabla T_p = k_m \nabla^2 T_p \tag{5.10}$$

where, $(\rho c_p)^* = \phi(\rho c_p)_f + (1-\phi)(\rho c_p)_s$. The source term, $\mathbf{S}$ is given by the Darcy-Forchheimer equation for homogeneous porous media:

$$\mathbf{S} = -(\mu D + \frac{1}{2}\rho_f \left|\phi \mathbf{u}\right| F)\phi \mathbf{u} \tag{5.11}$$

The first and second terms in S account for the viscous and inertial loss, respectively. In the present work, we use Ergun's equation [47] used for packed bed reactors giving:

$$D = \frac{150(1-\phi)^2}{d^2\phi^3} \tag{5.12}$$

$$F = \frac{3.5}{d}\frac{(1-\phi)}{\phi^3} \tag{5.13}$$

In addition to comparing results from fully resolved coarse grained media simulations to those obtained with the Darcy-Forchheimer model (Eq.(5.8)-(5.13)), we also compare our results to Darcy model (Eq.(5.8)-(5.12)) by setting the Forchheimer term (Eq.(5.13)) to zero.

5.2.2. NUMERICAL METHOD

The open-source, finite volume CFD solver OpenFOAM 2.4.0 [48] is used to carry out our simulations. Because of the complex nature of the geometry in the fully resolved simulations, making it difficult to use structured grids, the sphere packed cubical cavities are meshed with body-conforming unstructured tetrahedral grids. With all the flows studied in this paper being either stationary or slowly oscillatory, the use of unstructured grids is reported in literature to be justified in terms of accuracy. Finn and Apte [49] report that

OpenFOAM simulations of packed beds using unstructured meshes are comparable in accuracy to those on non-body-conforming cartesian grids, but with added computational costs. Similar studies on the acuracy of OpenFOAM simulations with unstructured grids are also reported in [50, 51].

The above set of equations, Eq.(5.2)-(5.5) are discretized and simulations are carried out using a modified version [13] of the standard conjugate heat transfer solver "chtMultiRegionFoam". The energy equation for the fluid region in the solver is modified as in "buoyantBoussinesqPimpleFoam" to account for the Boussinesq approximation. We treat the temperature equation for the solid phase as a passive scalar equation. A detailed solver validation is reported in [13].

The Darcy and Darcy-Forcheimer simulations Eq.(5.8)-(5.13) are solved by adding a porous zone to the "buoyantBoussinesqPimpleFoam" as discussed in [52].

In contrast to the fully resolved simulations, the Darcy simulations are carried out using a relatively coarse mesh consisting of hexahedral grid cells. The numerical schemes (available in OpenFOAM [48]) used to solve our equations are listed below:

1. Time stepping-backward scheme (2^{nd} order backward differencing scheme).
2. Convective and diffusive terms (Eq.(5.3)-(5.10))-limitedLinear (2^{nd} order central differencing scheme).

The pressure-velocity-coupling at each time step is handled by the iterative PISO algorithm [53]. We solve the energy transport equation (Eq.(5.4)) using the divergence-free velocity obtained in each time step.

For the fully resolved simulations, a grid independence study is carried out using three different unstructured tetrahedral grids with 1.2×10^6, 5.1×10^6 and 1.12×10^7 grid cells, respectively. In all the simulations reported, 9 probes were inserted at random locations in the pore-space to monitor the time dependence of the flow and temperature. We place 3 probes each close to the isothermal walls at different heights with one at the central plane and the other two close to the front and back walls, while the remaining 3 probes are placed at the central plane with one in the pore-space close to the center of the cavity and the other 2 close to the top and bottom walls. In all cases, the flow and temperature was steady or slowly oscillating and in the laminar regime. Thus, we choose the overall Nusselt number to be the criterion to check the grid independence. At $Ra_f = 10^7$ and $Ri_m = 0.4$ the deviation in overall Nusselt number obtained between the 5.1×10^6 and 1.12×10^7 grids is less than 3%. Consequently, the base grid cells for the presented simulations is set as 5.1×10^6 grid cells. This mesh is obtained by using a roughly uniform grid size $h \approx d/16 \approx L/80$ in the solid phase and in the core of the cavity. The same mesh size is used at the interfaces between the solid and fluid regions. Near the hot and cold walls the grid size is gradually refined to $h_{BL} \approx d/32 \approx L/160$.

A grid independence study for Darcy simulations is carried using 32^3, $64^3$and 128^3 hexahedral grid cells with an expansion factor of 1.2 close to the hot and cold walls. At $Ra_f = 10^7$ and $Ri_m = 0.4$, the deviation in overall Nusselt number obtained between the 64^3 and 128^3 hexahedral grid cells is less than 2%. Thus 128^3 hexahedral grid cells are used for our Darcy simulations.

An adaptive time stepping, with CFL number = 0.33, is used in all the simulations reported. The time steps are observed to be constant throughout a simulation at fixed

Ra_f, once the flow attains a (quasi) steady state.

5.3. RESULTS AND DISCUSSION

We study the combined effect of natural convection and forced convection in a cavity filled with a coarse-grained porous media, and compare results of fully resolved simulations to those of Darcy and Darcy-Forchheimer based volume averaged simulations. The temperature and velocities which are discussed below, are expressed in the non-dimensional form, such that the non-dimensional temperature, θ:

$$\theta = \frac{T - T_c}{T_h - T_c}$$

and non-dimensional velocity, $\mathbf{u}^*$:

$$\mathbf{u}^* = \frac{\mathbf{u}}{U_0}$$

where, $U_0 = \dfrac{{Ra_f}^{1/2}\alpha}{L}$ is the natural convection characteristic velocity scale defined as [54].

5.3.1. ANALYSIS: HEAT TRANSFER AT THE ISOTHERMAL WALLS

To understand the influence of the direction of the wall motion on the mixed convective heat transfer in a bead-filled cavity, we analyze the time and wall- averaged Nusselt number, Nu_f, as well as the scaled effective heat transfer (discussed below) in both assisting (Fig.5.3) and opposing (Fig.5.4) mixed convection, for $Ra_f = 10^6$ and 10^7 and $0.025 \leq Ri_m \leq 500$. The heat transfer results from the coarse-grained porous media simulations are compared with the results from Darcy simulations.

In assisting mixed convection (Fig.5.3(a)), Nusselt numbers at $Ri_m >> 1$ approach that for pure natural convection alone (indicated as $Ri_m \to \infty$), as expected. At fixed Ra_f, heat transfer increases with decreasing Ri_m, i.e. increasing forced convection. For $Ri_m << 1$, heat transfer is dominated by forced convection and indeed Nu_f scales as $Nu_f \sim Ri_m^{-0.33} \sim Re_m^{0.66}$, in agreement with what was found for forced convection heat transfer in a lid driven cavity [20, 55]. Thus, heat transfer is dominated by natural convection at $Ri_m >> 1$, whereas it increases with decreasing Ri_m due to the combined contribution of natural convection and forced convection, and approaches that of pure forced convection for $Ri_m << 1$. At $Ra_f = 10^6$, in the simulations at $Ri_m > 10$, the heat transfer in a coarse-grained porous media filled cavity is lower than that with Darcy assumption. The heat transfer due to natural convection alone exhibits the same behavior at $Ra_f = 10^6$. At $Ri_m < 10$, the heat transfer in coarse-grained simulations becomes higher than that in Darcy simulations. Unlike $Ra_f = 10^6$, at $Ra_f = 10^7$ and at all Ri_m, the heat transfer due to natural and assisting mixed convective flow in a coarse-grained porous media filled cavity is higher than that with Darcy assumption.

To quantify the range of Ri_m where natural convection and forced convection are of comparable strength, we define the effective heat transfer, Nu_{eff} as:

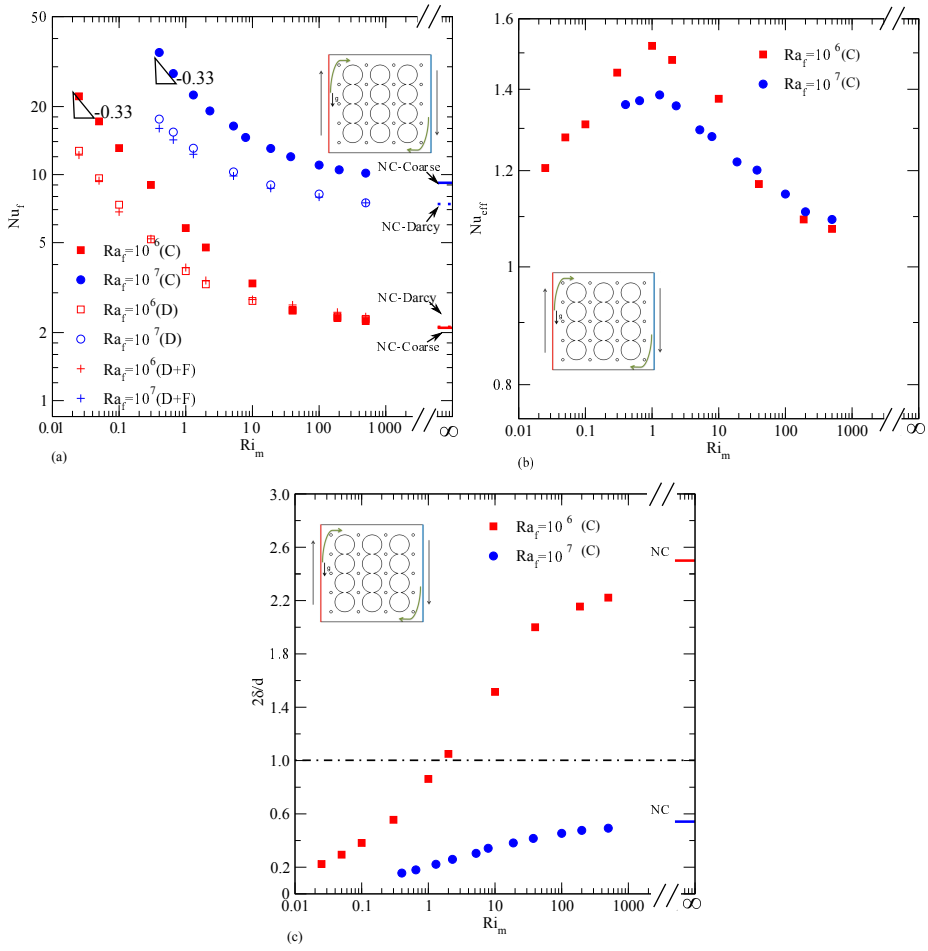

Figure 5.3: Heat transfer and thermal boundary layer thickness variation in a coarse-grained porous media filled cavity with assisting mixed convection, at different Ra_f and Ri_m. Solid dash indicate the heat transfer in the hydrogel bead filled cavity with natural convection at $Ra_f = 10^6$ (red), $Ra_f = 10^7$ (blue) (a) total heat transfer (b) scaled effective heat transfer (c) boundary layer thickness in coarse-grained filled cavity.

$$Nu_{eff} = \frac{Nu_{MC}}{Nu_{FC} + Nu_{NC} - 1} \tag{5.14}$$

with Nu_{MC} the observed mixed convection Nusselt number, Nu_{FC} the Nusselt number for forced convection only, and , Nu_{NC} the Nusselt number for natural convection only. Nu_{eff} quantifies the total heat transfer in mixed convection to the combined effect in natural convection alone and forced convection alone. We subtract 1 from the denominator to ensure that the effect of conduction is taken into account only once.

In assisting mixed convection Fig.5.3(b), at both studied values of Ra_f, the effective

heat transfer reaches a maximum at $Ri_m \approx 1$, i.e. when both natural and forced convection contribute equally to the heat transfer process. For $Ri_m << 1$ and $Ri_m >> 1$, heat transfer is dominated by forced convection and natural convection respectively, resulting in Nu_{eff} approaching 1.

Comparing the fully resolved simulations (indicated by (C) in Fig.5.3(a)), to those using Darcy-based and Darcy-Forchheimer based VAM models (indicated by (D) and (D+F) respectively), we observe that at $Ra_f = 10^6$ the heat transfer for natural convection dominated flows (i.e. large Ri_m, including pure natural convection at $Ri_m \rightarrow \infty$) in a coarse-grained porous medium filled cavity is lower than that obtained with the Darcy assumption, whereas at low Ri_m the heat transfer in coarse-grained simulations becomes higher than that in Darcy simulations. The cross-over is observed at $Ri_m \approx 10$. At $Ra_f = 10^7$ such a cross-over is not observed, and the heat transfer in a coarse-grained porous medium filled cavity is higher than that with the Darcy assumption at all Ri_m.

To understand this difference in behaviour at different Ra_f, we look at the relative thickness of the thermal boundary layers δ [11] compared to the radius $d/2$ of the beads:

$$\frac{2\delta}{d} = \frac{L/d}{Nu_f} \tag{5.15}$$

From Fig.5.3(c) it is observed that at $Ra_f = 10^6$ the Darcy and Darcy-Forchheimer simulations under predict heat transfer when the thermal boundary layer thickness at the isothermal walls is significantly smaller than the radius of the beads. With the thinning of thermal boundary layer at higher $Ra_f = 10^7$, $2\delta/d$ is always less than 1, and Darcy simulations always under predict heat transfer.

We now move from assisting to opposing mixed convection (Fig.5.4). As in assisting mixed convection, opposing mixed convection Nusselt numbers (see Fig.5.4(a)) approach those in pure natural convection at high Ri_m, as expected. In deviation from assisting mixed convection, Nusselt decreases with decreasing Ri_m, i.e. increasing forced convection, and attains a minimum at $1 \leq Ri_m \leq 10$. With a further decrease in Ri_m, a change in the trend occurs and the Nusselt number increases, as heat transfer is now dominated by forced convection. In opposing mixed convection, the effective heat transfer (Fig.5.4(b)), calculated as in Eq.5.14, reaches a minimum at $Ri_m \approx 1$, representing the region where natural and forced convection are of equal strength and opposite to each other.

Comparing the fully resolved simulations (indicated by (C) in Fig.5.4(a)), to those using Darcy-type VAM models (indicated by (D) and (D+F)), we observe that at $Ra_f = 10^6$ the heat transfer for high Ri_m natural convection dominated flows in a coarse-grained porous medium is lower than that obtained with the Darcy and Darcy-Forchheimer assumptions, whereas for low Ri_m forced convection dominated flows it becomes higher than that in Darcy-type simulations. At $Ra_f = 10^7$ the heat transfer in a coarse-grained porous medium filled cavity is lower than that with the Darcy and Darcy-Forchheimer assumptions for intermediate values of Ri_m, and approaches that of a Darcy-type medium for high Ri_m. This can again be understood by comparing the relative thickness of the thermal boundary layers to the radius of the beads. From Fig.5.4(c) it is observed that at $Ra_f = 10^6$, the Darcy and Darcy-Forchheimer simulations over-predict the heat transfer

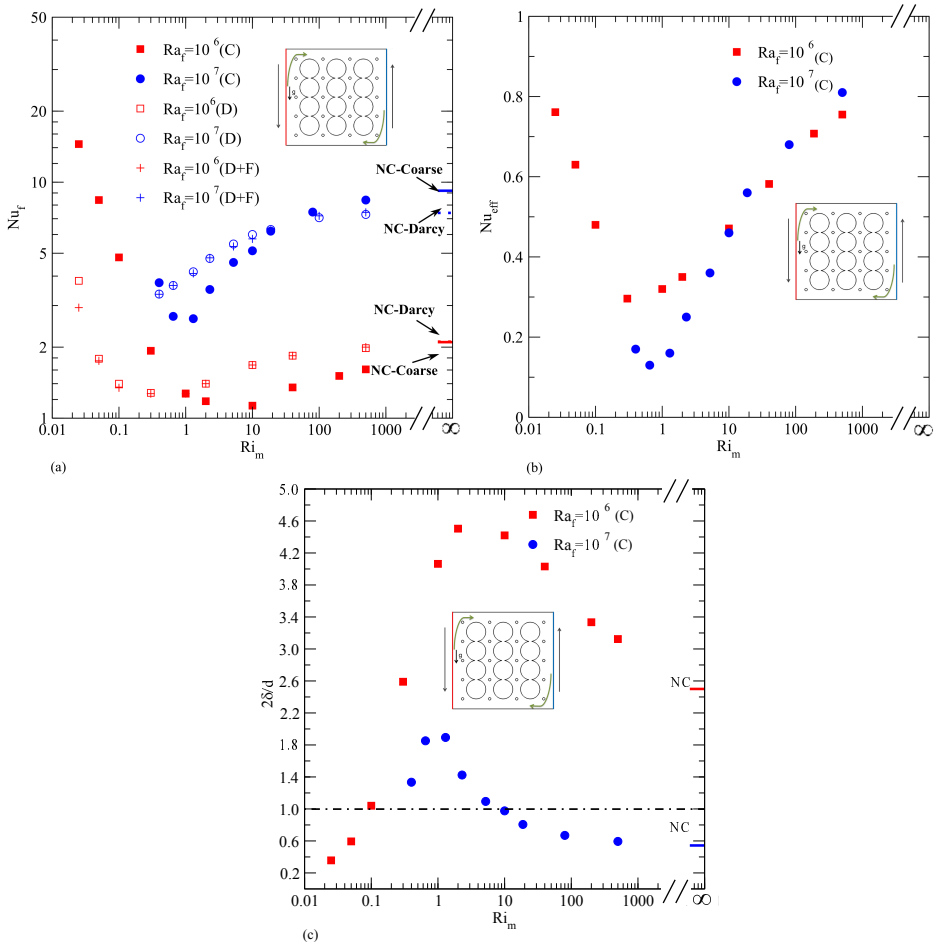

Figure 5.4: Heat transfer and thermal boundary layer thickness variation in a coarse-grained porous media filled cavity with opposing mixed convection, at different Ra_f and Ri_m. Solid dash indicate the heat transfer in the hydrogel bead filled cavity with natural convection at $Ra_f = 10^6$ (red), $Ra_f = 10^7$ (blue) (a) total heat transfer (b) scaled effective heat transfer (c) boundary layer thickness in coarse-grained filled cavity.

when the thermal boundary layer thickness is significantly larger than the bead size and under-predict it when the boundary layer thickness is significantly smaller. At $Ra_f = 10^7$, the thermal boundary layer thickness is larger than the bead size for all simulated $0.4 < Ri_m < 10$, in agreement with the range of Ri_m for which the coarse grained medium has a lower heat transfer than the Darcy-type medium.

To understand how the local heat transfer varies with the direction of the forced convection (i.e. of the moving wall), we compare the local instantaneous Nusselt number at the hot wall at $Ra_f = 10^7$ (Fig.5.5). Compared to pure natural convection (Fig.5.5(N1)), in assisting mixed convection (Fig.5.5(A1,A2)) the overall heat transfer is increased and

the regions of higher heat transfer extend further up along the hot wall.

On the other hand, in opposing mixed convection (Fig.5.5(O1,O2)), the overall heat transfer is lower than that in natural convection, and with decreasing Ri_m, the regions where maximum heat transfer occurs shift to the top of the hot wall. This shows the change in the mode of heat transfer from natural convection to forced convection. The anti-clockwise motion of the fluid induced by the moving isothermal walls results in the change in the region of maximum heat transfer from the bottom to the top.

A comparison of heat transfer at the wall in coarse-grained porous media with Darcy simulations is reported in Fig.5.6. As observed with coarse-grained media simulations, the simulations with Darcy assumption also show an increased overall heat transfer in assisting mixed convection and a change in the location of maximum heat transfer in opposing mixed convection. The heat transfer is observed to be uniform along the horizontal direction in Darcy simulations Fig.5.6(A1,O1,N1), unlike the coarse-grained media simulations where the maximum heat transfer is limited to the pore-space Fig.5.6(A2,N2,O2).

5.3.2. SPATIAL TEMPERATURE AND FLOW FEATURES AT DIFFERENT Ri_m

To understand the spatial variations in heat transfer we analyze the local temperature and velocity fields from both fully resolved and Darcy simulations. The nature of the flow structures at $Ra_f = 10^7$ is visible in Fig.5.7, showing instantaneous $u_y - u_z$ velocity vectors in a characteristic vertical plane at $X/L = 0.79$. The flow field has reached a quasi steady-state, not changing over a period of $30t_0$, and the velocity field is interpolated on a 32-32 uniform grid for visualization purposes.

In pure natural convection (Fig.5.7(N1,N2)), the temperature distribution and flow in coarse-grained and Darcy simulations are quite similar, but the flow velocities along the isothermal walls are a bit higher in the free pore spaces of the coarse-grained porous medium, because of the locally higher porosity and permeability. More importantly, and for similar reasons, higher velocities are observed in the free pore spaces along the horizontal adiabatic walls, causing cold fluid to impinge on the lower part of the hot wall, and hot fluid to impinge on the top part of the cold wall. Together this explains the slightly higher average Nusselt number observed for the coarse grained medium, as compared to the Darcy medium, shown in Fig.5.3(a), as well as the increased local Nusselt number of the lower part of the hot wall, shown in Fig.5.6(N2).

In assisting mixed convection (Fig.5.7(A1,A2)), the velocities close to the isothermal walls increase compared to pure natural convection, leading to thinner thermal boundary layers. In the coarse grained medium, hot fluid impinges on the upper part of the cold wall with increased velocity, as does cold fluid on the lower part of the hot wall, explaining the 30% higher average Nusselt number for the coarse grained medium, shown in Fig.5.3(a), and the increased local Nusselt number of the lower part of the hot wall, shown in Fig.5.6(A2).

When the forced convection induced by the moving vertical walls is in the opposite direction w.r.t that in natural convection Fig.5.7(O1,O2), we observe a change in the direction of flow close to the walls. The fluid close to the walls moves in the direction of the moving wall with the convective flow induced by natural convection in the opposite direction. The opposing nature of the flow results in thickening of the thermal boundary layer in both Darcy and coarse-grained media cavities.

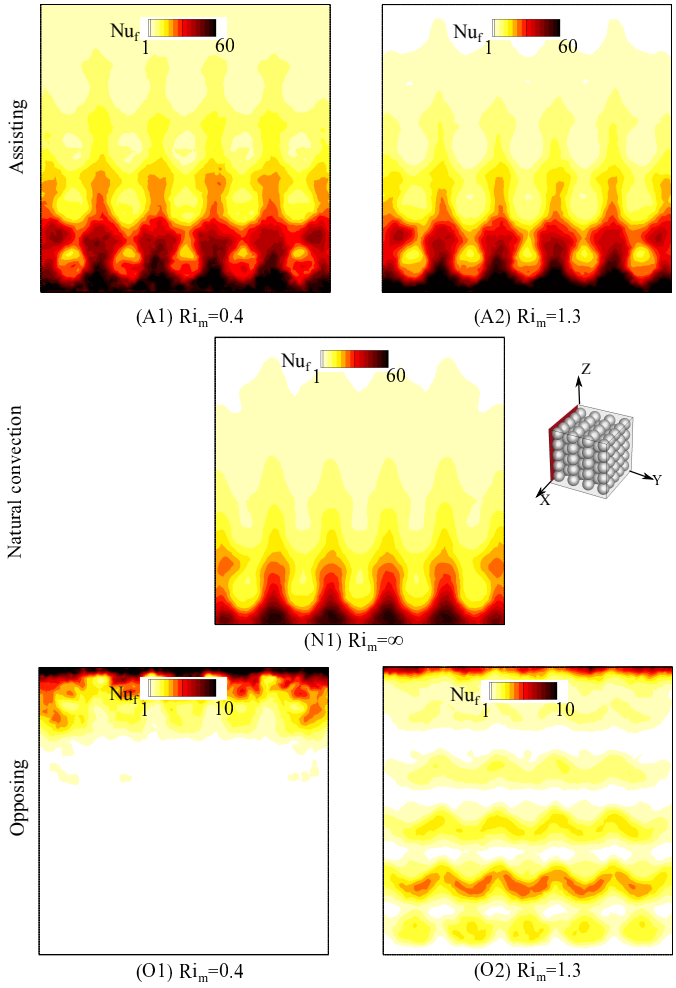

Figure 5.5: Instantaneous Nusselt number Nu_f distributions at the hot wall in a cavity packed with hydrogel beads, at $Ra_f = 10^7$, at different Ri_m in assisting mixed convection (top row), natural convection (center) and opposing mixed convection (bottom row). The Nu_f distributions reported are at $t/t_0 = 30$, after a quasi steady-state has been reached.

In opposing mixed convection (Fig.5.7(O1,O2)) we observe a flow direction reversal within the thermal boundary layers, resulting in two circulation zones extending from the bottom to the top of the cavity, close to the isothermal walls. Very close to the walls, the fluid moves in the direction of the moving wall, whereas a bit further away from the wall the flow is in the opposite direction due to buoyancy. This flow recirculation results in thickening of the thermal boundary layers and reduced average heat transfer (Fig.5.3(a)), in both Darcy and coarse-grained medium. However, in the coarse-grained porous medium (Fig.5.7(O2)), the opposing nature of forced and natural convection results in a local rotational flow in the pore-spaces close to the vertical

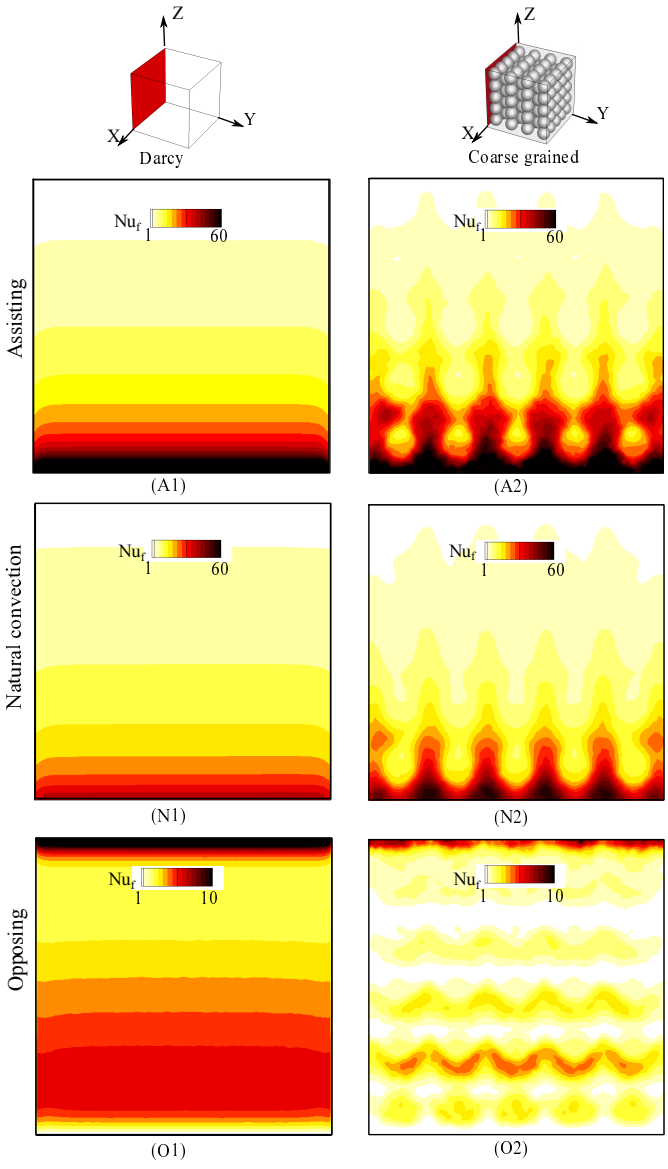

Figure 5.6: Instantaneous Nusselt number Nu_f distributions at the hot wall at $Ra_f = 10^7$, $Ri_m = 1.3$ in assisting mixed convection (top row), natural convection (center) and opposing mixed convection (bottom row), with Darcy **(D)** assumption (left column) and coarse-grained **(C)** porous media filled cavity (right column). The Nu_f distributions reported are at $t/t_0 = 30$, after a quasi steady-state has been reached.

walls. Due to increased mixing this leads to thick thermal boundary layers of uniform thickness, unlike the developing boundary layers in natural and assisting mixed convection (Fig.5.7(N2,A2)), explaining the 40% lower average Nusselt number for the coarse

grained medium, as shown in Fig.5.3(a), and the decreased and more uniform local Nusselt number on the hot wall, as shown in Fig.5.6(A2), both compared to the Darcy medium.

5.3.3. LOCAL TEMPERATURE AND FLOW FEATURES AT DIFFERENT Ri_m

From the above discussion it is clear that important differences in overall and local heat transfer between coarse-grained and Darcy-type simulations are due to differences in the local flow and temperatures. In the following sections we take a closer look at the local velocities and temperatures in the coarse-grained medium.

Fig.5.8 shows the non-dimensional vertical velocity, u_z^* along the horizontal line at $Z/L = 0.5$ and $X/L = 0.4$, at $Ra_f = 10^7$ for different Ri_m. In assisting mixed convection (Fig.5.8(a)), a transition from a natural convection boundary layer with a velocity extremum away from the wall, to a forced convection boundary layer with a velocity extremum at the wall, is observed for decreasing Ri_m (corresponding to an increasing Re_m). In opposing mixed convection (Fig.5.8(b)), on the other hand, the local circulating flow induced by the opposing effects of wall motion and natural convection as discussed in Fig.5.7(O1,O2), results in secondary extrema in the vertical velocities close to the first layer of hydrogel beads near the vertical walls.

Fig.5.9 shows the local non-dimensional temperature, θ, both in the fluid and the hydrogel beads, along the horizontal line at $Z/L = 0.5$ and $X/L = 0.4$, at $Ra_f = 10^7$ for different Ri_m. In assisting mixed convection (Fig.5.9 (a)), the temperature distribution exhibits clear and relatively thin thermal boundary layers for all $Ri_m \geq 0.4$, indicating the dominance of (either forced or natural) convective heat transfer. With increased contribution of forced convection (i.e. decreased Ri_m), the boundary layers get thinner and the local extrema close to isothermal walls become more prominent. In opposing mixed convection (Fig.5.9(b)), on the other hand, the dominant mode of heat transfer switches from natural convection at high Ri_m to forced convection at low Ri_m via a "conduction only" mode at $Ri_m \sim 1$.

5.4. SUMMARY AND CONCLUSION

We performed numerical simulations of assisting and opposing mixed convection in a side-heated, side-cooled lid driven cavity, packed with relatively large hydrogel beads, over a range of Richardson numbers, at fluid Rayleigh numbers 10^6 and 10^7. We focused on explaining overall heat transfer from local flow and temperature variations. The results are compared with Darcy and Darcy-Forchheimer simulations to understand the influence of the coarse-grained nature of the medium on the heat transfer. As in fluids-only mixed convection, in assisting mixed convection for a given Rayleigh number we find a maximum scaled effective heat transfer (and in opposing mixed convection we similarly find a scaled minimum effective heat transfer) at a Richardson number of approximately one, when the Richardson number is modified with the Darcy number Da and the Forchheimer coefficient $C_f = 0.1$ as $Ri_m = Ri \times Da^{1/2}/C_f$.

In assisting mixed convection we found a maximum heat transfer increase of 40−50% for Rayleigh numbers between 10^6 and 10^7, compared to the summated heat transfer effects of natural and forced convection alone. In opposing mixed convection we found

a maximum heat transfer decrease by a factor 3-10, for Rayleigh numbers between 10^6 and 10^7, compared to the summated heat transfer effects of natural and forced convection alone. We found that the ratio between the thermal boundary layer thickness at the isothermal walls and the average pore and sphere size plays an important role in the heat transfer mechanism and in the effect that the grain size has on the heat transfer. When this ratio is relatively large (i.e. at large solid object dimensions and/or high Rayleigh numbers), the thermal boundary layer is locally disturbed by the solid objects and these objects cause local velocities and flow recirculation perpendicular to the walls. As a result, for a coarse grained medium we not only find strong local variations in heat transfer, but also significant differences in the wall-average heat transfer. Our ongoing experimental study on mixed convection in porous-media filled cavities with an inlet and outlet also hints at the influence of coarse-grained porous media on local and integral heat transfer. For such coarse grained media, either fully resolved simulations, or simulations applying more sophisticated VAM models than Darcy-type models, are needed to predict both local and average heat transfer. From our previous work on natural convection with similar packing, we find a strong influence of material properties on heat transfer at low Rayleigh numbers which decreases with the increase in Rayleigh number. It would also be interesting to investigate the influence of material properties on the flow and heat transfer in coarse-grained porous media filled cavities under mixed convection. As observed in the current work, we expect a transition from heat transfer dominated by natural convection to that by forced convection to occur in assisting and opposing cases, but at different Richardson numbers depending on the thermal properties of the porous media.

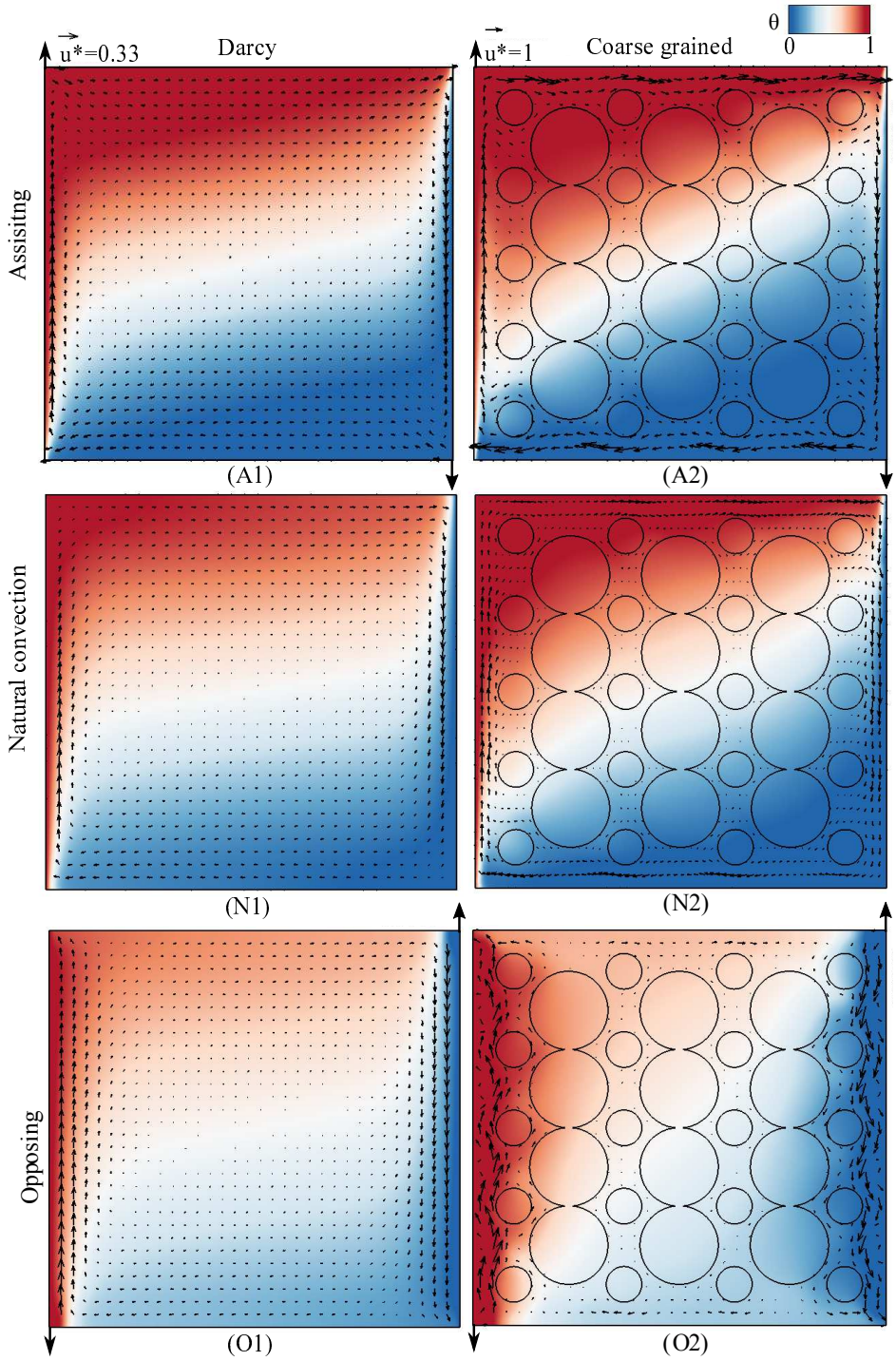

Figure 5.7: Instantaneous velocity vectors and temperatures in a characteristic vertical plane, $X/L = 0.79$ at $Ra_f = 10^7$, $Ri_m = 1.3$ in assisting mixed convection (top row), natural convection (center) and opposing mixed convection (bottom row) with Darcy **(D)** assumption (left column) and coarse-grained **(C)** porous media filled cavity (right column). The instantaneous data reported is at $t/t_0 = 30$, after a quasi steady-state has been reached.

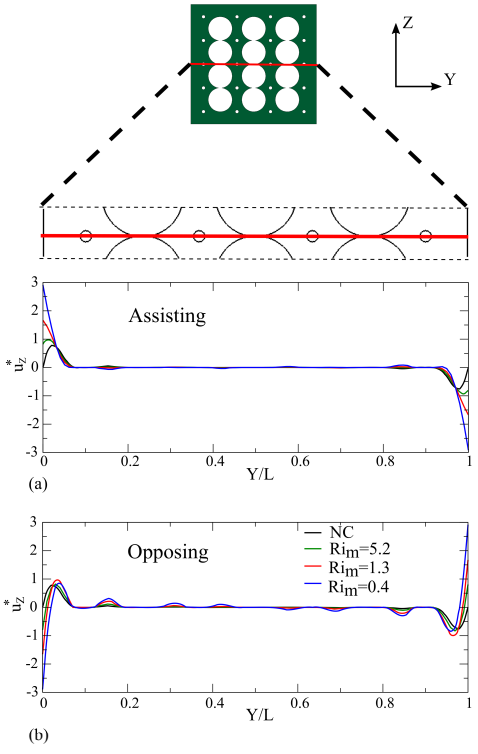

Figure 5.8: Non-dimensional vertical velocity, u_z^* along the line at $Z/L = 0.5$ in the plane $X/L = 0.4$, at $Ra_f = 10^7$ in (a) assisting mixed convection (b) opposing mixed convection at different Ri_m. The instantaneous vertical velocity reported is at $t/t_0 = 30$, after a quasi steady-state has been reached.

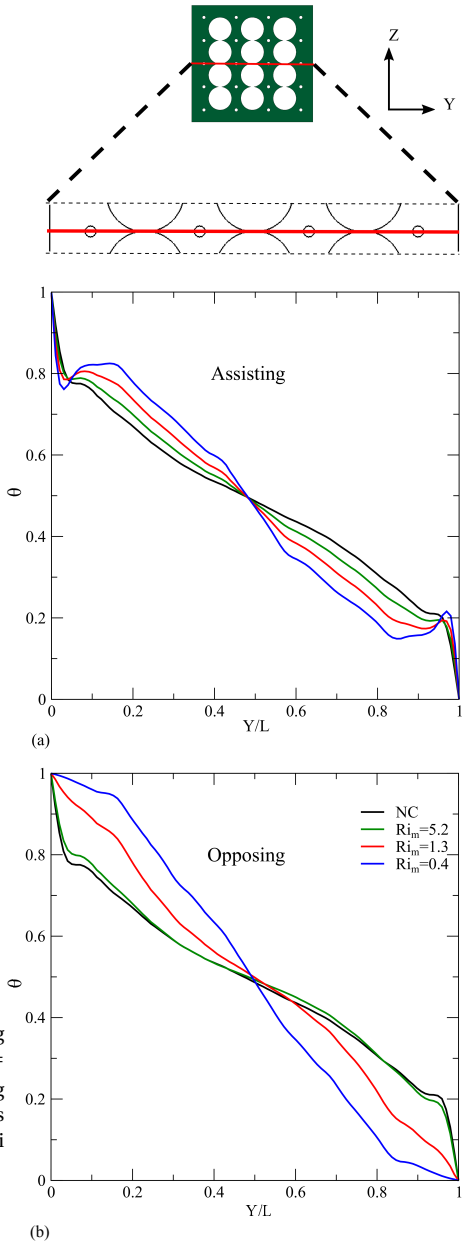

Figure 5.9: Non-dimensional temperature along the line at $Z/L = 0.5$ in the plane $X/L = 0.4$, at $Ra_f = 10^7$ in (a) assisting mixed convection (b) opposing mixed convection at different Ri_m. The instantaneous temperature reported is at $t/t_0 = 30$, after a quasi steady-state has been reached.

REFERENCES

[1] A. Raji and M. Hasnaoui, *Mixed convection heat transfer in a rectangular cavity ventilated and heated from the side,* Numerical Heat Transfer, Part A: Applications **33**, 533 (1998).

[2] H. F. Oztop and I. Dagtekin, *Mixed convection in two-sided lid-driven differentially heated square cavity,* International Journal of Heat and Mass Transfer **47**, 1761 (2004).

[3] A. K. Prasad and J. R. Koseff, *Combined forced and natural convection heat transfer in a deep lid-driven cavity flow,* International Journal of Heat and Fluid Flow **17**, 460 (1996).

[4] T. S. Ro and N. E. Todreas, *Energy transfer mechanisms in LMR rod bundles under mixed convection conditions,* Nuclear Engineering and Design **108**, 343 (1988).

[5] J. Sillekens, C. Rindt, and A. V. Steenhoven, *Developing mixed convection in a coiled heat exchanger,* International Journal of Heat and Mass Transfer **41**, 61 (1998).

[6] N. Ghorbani, H. Taherian, M. Gorji, and H. Mirgolbabaei, *Experimental study of mixed convection heat transfer in vertical helically coiled tube heat exchangers,* Experimental Thermal and Fluid Science **34**, 900 (2010).

[7] Z. Li, Z. Huang, and W. Tao, *Three-dimensional numerical study on turbulent mixed convection in parabolic trough solar receiver tube,* Energy Procedia **75**, 462 (2015).

[8] M. C. Moghadam, M. Edalatpour, and J. P. Solano, *Numerical study on conjugated laminar mixed convection of alumina/water nanofluid flow, heat transfer, and entropy generation within a tube-on-sheet flat plate solar collector,* Journal of Solar Energy Engineering **139**, 041011 (2017).

[9] A. J. Smith, *Mixed convection and density-dependent seawater circulation in coastal aquifers,* Water Resources Research **40** (2004), 10.1029/2003wr002977.

[10] F. P. Incropera, *Convection heat transfer in electronic equipment cooling,* Journal of Heat Transfer **110**, 1097 (1988).

[11] D. J. Keene and R. J. Goldstein, *Thermal Convection in Porous Media at High Rayleigh Numbers,* Journal of Heat Transfer **137**, 1 (2015).

[12] I. Ataei-Dadavi, M. Chakkingal, S. Kenjereš, C. R. Kleijn, and M. J. Tummers, *Flow and heat transfer measurements in natural convection in coarse-grained porous media,* International Journal of Heat and Mass Transfer **130**, 575 (2019).

[13] M. Chakkingal, S. Kenjereš, I. Ataei-Dadavi, M. Tummers, and C. R. Kleijn, *Numerical analysis of natural convection with conjugate heat transfer in coarse-grained porous media,* International Journal of Heat and Fluid Flow **77**, 48 (2019).

[14] T. Jonsson and I. Catton, *Prandtl number dependence of natural convection in porous media,* Journal of Heat Transfer **109**, 371 (1987).

[15] C. R. B. Lister, *An explanation for the multivalued heat transport found experimentally for convection in a porous medium,* Journal of Fluid Mechanics **214**, 287–320 (1990).

[16] V. Calmidi and R. Mahajan, *Forced convection in high porosity metal foams,* Journal of heat transfer **122**, 557 (2000).

[17] D. Nield, A. Kuznetsov, and M. Xiong, *Thermally developing forced convection in a porous medium: parallel plate channel with walls at uniform temperature, with axial conduction and viscous dissipation effects,* International Journal of Heat and Mass Transfer **46**, 643 (2003).

[18] B. Buonomo, O. Manca, and G. Lauriat, *Forced convection in micro-channels filled with porous media in local thermal non-equilibrium conditions,* International Journal of Thermal Sciences **77**, 206 (2014).

[19] D. B. Ingham and I. Pop, *Transport phenomena in porous media II* (2002) p. 449.

[20] D. A. Nield and A. Bejan, *Convection in Porous Media* (Springer New York, 2013).

[21] J. Koh and R. Colony, *Heat transfer of microstructure for integrated circuits,* International Communications in Heat and Mass Transfer **13**, 89 (1986).

[22] K. M. Khanafer and A. J. Chamkha, *Mixed convection flow in a lid-driven enclosure filled with a fluid-saturated porous medium,* International Journal of Heat and Mass Transfer **42**, 2465 (1999).

[23] F.-C. Lai, V. Prasad, and F. Kulacki, *Aiding and opposing mixed convection in a vertical porous layer with a finite wall heat source,* International Journal of Heat and Mass Transfer **31**, 1049 (1988).

[24] K. Muralidhar, *Mixed convection flow in a saturated porous annulus,* International journal of heat and mass transfer **32**, 881 (1989).

[25] A. Hadim, *Numerical study of non-darcy mixed convection in a vertical porous channel,* Journal of Thermophysics and Heat Transfer **8**, 371 (1994).

[26] A. Hadim and G. Chen, *Non-darcy mixed convection in a vertical porous channel with discrete heat sources at the walls,* International Communications in Heat and Mass Transfer **21**, 377 (1994).

[27] Y. Chen, J. Chung, C. Wu, and Y. Lue, *Non-darcy mixed convection in a vertical channel filled with a porous medium,* International Journal of Heat and Mass Transfer **43**, 2421 (2000).

[28] N. H. Saeid, *Analysis of mixed convection in a vertical porous layer using non-equilibrium model,* International Journal of Heat and Mass Transfer **47**, 5619 (2004).

[29] K.-C. Wong and N. H. Saeid, *Numerical study of mixed convection on jet impingement cooling in a horizontal porous layer under local thermal non-equilibrium conditions,* International Journal of Thermal Sciences **48**, 860 (2009).

[30] G. Venugopal, C. Balaji, and S. Venkateshan, *Experimental study of mixed convection heat transfer in a vertical duct filled with metallic porous structures,* International Journal of Thermal Sciences **49**, 340 (2010).

[31] N. S. Ahmed, I. A. Badruddin, J. Kanesan, Z. Zainal, and K. N. Ahamed, *Study of mixed convection in an annular vertical cylinder filled with saturated porous medium, using thermal non-equilibrium model,* International Journal of Heat and Mass Transfer **54**, 3822 (2011).

[32] M. K. Khandelwal and P. Bera, *A thermal non-equilibrium perspective on mixed convection in a vertical channel,* International Journal of Thermal Sciences **56**, 23 (2012).

[33] B. Buonomo, G. Cresci, O. Manca, P. Mesolella, and S. Nardini, *Transient mixed convection in a channel with an open cavity filled with porous media,* Journal of Physics: Conference Series **395**, 012149 (2012).

[34] H. Çelik, M. Mobedi, O. Manca, and U. Ozkol, *A pore scale analysis for determination of interfacial convective heat transfer coefficient for thin periodic porous media under mixed convection,* International Journal of Numerical Methods for Heat & Fluid Flow **27**, 2775 (2017).

[35] H. F. Oztop, *Combined convection heat transfer in a porous lid-driven enclosure due to heater with finite length,* International Communications in Heat and Mass Transfer **33**, 772 (2006).

[36] E. Vishnuvardhanarao and M. K. Das, *Laminar mixed convection in a parallel two-sided lid-driven differentially heated square cavity filled with a fluid-saturated porous medium,* Numerical Heat Transfer, Part A: Applications **53**, 88 (2007).

[37] E. Vishnuvardhanarao and M. K. Das, *Mixed convection in a buoyancy-assisted two-sided lid-driven cavity filled with a porous medium,* International Journal of Numerical Methods for Heat & Fluid Flow **19**, 329 (2009).

[38] P. N. Shankar and M. D. Deshpande, *Fluid mechanics in the driven cavity,* Annual Review of Fluid Mechanics **32**, 93 (2000).

[39] D. J. Goering and P. Kumar, *Winter-time convection in open-graded embankments,* Cold Regions Science and Technology **24**, 57 (1996).

[40] D. J. Gunn, *Transfer of heat or mass to particles in fixed and fluidised beds,* International Journal of Heat and Mass Transfer **21**, 467 (1978).

[41] S. Ueda, S. Natsui, H. Nogami, J.-I. Yagi, and T. Ariyama, *Recent progress and future perspective on mathematical modeling of blast furnace,* ISIJ International **50**, 914 (2010).

[42] I. Ataei-Dadavi, N. Rounaghi, M. Chakkingal, S. Kenjeres, C. R. Kleijn, and M. J. Tummers, *An experimental study of flow and heat transfer in a differentially side heated cavity filled with coarse porous media,* International Journal of Heat and Mass Transfer **143**, 118591 (2019).

[43] M. Kandula, *On the effective thermal conductivity of porous packed beds with uniform spherical particles,* Journal of Porous Media **14** (2011).

[44] V. Kathare, J. H. Davidson, and F. A. Kulacki, *Natural convection in water-saturated metal foam,* International Journal of Heat and Mass Transfer **51**, 3794 (2008).

[45] D. D. Gray and A. Giorgini, *The validity of the boussinesq approximation for liquids and gases,* International Journal of Heat and Mass Transfer **19**, 545 (1976).

[46] P. Nithiarasu, K. Seetharamu, and T. Sundararajan, *Natural convective heat transfer in a fluid saturated variable porosity medium,* International Journal of Heat and Mass Transfer **40**, 3955 (1997).

[47] S. Ergun and A. A. Orning, *Fluid flow through randomly packed columns and fluidized beds,* Industrial & Engineering Chemistry **41**, 1179 (1949).

[48] H. G. Weller, G. Tabor, H. Jasak, and C. Fureby, *A tensorial approach to computational continuum mechanics using object-oriented techniques,* Computers in Physics **12**, 620 (1998).

[49] J. Finn and S. V. Apte, *Relative performance of body fitted and fictitious domain simulations of flow through fixed packed beds of spheres,* International Journal of Multiphase Flow **56**, 54 (2013).

[50] A. Zenklusen, S. Kenjereš, and P. R. von Rohr, *Vortex shedding in a highly porous structure,* Chemical Engineering Science **106**, 253 (2014).

[51] A. Zenklusen, S. Kenjereš, and P. R. von Rohr, *Mixing at high Schmidt number in a complex porous structure,* Chemical Engineering Science **150**, 74 (2016).

[52] H. E. Hafsteinsson, *Porous Media in OpenFOAM, CFD with OpenSource Software*, Tech. Rep. (Chalmers University of Technology, 2009).

[53] R. Issa, *Solution of the implicitly discretised fluid flow equations by operator-splitting,* Journal of Computational Physics **62**, 40 (1986).

[54] J. Patterson and J. Imberger, *Unsteady natural convection in a rectangular cavity,* Journal of Fluid Mechanics **100**, 65 (1980).

[55] N. Wakao and S. Kaguei, *Heat and Mass Transfer in Packed Beds* (1982).

6

CONCLUSION AND OUTLOOK

6.1. CONCLUSIONS

Heat transfer in porous media with porous length scales comparable to flow and thermal length scales are common in various industrial and daily life applications. This thesis numerically investigates the influence of such coarse-grained porous media on natural convection and mixed convection heat transfer in cavities. The open-source finite volume solver package OpenFOAM is used in our research. We look into flow situations over a wide range of relative sizes of the flow and thermal scales w.r.t the pore-scale. The influence of the location of the porous media and its material properties under different flow situations are also investigated.

In Chapter 2, we investigate the influence of the presence, location and thickness of a layer of coarse-grained porous medium on the heat transfer in a bottom-heated, top-cooled cavity. This is relevant for applications in for instance in electronic devices, nuclear reactors, blast furnace, etc. We compare the heat transfer as calculated from - computationally expensive - fully resolved simulations to that obtained with a - computationally less expensive - so-called Representative Elementary Volume (REV) approach using the Darcy-Forchheimer model. The latter approach can be seen as modelling the coarse grained porous medium as a fine-grained medium with the same average porosity and permeability, while neglecting local variations in porosity and permeability. When the porous medium layer touches an isothermal wall, the heat transfer at low Rayleigh numbers is adversely affected by the presence of the porous medium, and further decreases with increasing porous medium layer thickness. However, the heat transfer reduction due to the presence of the porous layer, and its dependence on the porous layer thickness, both vanish at high Rayleigh numbers, where heat transfer in coarse-grained porous medium filled cavities approaches that in fluid-only cavities. For all studied geometries with the porous media touching the isothermal walls, the Darcy-Forchheimer REV approach predicts heat transfer close to that obtained in fully resolved coarse-grained simulations at low Rayleigh numbers, whereas it under-predicts heat transfer at high Rayleigh numbers. We attribute this observation to the fact that the thick

thermal plumes at low Rayleigh numbers are equally obstructed by fine grained and coarse grained porous media, whereas the thinner thermal plumes at higher Rayleigh are still being obstructed by fine grained porous media, whereas they can freely penetrate coarse pore-spaces, resulting in heat transfer comparable to that in fluid-only filled cavities. Unlike in cavities in which the porous medium touches an isothermal wall, the inclusion of a porous layer away from the isothermal walls does not significantly reduce the heat transfer. Though we observe a deviation in heat transfer between Darcy-Forchheimer and coarse-grained simulations at low Rayleigh number, they predict heat transfer that is comparable to the coarse-grained simulations at high Rayleigh numbers.

The observation that the flow through the pore-spaces becomes unobstructed at reduced length scales of the flow structures is further confirmed in Chapter 3. In this chapter, we investigate the influence of the thermal properties of the porous material on the heat transfer at different Rayleigh numbers. The results are validated against experiments conducted in our group. The total heat transfer is due to the combined effect of conductive heat transfer in the solid porous medium and convective heat transfer in the flowing fluid. At lower Rayleigh numbers, when the flow length scales are larger than the pore-scale, the flow and thus convective heat transfer are suppressed due to the presence of the porous medium. Consequently, heat transfer is dominated by conduction and strongly dependent on the thermal properties of the porous material. With increasing Rayleigh number, the flow length scales become smaller and the flow is no longer obstructed by the porous medium. Then, heat transfer is dominated by convection, becomes independent of the properties of the porous material, and approaches that in a fluid-only filled cavity.

With the gained understanding of pore-scale flow phenomena in relation to the length scales of flow phenomena, in Chapter 4 we extend our studies to situations with non-uniform wall temperatures. Thus, we closer approach more realistic situations, such as in the industrial application of our interest, viz. the hearth of a blast furnace. We generalize non-uniform thermal boundary conditions at the walls by studying sinusoidal wall temperature distributions around a constant average wall temperature difference. Variations in the amplitude and phase shift of this sinusoidal distribution lead to an enhancement or reduction of the overall heat transfer. Though a similar behaviour is observed in fluid-only filled cavities, maximum and minimum heat transfer in fluid only filled cavities are observed for different phase shifts in the sinusoidal wall temperature distribution as compared to porous medium filled cavities. This is attributed to the importance of the location of pore spaces with respect to hot and cold parts of the walls. Such local effects cannot be accounted for in REV type simulations.

In Chapter 5, we further extend our research to understand mixed convection flow and heat transfer in a differentially heated, lid driven cavity filled with a coarse grained porous medium. The mixed convection flow is induced by the combined effect of natural convection and forced flow due to the movement of the isothermal walls, where the latter may assist or oppose the natural convection depending on the direction in which the walls are moved. As observed in Chapter 2 for natural convection, the heat transfer obtained in fully resolved coarse-grained simulations is higher compared to that obtained with REV simulations when the thermal boundary layers are thinner than the pore size. This is particularly the case in cavities with assisting mixed convection, where

the presence of the coarse grained porous medium leads to local rotational flows in the pore-spaces close to the walls, resulting in higher heat transfer. Local variations in wall heat transfer strongly depend on the locations of the near wall pores, and on the relative strength and direction of the forced and natural convection flows. All these effects cannot be accounted for in REV type simulations.

From all the observations above, we conclude that the length scales of the flow and thermal structures in natural and mixed convection, with respect to the length scales of the pores, have a determining effect on the heat transfer in coarse grained porous media. When length scales of thermal plumes or thermal boundary layers decrease, for instance at higher Rayleigh numbers, the flow obstruction due to the porous medium vanishes and the flow and heat transfer approach that in a fluid-only situation. The Rayleigh number at which the thermal boundary layers (in side heated situations) or the thermal plumes (in bottom heated situations) become thinner than the pore-space may vary with the geometry and material of the porous material. However, at sufficiently high Rayleigh numbers, the thermal boundary layers or plumes become so thin that they no more feel the porous medium. Under these conditions, the use of an REV simulation approach (based on e.g. Darcy or extended-Darcy models) will result in an under-prediction of heat transfer. The influence of the presence of a porous medium on flow and heat transfer diminishes when this porous medium is away from the isothermal walls. In such situations, REV simulations based on Darcy or Darcy-Forchheimer models may be sufficient to accurately determine the global heat transfer.

6.2. FUTURE WORK

The studies addressed in the present thesis were limited to coarse grained porous packings consisting of mono-disperse, spherical, non-permeable particles with uniform thermal properties. This clearly suggests three interesting directions for follow-up research:

6.2.1. PACKINGS OF POLY-DISPERSE AND NON-SPHERICAL PARTICLES

The numerical simulation studies presented in this thesis investigated the influence of the presence of a packed bed made of *mono-disperse, spherical* beads on natural and mixed convection flow and heat transfer in cubical cavities. For natural convection in cavities with a vertical temperature gradient, the flow is found to be dominant close to the verticals walls, and heat transfer is found to no longer be influenced by the presence of the packing at high Rayleigh numbers. An interesting topic for further studies would be the difference between mono-disperse spherical packings, and poly-disperse, non-spherical packings.

In the literature, studies on hydrodynamics [1] and forced convective heat transfer in *cylindrical* cavities with mono-disperse [2] and poly-disperse particles of different sizes and shapes [3] report that the highest flow velocities occur close to the cavity walls, where the local porosity is the highest. In such cavities, the radial distribution of local velocity scales with the radial distribution of local porosity. It is also observed that, depending on the shape of the poly-disperse particle, there may be large local variations in the contact surface between the cavity walls and the particles, resulting in radial variations in porosity, and thus the local flow velocity.

Combining our own findings with those reported in literature, we expect important differences between natural convection in cubical cavities filled with poly-disperse or differently shaped particles, compared to mono-disperse spherical particles, due to decreased near-wall porosity. At low Rayleigh numbers, heat transfer is therefore expected to decrease compared to that in cavities with a spherical packed bed of mono-disperse particles. At higher Rayleigh numbers these differences are expected to disappear, but the Rayleigh number at which the heat transfer approaches that of an empty cavity is expected to be higher than in the case of mono-disperse spherical particles. The above expectations should be verified by further studies on cavities filled with poly-disperse and non-spherical particles.

6.2.2. PACKINGS WITH LOCAL VARIATIONS IN THERMAL PROPERTIES

Our studies on natural convection in bottom-heated, top-cooled porous media-filled-cavities show that the thermal *conduction* properties of the porous medium have a strong impact on the *convective* heat transfer, with a high thermal conductivity leading to reduced convection.

Many applications, like catalytic reactors, prefer isothermal operating conditions [4]. This could either be achieved by enhancing convective heat transfer, or by using packing material with a high thermal conductivity. The latter, however, counteracts the first.

We expect that the above conundrum can be circumvented by applying a radial variation in the thermal conductivity of the packing material. Our studies indicate that that the convective heat transfer will be triggered earlier when a low conductivity packing material is put close to the isothermal walls. At the same time, a packing material of higher conductivity can thus be utilized to enhance conduction in the core of the reactor, where convection is less dominant. The above expectations should be verified by further studies on cavities filled with packings of varying thermal conductivities.

6.2.3. PACKINGS OF PERMEABLE SOLID PARTICLES

The current work investigated packed beds consisting of *non-permeable* solid particles. However, in many applications, such as in the food industry, in catalytic reactors, etc., the particles themselves are permeable (with a low porosity). Forced convection in such permeable packed beds has been studied in literature [3], but no information is available on flow and heat transfer in such systems under natural and mixed convection conditions. A variable 3D porosity field approach, as discussed in [3], can be utilized to study the combined effect of natural or mixed convection flow within the permeable particles and in inter-particle spacing. This can alternatively be analysed by using an REV approach, solving Volume Averaged Navier-Stokes equations within the permeable solids, while solving the fully resolved Navier-Stokes equations in the inter-particles pore-spaces.

6.3. OUTLOOK

The studies presented in the present thesis were limited to natural and mixed convection in very simple geometries (viz. cubical cavities), filled with coarse grained porous packings. However, our studies were motivated by an interest in, and relevant for, such flows in real-life and industrially applied complex geometries. Moreover, the simulation tools developed in this thesis are relevant for the study of the flow in such complex geometries. This is discussed below.

6.3.1. BLAST FURNACE HEARTH MODELLING

The hearth of the blast furnace can be visualized as an enclosure filled with a coarse grained packing, with an inlet at the top and an outlet at the cooled sidewalls. Within the hearth, depending on the stage of operation, natural or forced convection may occur and we may find regions with stable or unstable vertical temperature gradients, regions with horizontal temperature gradients, etc. as all addressed in this thesis. Furthermore, dissolution of the carbon lining at the walls [5] may result in so called hot-spots, i.e. regions with locally very high temperatures. 2D simulations and experiments on geometries similar to the blast furnace hearth [6, 7] report the influence of locally high flow velocities and flow recirculation close to the wall to be responsible for the wear of the carbon lining and thus the hot spot formation.

Inspired by the above, the current work aimed at numerically analysing flow and heat transfer in coarse-grained solid packings, using the OpenFOAM simulation environment. To this end, we integrated the Boussinesq natural convection solver with the conjugate heat transfer solver, as were both individually, but non-simultaneously, available within OpenFOAM. Furthermore, a volume-averaged solver was developed within OpenFOAM, allowing for REV type simulations. Both novel solvers were validated against experiments conducted simultaneously and within the same research group by PhD student Iman Ataei Dadavi [8–10]. Both solvers can now be used by TATA steel R&D IJmuiden, Netherlands, to carry out simplified simulations of e.g. the blast furnace hearth, in combination with water-model experiments for further validation. In these studies, the following aspects deserve special attention:

From our 3D numerical simulations we observe that the increased porosity close to the walls results in locally high flow velocities. We also find that the near-wall temperature is strongly influenced by the thermal properties and local configuration of the packing material. A larger pore-space close to the wall results in the fluid to impinge at the wall at a higher temperature. The vertical downward flow through the pore-space along cooled walls results in local circulation zones, both in natural and mixed convective flow. The formation of these recirculation zones becomes even more prominent when there are local variations in the wall temperature.

Studies of the influence of carbon concentration gradients, due to double diffusion effects, will help to understand the combined effect of carbon dissolution and thermal convection flow on the hot-spot formation at the walls. We also suggest to carry out experimental studies on effect of the dissolution of wall coating alone on hot-spot formation. For example, we suggest to evaluate the feasibility of using an ethyl-cellulose coated wall and study its dissolution in methanol filled bottom or side-heated cavity with a methanol resistant solid packing [11].

In order to simulate the expected turbulent flows at the very high Rayleigh numbers encountered in real-size blast furnaces, we suggest to investigate the possibility of including the turbulent closure terms in a VANS model based REV approach, similar to that reported in [12], and to carry out transient simulations [13, 14].

6.3.2. REFRIGERATION AND TEMPERATURE CONTROL IN BUILT ENVIRONMENTS

The storage and transportation of medicines, processed food, vegetables, etc., demand proper temperature [15, 16] and moisture conditions to keep them fresh. Air temperature and moisture content distributions also play an important role in human comfort [17–19] in the built environments.

Studies on the combined heat and moisture transfer in fluid-only filled enclosures are widely available in the literature, e.g. [20, 21]. However, our studies as presented in this thesis point at the importance of considering the influence of the stored objects themselves, as well as other obstructions, on the moisture and temperature distribution in e.g. storage spaces.

We find the positioning of the objects within the enclosure to play a role in the temperature and moisture content. We also observe an influence of the thermal properties of the stored objects on local flow and temperature. We reported the convective flow to be wall dominated at low Rayleigh numbers, resulting in larger thermal non-uniformities within the enclosure. These non-uniformities decrease at higher Rayleigh numbers. The temperature and flow distribution within the enclosure were also found to be influenced by the local wall temperature distribution *w.r.t* the pore-spaces close to the wall, possibly resulting in stagnant regions with high or low temperatures.

6.3.3. ELECTRONIC COOLING

Most electronic devices require precise temperature control to ensure efficient operation. Most of these are cooled by forced convection, but in applications where vibrations, noise, etc. can adversely influence the performance, manufacturers resort to natural convective cooling or a combination of forced and natural convection cooling [22–24]. From our current work, we find that - although the presence of conductive obstructions close to isothermal walls increases the effective surface area for heat transfer - stacking them together may result in reduced natural convection at low or intermediate Rayleigh numbers. This may even result in a reduction of the total heat transfer. The cooling can be optimized by properly placing the components such (e.g. staggered high conductive and low conductive blocks) that convective heat transfer is enhanced even at low Rayleigh number.

REFERENCES

[1] V. Pozzobon, J. Colin, and P. Perré, *Hydrodynamics of a packed bed of non-spherical polydisperse particles: A fully virtual approach validated by experiments,* Chemical Engineering Journal **354**, 126 (2018).

[2] S. Das, N. G. Deen, and J. Kuipers, *A DNS study of flow and heat transfer through slender fixed-bed reactors randomly packed with spherical particles,* Chemical Engineering Science **160**, 1 (2017).

[3] S. Das, N. Deen, and J. Kuipers, *Multiscale modeling of fixed-bed reactors with porous (open-cell foam) non-spherical particles: Hydrodynamics,* Chemical Engineering Journal **334**, 741 (2018).

[4] Q. Jing, H. Lou, L. Mo, and X. Zheng, *Comparative study between fluidized bed and fixed bed reactors in methane reforming with CO2 and o2 to produce syngas,* Energy Conversion and Management **47**, 459 (2006).

[5] K.-X. Jiao, J.-L. Zhang, Z.-J. Liu, C.-L. Chen, and Y.-X. Liu, *Analysis of blast furnace hearth sidewall erosion and protective layer formation,* ISIJ International **56**, 1956 (2016).

[6] J. R. Post, T. Peeters, Y. Yang, and M. A. Reuter, *Hot metal flow in the blast furnace hearth: thermal and carbon dissolution effects on buoyancy, flow and refractory wear,* in *Third International Conference on CFD in the Minerals and Process Industries, CSIRO, Melbourne, Australia* (2003) pp. 433–440.

[7] J. Post, D. Togarelli, J. van der Stel, Y. Yang, and M. Reuter, *Hot metal flow in the hearth of a blast furnace: influence of dynamic changes dead man porosity due to coke dissolution and coke size changes,* in *Proc. 5th European coke and ironmaking congress–5th ECIC, Stockholm, Sweden* (2005) pp. 1–16.

[8] I. Ataei-Dadavi, M. Chakkingal, S. Kenjereš, C. R. Kleijn, and M. J. Tummers, *Flow and heat transfer measurements in natural convection in coarse-grained porous media,* International Journal of Heat and Mass Transfer **130**, 575 (2019).

[9] I. Ataei-Dadavi, N. Rounaghi, M. Chakkingal, S. Kenjereš, C. R. Kleijn, and M. J. Tummers, *An experimental study of flow and heat transfer in a differentially side heated cavity filled with coarse porous media,* International Journal of Heat and Mass Transfer **143**, 118591 (2019).

[10] I. Ataei-Dadavi, M. Chakkingal, S. Kenjeres, C. R. Kleijn, and M. J. Tummers, *Experiments on mixed convection in a vented differentially side-heated cavity filled with a coarse porous medium,* International Journal of Heat and Mass Transfer **149**, 119238 (2020).

[11] M. Davidovich-Pinhas, S. Barbut, and A. G. Marangoni, *Physical structure and thermal behavior of ethylcellulose,* Cellulose **21**, 3243 (2014).

[12] M. J. de Lemos, *Turbulence in Porous Media Turbulence in Porous Media Modeling and Applications*.

[13] S. Kenjereš and K. Hanjalić, *LES, T-RANS and hybrid simulations of thermal convection at high Ra numbers,* International Journal of Heat and Fluid Flow **27**, 800 (2006).

[14] S. Kenjereš and K. Hanjalić, *Tackling complex turbulent flows with transient RANS,* Fluid Dynamics Research **41**, 012201 (2009).

[15] K. Beukema, S. Bruin, and J. Schenk, *Heat and mass transfer during cooling and storage of agricultural products,* Chemical Engineering Science **37**, 291 (1982).

[16] O. Laguerre, *Chapter16: Heat transfer and air flow in a domestic refrigerator,* in *Mathematical Modeling of Food Processing* (CRC Press, 2010) pp. 473–502.

[17] K. Hanjalić, S. Kenjereš, and F. Durst, *Natural convection in partitioned two-dimensional enclosures at higher Rayleigh numbers,* International Journal of Heat and Mass Transfer **39**, 1407 (1996).

[18] Q. Ma, R. Wang, Y. Dai, and X. Zhai, *Performance analysis on a hybrid air-conditioning system of a green building,* Energy and Buildings **38**, 447 (2006).

[19] S. Lee, M. Nogami, S. Yamaguchi, T. Kurabuchi, and N. Ohira, *Evaluation of heat transfer coefficients in various air-conditioning modes by using thermal manikin,* in *Proc. 13th International Building Performance Simulation Association Conference (BS2013), Chambéry, France* (2013) pp. 2289–2296.

[20] H. Wee, R. Keey, and M. Cunningham, *Heat and moisture transfer by natural convection in a rectangular cavity,* International Journal of Heat and Mass Transfer **32**, 1765 (1989).

[21] L. Zhang, K. L. Chong, and K.-Q. Xia, *Moisture transfer by turbulent natural convection,* Journal of Fluid Mechanics **874**, 1041 (2019).

[22] E. Papanicolaou and Y. Jaluria, *Mixed convection from an isolated heat source ina rectangular enclosure,* Numerical Heat Transfer, Part A: Applications **18**, 427 (1991).

[23] C. S. F. T. C. Hung, *Conjugate heat transfer analysis for the passive enhancement of electronic cooling through geometric modification in a mixed convection domain,* Numerical Heat Transfer, Part A: Applications **35**, 519 (1999).

[24] S. Bhopte, M. S. Alshuqairi, D. Agonafer, and G. Refai-Ahmed, *Mixed convection of impinging air cooling over heat sink in telecom system application,* Journal of Electronic Packaging **126**, 519 (2004).

ACKNOWLEDGEMENTS

I would like to thank each and everyone who supported me. I would like to thank **Prof. Chris Kleijn** and **Prof. Saša Kenjereš** for allowing me to work at TP. I still remember the day I joined as a Ph.D. student, April FOOL'S Day in our old building at Juilanalaan. It was a nice experience working in the group. It was great to have scientific discussions with you during our meetings. It has helped me a lot to improve my work. The effort **Chris** and **Sasa** put in making our manuscripts look nicer was really helpful. The time that you both spent on the work with the Master students whom I supervised also helped me to learn a lot. **Dr. Mark Tummers** who was involved in my work concentrating more on the experiments always gave me a new dimension in which I could think, considering what we could achieve experimentally. It was great, discussing with you.

It was nice to have wonderful office-mates, **Cees, Sid, Xiaolin, Sayeed, Peng, Harish, Ozgur** during my Ph.D. The cheeky jokes from **Cees** always stood out. **Sayeed**, if you found your computer mouse moving occasionally when you worked remotely, I had nothing to do with it. **Xiaolin** and your triplets were always nice to talk to. **Peng**, you are one among the nicest people whom I know. **Sid**, I enjoyed the songs we played in our office, your street photographs....and our stay at Udine, for the course. You were always there to discuss technical stuff and for small talks. **Wenjie**, though we had a small overlap at TP, I enjoyed our conversations and our lunch/dinner outings to Chinese restaurants.

Elin, it was nice working with you, who was always there for any technical/non-technical support. People working in OpenFOAM will always be grateful to you ☺. It was a great time chatting with you and **Sid** during the breaks.. **Hrushi, Chirag, Gerasimos** it was nice to work with you in the group and discuss topics ranging from engineering to politics. **Peng, Annekatrien**, you both always made sure the plants in my office did not die without water, thanks for that. **Manas**, you are the one who took me to Rotterdam on cycle for the first time. It was nice to be with you in the group, such a joyful and pumped up person. The dance skills you showed us on your birthday were amazing. It was nice chatting with you **Romana, Matheus** at our coffee breaks. I liked bugging you **Matheus** and **Debasish** by randomly dropping by your office when I was bored.. of-course, you did the same. **Fie, Rose, Saidah**, I enjoyed the conversations with you all. **Fie**, the boating during our team outing was really a nice experience. It was nice to have lunch as a group with you all; **Sasa, Valeria, David, Brice, Elin, Kosta, Lorenz, Aartem, Romana**. **Kevin**, you supported me a lot with OpenFOAM, RP, and many more. I would love to have a teacher like you. Thanks for the occasional witty discussions **Maulik, Shaurya, Karthik**. **Maulik** you are such a nice, calm person with whom everyone would love to talk and work with. **Shridhar**, I enjoyed our discussion on FLUENT and more, during our breaks.

Luis, you always found time for me and almost everyone to discuss either in your office or during your walk back home. I like the passion with which you approach everything whether its research, card-game, or sumo wrestling ..... I would also like to thank

Anita, Jennifer, Sandra fur their help and support during my time at TP. I would like to thank Christiaan for the card games and outings he organized. **Evert**, thank you for the cheeky jokes and making us win in the toilet seat race. Your driving skills with the toilet seat car was amazing.

It was great working with you **Iman** on our Ph.D. topics. You were always there for any questions, on research, and more. I enjoyed working with you and discussing our work mostly through Facebook messenger. You are the one who opened up the use of social media for scientific discussions for me. It was great working with you, **Dimitri, Julia, Sharon, Sabino, Rense, Roland & Sebastian**. It was a nice learning experience for me. I hope I helped you to learn something new and made your stay at TP worth remembering. If I get an opportunity, I would love to work with you all again. Welcome to the group **Jorit, Nathalie, Mathäa**.

I would like to thank our industrial partner TATA, especially Dirk, Tim, Andre, Saskia, Sjaak, Daniel, and Margot for being a part of our project discussions, interest in the research, and their support during my short internship at TATA. Thank you **Viktoria** and the whole m2i team involved in our project, for making sure that our work and meeting were well organized.

The stay at DUWO for the first 3 months of my Ph.D. was great, making new wonderful friends **AJ**, **Jishnu, Kamath,** and **AM**, who supported me whenever I needed it. All of us stayed at some point in the same place, which was a lot of fun and helped me handle my life at Delft. I enjoyed the benefit of being a Vegetarian, as you guys had to cook for me always. The random recipes of **AJ**, fast cooking by **Kamath**, slow cleaning by **Jishnu** all made my stay at Delft relaxed. Our trip to Maastricht with **Aswin Muralidharan**, it was amazing... I still cannot understand how you **AJ, AM, Jishnu** managed to reach late exactly, when the fort was about to close.

Rahul machan, Nithin and **Aswin, Amith** coffee breaks during your master thesis at TP, at our OWN corner, was great and relaxing. The topics we discussed were endless. Thanks for making the "vishramavelakal anandakaram ☺".

Shyam ettan & Ranjani chechi you both always made sure that I have Indian food once a while (almost every weekend), of course, I showed up un-invited. At your place I met **Prashantettan, Seshanji, Anjana chechi, Divya, Devina, Minu, Kamakshi, Gautam, Sriram** ... with whom we had a lot of planned/unplanned dinners, barbecue... **Freddy & Amy**, it was great to have get-togethers with our friends, at your place. **Chris, Rueben, Geo, Aswin George, Lee, Jesil, Ashish, Ashil, Arun Dominic** it was a great time with you guys during our occasional cooking, at our place. **Manoj Master, Agustine, Anoop, Pious, Robo, Raga, Vikas** it was always refreshing to meet and chat with you.

Ammamma, Amma, Mama, Appu... you made the thesis possible..

A

THEORETICAL AND ANALYTICAL RELATIONS

A.1. RELATION BETWEEN THERMAL BOUNDARY LAYER THICKNESS AND NUSSELT NUMBER

In a bottom- heated top-cooled cavity with the isothermal walls at a distance L and a temperature difference $\Delta = T_h - T_c$ (Fig.A.1), the temperature drops by $\approx \Delta/2$ in the thermal boundary layer attaining a $T_m(z)$ temperature. Thus, in the thermal boundary layer:

$$Q_{total} \approx Q_{cond} \approx \alpha \frac{\Delta/2}{\delta_{th}} \tag{A.1}$$

where Q_{total}, Q_{cond}, α and δ_{th} are the total heat flux, conductive heat flux, thermal diffusivity and thermal boundary layer thickness respectively. The Nusselt number, Nu can be expressed as:

$$Nu \approx \frac{Q_{total}}{Q_{cond}} \approx \frac{Q_{total}}{\alpha\Delta/L} \approx \frac{L}{2\delta_{th}} \tag{A.2}$$

Thus the thermal boundary layer thickness can be expressed in terms of Nu as:

$$\delta_{th} = \frac{L}{2Nu} \tag{A.3}$$

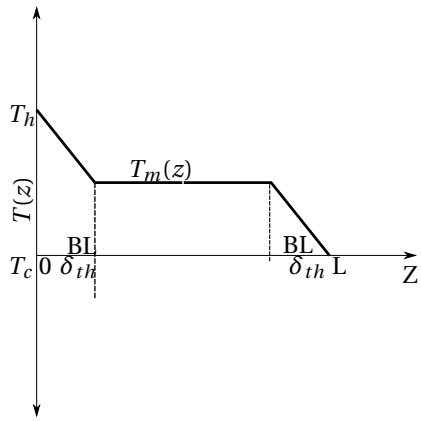

Figure A.1: Calculation of thermal boundary layer thickness from mean temperature profile for RBC convection. $T(z)$ denotes the $X-Y$ plane averaged temperature $\langle T \rangle_{xy}$ at different height along the direction of gravity.

B

THERMAL PROPERTIES OF MOLTEN IRON AND POROUS MEDIA

Table B.1: Thermal properties of molten iron and coarse-grained coke particles [1, 2]. Some of the properties* are obtained from TATA IJmuiden, The Netherlands

Property	Molten iron	Coarse-grain
Viscosity, $kg/(m.s)$	7.15×10^3	-
Density, kg/m^3	7000	$400 - 2200^*$
Heat Capacity, $J/(kg.K)$	850	$300 - 500^*$
Thermal conductivity, $W/(m.K)$	16.5	2-5
Coefficient of volume expansion, K^{-1}	1.4×10^{-4}	-

REFERENCES

[1] V. Panjkovic, J. S. Truelove, and P. Zulli, *Numerical modelling of iron flow and heat transfer in blast furnace hearth,* Ironmaking & Steelmaking **29**, 390 (2002).

[2] B.-Y. Guo, D. Maldonado, P. Zulli, and A.-B. Yu, *CFD modelling of liquid metal flow and heat transfer in blast furnace hearth,* ISIJ International **48**, 1676 (2008).

C

REV EQUATIONS FOR POROUS MEDIA

The momentum equation in ANSYS Fluent Manual differs in its representation from that in literature [1]. However it seems to be consistent with that in literature, after some re-arrangements.

C.1. EQUATION IN ANSYS FLUENT

$$\frac{\partial \mathbf{u}}{\partial t} + \mathbf{u} \cdot \nabla \mathbf{u} = -\frac{1}{\rho_f} \nabla p + \nu \nabla^2 \mathbf{u} + \mathbf{g} \beta (T - T_{ref}) + \frac{1}{\rho_f} \mathbf{S_{ANSYS}} \tag{C.1}$$

(C.2)

The source term in ANSYS Fluent is given as:

$$\mathbf{S_{ANSYS}} = -\frac{\mu}{C_0} \mathbf{u_d} - C_1 \frac{1}{2} \rho_f \mathbf{u_d} \mid \mathbf{u_d} \mid \tag{C.3}$$

implemented as a source term in the momentum equation (Eq.C.1). For a packed bed cavity C_0 and C_1 are calculated using Ergun's equation as:

$$C_0 = \frac{d^2}{150} \frac{\phi^3}{(1-\phi)^2} \tag{C.4}$$

$$C_1 = \frac{3.5}{d} \frac{1-\phi}{\phi^3} \tag{C.5}$$

C.2. EQUATION IN LITERATURE

In literature [1] the momentum equation is expressed in terms of Darcy velocity. Re-writing Eq.C.1 in terms of Darcy velocity defined as $\mathbf{u_d}$=$\phi\mathbf{u}$:

$$\frac{1}{\phi}\frac{\partial \mathbf{u_d}}{\partial t} + \frac{1}{\phi}\mathbf{u_d}\cdot\nabla\frac{\mathbf{u_d}}{\phi} = -\frac{1}{\rho_f}\nabla p + \frac{\nu}{\phi}\nabla^2\mathbf{u_d} + \mathbf{g}\beta(T - T_{ref}) + \frac{1}{\rho_f}\mathbf{S_{LIT}} \tag{C.6}$$

The source term in literature is given as:

$$\mathbf{S_{LIT}} = -A\mathbf{u_d} - B\mathbf{u_d}\,|\,\mathbf{u_d}\,| \tag{C.7}$$

Using Ergun's correlation the constants A and B is given by:

$$A = 150\frac{(1-\phi)^2}{\phi^3}\frac{\mu}{d^2} \tag{C.8}$$

$$B = 1.75\frac{\rho_f}{d}\frac{1-\phi}{\phi^3} \tag{C.9}$$

We could see that $A = \frac{\mu}{C_0}$ and $B = C_1\frac{1}{2}\rho_f$. Thus both Eq.C.1 and Eq.C.6 are the same.
In some literature the source term $\mathbf{S_{LIT}}$ is re-written in terms of the permeability $K = \frac{d^2}{150}\frac{\phi^3}{(1-\phi)^2}$ (same as C_0). If we substitute K in A and B we get:

C

$$A = \frac{\mu}{K} \tag{C.10}$$

$$\begin{aligned} B &= 1.75 \times \frac{\rho_f}{d} \times \frac{1-\phi}{\phi^3} \\ &= \frac{1.75}{\sqrt{150}} \times \frac{\rho_f}{d} \times \sqrt{150}\frac{1-\phi}{\phi^3} \\ &= \frac{1.75}{\sqrt{150}} \times \frac{\rho_f}{\phi^{3/2}} \times \sqrt{\frac{150}{d^2}} \times \frac{(1-\phi)^{2/2}}{\phi^{3/2}} \\ &= \frac{1.75}{\sqrt{150}} \times \frac{\rho_f}{\phi^{3/2}} \times \sqrt{\frac{150}{d^2}} \times \sqrt{\frac{(1-\phi)^2}{\phi^3}} \\ &= \frac{1.75}{\sqrt{150}} \times \frac{\rho_f}{\phi^{3/2}} \frac{1}{\sqrt{K}} \end{aligned} \tag{C.11}$$

Some literature also simplify Eq.C.11 as:

$$B = \frac{1.75}{\sqrt{150\phi^5}} \times \frac{\phi\rho_f}{\sqrt{K}}$$

REFERENCES

[1] P. Nithiarasu, K. Seetharamu, and T. Sundararajan, *Effect of porosity on natural convective heat transfer in a fluid saturated porous medium,* International Journal of Heat and Fluid Flow **19**, 56 (1998).

CURRICULUM VITÆ

Manu CHAKKINGAL

31-05-1991	Born in Kerala, India.

EDUCATION AND WORK EXPERIENCE

1996-2006	Sree Narayana Public School Vadakkencherry, Kerala, India
2006-2008	A.S.M.M. Higher Secondary School Alathur, Kerala, India
2008-2012	Bachelor of Technology, Mechanical Engineering Government Engineering College Thrissur, Kerala, India
2012-2014	Master of Technology, Applied Mechanics Indian Institute Of Technology-Delhi New Delhi, India
2014-2015	Senior Engineer Robert Bosch Engineering & Business Solutions PVT LTD Coimbatore, India
2016-2020	Ph.D. student, Faculty Of Applied Sciences Dept. Of Chemical Engineering, TU Delft Netherlands
Thesis:	Convective heat transfer in coarse-grained porous media A numerical investigation of natural and mixed convection
Promotor:	Prof. dr. Chris R. Kleijn & Prof. dr. Saša Kenjereš
2020-	Jr. credit risk analyst ABN AMRO Bank Amsterdam, Netherlands

LIST OF PUBLICATIONS

9. **M. Chakkingal**, S. Bosch, E. Vesper, C.R. Kleijn, S. Kenjereš *Thermal charcterisitics in a cavity with cylindrical obstructions under natural convective and mixed convective flows*, Under preparation.

8. **M. Chakkingal**, S. Schiavo, I. Ataei-Dadavi, M.J. Tummers, C.R. Kleijn, S. Kenjereš *Effect of packing height and location of porous media on heat transfer in a cubical cavity: Are extended Darcy simulations sufficient?*, Int. J. Heat Fluid Flow **84**, 108617 (2020).

7. **M. Chakkingal**, R. Voigt, C.R. Kleijn, S. Kenjereš *Effect of double-diffusive convection with cross gradients on heat and mass transfer in a cubical enclosure with adiabatic cylindrical obstacles*, Int. J. Heat Fluid Flow **83**, 108574 (2020).

6. **M. Chakkingal**, J. de Geus, S. Kenjereš, I. Ataei-Dadavi, M.J. Tummers, C.R. Kleijn *Assisting and opposing mixed convection with conjugate heat transfer in a differentially heated cavity filled with coarse-grained porous media*, Int. Commun. Heat Mass Transf. **111**, 104457 (2020).

5. **M. Chakkingal**, S. Kenjereš, I. Ataei-Dadavi, M.J. Tummers, C.R. Kleijn *Numerical analysis of natural convection in a differentially heated packed bed with non-uniform wall temperature*, Int. J. Heat Mass Transf. **149**, 119168 (2020).

4. I. Ataei-Dadavi, **M. Chakkingal**, S. Kenjereš, C.R. Kleijn, M.J. Tummers *Experiments on mixed convection in a vented differentially side-heated cavity filled with a coarse porous medium*, Int. J. Heat Mass Transf. **149**, 119238 (2020).

3. I. Ataei-Dadavi, N. Rounaghi, **M. Chakkingal**, S. Kenjereš, C.R. Kleijn, M.J. Tummers *An experimental study of flow and heat transfer in a differentially side heated cavity filled with coarse porous media*, Int. J. Heat Mass Transf. **143**, 118591 (2019).

2. **M. Chakkingal**, S. Kenjereš, I. Ataei-Dadavi, M.J. Tummers, C.R. Kleijn *Numerical analysis of natural convection with conjugate heat transfer in coarse-grained porous media*, Int. J. Heat Fluid Flow **77**, 48 (2019).

1. I. Ataei-Dadavi, **M. Chakkingal**, S. Kenjereš, C.R. Kleijn, M.J. Tummers *Flow and heat transfer measurements in natural convection in coarse-grained porous media*, Int. J. Heat Mass Transf. **130**, 575 (2019).